

# **UV light-driven prebiotic synthesis of iron-sulfur clusters**

Claudia Bonfio, Luca Valer, Simone Scintilla, Sachin Shah, David J. Evans, Lin Jin, Jack W. Szostak, Dimitar D. Sasselov, John D. Sutherland, Sheref S. Mansy

Materials and Methods

Figs. S1 to S65

Tables S1 to S8

References

## Materials and Methods

Unless otherwise specified, all reactions and manipulations were carried out at room temperature using vinyl anaerobic chambers that provide a strict anaerobic atmosphere of 0-5 parts per million (ppm) using a palladium catalyst and a hydrogen gas mix of 5%. The products were maintained under inert atmosphere and transferred to NMR tubes sealed with rubber septa, anaerobic sealed Hellma quartz cuvettes, or sealed glass vials for NMR, UV-Vis spectroscopy, and Mössbauer spectroscopy, or vesicle experiments, respectively. Reagents and solvents were from Sigma-Aldrich, including  $^{57}\text{Fe}$ , and VWR International and were used without further purification, unless otherwise stated. Peptides ACG, ECG, FCG, KCG, QCG, WCG, and GMG were bought from ProteoGenix SAS. The *N*-acetylated compounds Ac-Ala-OH and Ac-Ala-OMe were prepared according to published procedures<sup>1</sup>.

A Mettler Toledo InLab Flex-Micro pH Meter was used to monitor pH. H<sub>2</sub>O was degassed by the freeze-pump-thaw method. Unless otherwise stated, all irradiations were carried out in a RPR-200 Rayonet reactor using 8 lamps with principal emission at 254 nm and with the cooling fan turned on resulting in an internal reactor temperature of ca. 35 °C. Kinetic irradiation studies at variable wavelengths were carried out with a Photon Technology International UV tunable lamp with a 75 W Xenon lamp as the power source. Tunable wavelength selection was enabled by adjusting the angle between the diffraction grating and the slit. The bandwidth of radiation used for all trials was set to 10 nm. Kinetic values obtained from these studies were normalized by the incident photon flux, as the flux varies from one wavelength to another. <sup>1</sup>H-NMR spectra were acquired using a Bruker Ultrashield 400 Plus operating at 400.1 MHz <sup>1</sup>H frequency, equipped with a cryogenic inverse probe. The sample temperature was 298 K. Samples consisting of H<sub>2</sub>O/D<sub>2</sub>O mixtures were analyzed using HOD suppression to collect <sup>1</sup>H-NMR data. Chemical shifts ( $\delta$ ) are shown in ppm. The yields of conversion were determined by relative integrations of the signals in the <sup>1</sup>H-NMR spectrum or by spiking with internal standards, unless otherwise stated. UV-Vis absorption spectra of freshly prepared solutions were recorded with an Agilent 8453 UV-Vis diode array spectrophotometer with an integration time of 0.5 s and an interval of 1 nm. Mössbauer spectra were recorded at 80 K in zero magnetic field in the solid state on an ES-Technology MS-105 Mössbauer spectrometer with a 60 MBq <sup>57</sup>Co source in a rhodium matrix at ambient temperature. Spectra were referenced against a 25  $\mu\text{m}$  iron foil at 298 K and spectrum parameters obtained by fitting with Lorentzian lines. Samples were prepared by grinding with boron nitride under an inert atmosphere. Mass spectra for glutathione samples were acquired on an Agilent 1200 LC-MS system that employs a 6130 Quadrupole spectrometer. The solvent system used for liquid chromatography (LC) was 0.2 % formic acid in H<sub>2</sub>O as buffer A, and 0.2 % formic acid in acetonitrile (MeCN) as buffer B. Samples were injected into Phenomenex Jupiter C18 column (150 x 200 mm, 5  $\mu\text{m}$ ) and subsequently into the mass spectrometer using a fully automated system. Spectra were acquired in the positive mode and analyzed using the MS Chemstation software (Agilent Technologies). The deconvolution program provided by the software was used to obtain the mass spectra. Absorbance and fluorescence analyses of vesicle experiments were performed with a SpectraMax i3x Multi-Mode Detection Platform (Molecular Devices).

### Solid-phase peptide synthesis (SPPS)

All the peptides were synthesized according to previously published SPPS procedures by using Fmoc-protected L-amino acids<sup>2</sup>. *N,N*-dimethyl formamide (DMF) was used as the solvent and preloaded fluorenylmethyloxycarbonyl-glycyl-Wang resin (Fmoc-Gly-Wang) was used as the starting polymeric support. Trityl-protected Fmoc-Cysteine (Fmoc-Cys(Trt)-OH) and tert-butyl (OtBu) side chain-protected Fmoc- $\alpha$ -amino acid were used as building blocks. In general, the peptide chain was elongated by sequential Fmoc deprotection of the residue anchored to the resin and Fmoc-AA-OH coupling. Acetic anhydride in DMF was used to achieve *N*-acetylation. Fmoc deprotection was obtained by washing the mixture with 20% (v/v) solution of piperidine in DMF. For each coupling, an excess (Fmoc-AA-OH: anchored AA, 4:1) of the Fmoc- $\alpha$ -amino acid

derivative was added to the resin. Apart from Fmoc-Cys(Trt)-OH, Fmoc- $\alpha$ -amino acid derivatives were activated with a mixture of hydroxyl-benzotriazole (HOBt), *N,N,N',N'*-tetramethyl-*O*-(benzotriazol-1-yl)uronium tetrafluoroborate (TBTU), and *N,N*-diisopropylethyl amine (DIPEA). Fmoc-Cys(Trt)OH was activated with a *N,N'*-diisopropylcarbodiimide (DIC)/HOBt mixture. At the end of the coupling, the polymers were cleaved from the resin and deprotected by treatment with a solution of trifluoroacetic acid (TFA):H<sub>2</sub>O:triisopropyl silane (TIS):1,2-ethanedithiol (EDT) (volume ratio 97:1:1:1) for 2 h. The volume was successively reduced under nitrogen atmosphere to avoid cysteinyl thiol oxidation, and the product was precipitated with a cold solution of diethyl ether/petroleum ether (30:70 (v/v)) followed by washing cycles with diethyl ether or extracted 3 times with 20% acetic acid/chloroform and finally dried under inert atmosphere.

### Sulfide-release studies

An aqueous solution containing each thiol (5 mL, 0.24 M) was prepared and the pH was adjusted to the pK<sub>a</sub> of the thiol under anaerobic conditions. Subsequently, the solution was transferred to an NMR tube, capped with a rubber septum, and irradiated at 254 nm. Hypophosphite was used only in the set of experiments described in Fig. 2a-2b. That is, hypophosphite was not used for the synthesis of iron-sulfur clusters unless specifically indicated.

### Photo-oxidation colorimetric assay

An aqueous solution of Fe<sup>2+</sup> (1 mL, 0.001 M) and an aqueous glutathione-Fe<sup>2+</sup> solution (1 mL, glutathione 0.24 M, Fe<sup>2+</sup> 0.001 M) were irradiated (254 nm) for 5 min. An excess of 1,10-phenantroline (0.005 M), which reacts with Fe<sup>2+</sup> ions, or potassium thiocyanate (0.005 M) solution, which reacts with Fe<sup>3+</sup> ions, was added to each solution before transfer to anaerobic sealed Hellma quartz cuvettes.

### [2Fe-2S] cluster synthesis

Ferric chloride hexahydrate (25  $\mu$ L, 0.1 M) was added to an aqueous solution containing each thiol (5 mL, 0.24 M) and sodium sulfide nonahydrate (10  $\mu$ L, 0.1 M) after pH adjustment under anaerobic conditions. For UV-driven experiments, ferric chloride hexahydrate (25  $\mu$ L, 0.1 M) was added to an aqueous solution containing each thiol (5 mL, 0.24 M) after pH adjustment under anaerobic conditions. Subsequently, the solution was transferred to a NMR tube capped with a rubber septum or an anaerobic sealed Hellma quartz cuvette and irradiated with UV light. For Mössbauer experiments, degassed 2-propanol was added in a 40-fold excess to solutions containing glutathione mononuclear Fe<sup>2+</sup> complex, a [2Fe-2S] cluster, and a [4Fe-4S] cluster to induce precipitation. The solution was centrifuged for 20 min at 5000 g and the solvent was discarded. The obtained precipitate was dried under N<sub>2</sub> atmosphere.

### Vesicle formation

Under anaerobic conditions, 100 mM oleic acid and 100 mM decanoic acid:decanol:glycerol monodecanoate 4:1:1 vesicles were prepared as previously described<sup>3</sup> by direct dispersion of the amphiphiles in either buffer (0.2 M glutathione, pH 8.6) or in solution containing the Fe<sup>2+</sup> mononuclear complex (0.2 M glutathione, 5 mM Fe<sup>2+</sup>, pH 8.6) with 0.5 equivalents of NaOH. Samples were briefly vortexed, tumbled at room temperature for 2 h, then extruded with 11 passages through a 400 nm pore membrane (Avanti Polar Lipids) using a Mini-Extruder (Avanti Polar Lipids). Vesicles containing Fe<sup>2+</sup> mononuclear complex were then loaded for purification onto a Sepharose 4B (6 mL bed volume) size exclusion column to remove unencapsulated material, using 0.2 M Tris-HCl pH 8.5 as the running buffer supplemented with 0.25 mM of oleic acid or 25 mM 4:1:1 decanoic acid:decanol:glycerol monodecanoate. Elution was monitored at 420 nm and the fractions containing vesicles were collected.

### Vesicle stability assay

100 mM oleic acid and 100 mM 4:1:1 decanoic acid:decanol:glycerol monodecanoate vesicles containing 0.1 mM FITC-dextran (MW 4000) were prepared and purified by size exclusion chromatography with a Sepharose 4B column. 500  $\mu$ L of the vesicle solution was then incubated for 60 min with 500  $\mu$ L of 200 mM Tris-HCl, pH 8.5, 500  $\mu$ L of 200 mM glutathione, pH 8.6, and 500  $\mu$ L of a glutathione-Fe<sup>2+</sup> mononuclear complex (5 mM Fe<sup>2+</sup>, 200 mM GSH) or an aqueous solution containing 5 mM Fe<sup>2+</sup>. All the samples were loaded onto a Sepharose 4B (6 mL bed volume) size exclusion column to assess vesicle stability, using 0.2 M Tris-HCl, pH 8.5 as the running buffer supplemented with 0.25 mM oleic acid or 25 mM 4:1:1 decanoic acid:decanol:glycerol monodecanoate. The elution profile was monitored by fluorescence (emission 525 nm, excitation 490 nm).

#### Vesicle sulfide-release assay

A fluorescence assay was performed to detect the release of sulfide from glutathione-encapsulated within oleate vesicles. Freshly prepared 100 mM 7-azido-4-methyl coumarin in DMSO was added to each fraction (200  $\mu$ L) of 100 mM oleate vesicles containing 200 mM glutathione that was previously exposed to UV light (254 nm). The formation of 7-amino-4-methyl coumarin upon reaction with sulfide ions was detected by fluorescence (excitation wavelength: 345 nm, emission wavelength: 440 nm).

#### Colorimetric assays for iron-sulfur cluster formation within fatty acids vesicles

A tiron assay was performed to detect fractions containing iron. Freshly prepared 100 mM tiron in 0.20 mM Tris-HCl, 0.25 mM oleic acid, pH 8.6 was added to each fraction (2.5 mM) that was previously incubated with ethanol (25% v/v) for 5 min. The formation of the tiron complex was detected by absorbance at 484 nm. Alternatively, a methylene blue assay was employed to detect fractions containing sulfide<sup>4</sup>. *N,N*-dimethyl-*p*-phenylenediamine (DMPD) (10 mg) was dissolved in 10 mL 35% (v/v) HCl to make a DMPD stock solution. DMPD was added to each fraction (2.5 mM) in the presence of Fe<sup>3+</sup> (1.25 mM) to increase the sensitivity of the assay and left to react for 1 h. The samples were then centrifuged and the absorbance at 668 nm recorded.

**Fig. S1.**

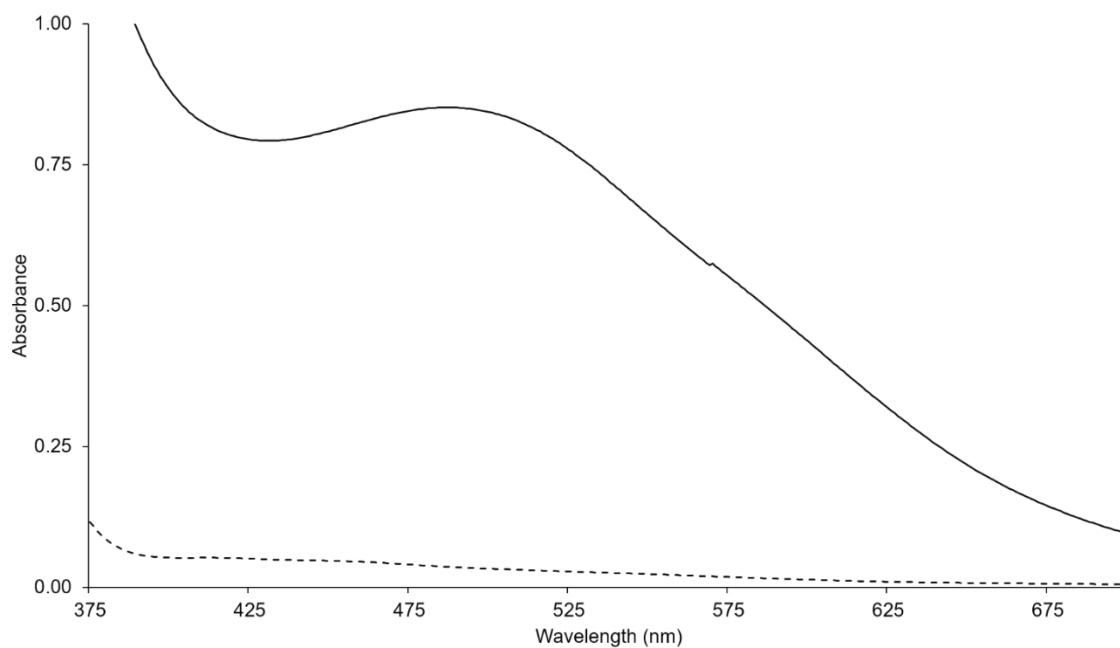


Fig. S1 | UV-vis absorption spectra of non-irradiated L-glutathione solution with Fe<sup>3+</sup>. In the absence of UV light the Fe<sup>3+</sup> mononuclear complex (solid line) undergoes reduction to the Fe<sup>2+</sup> mononuclear complex (dashed line) without conversion to the corresponding [2Fe-2S] cluster up to 24 h.

**Fig. S2.**

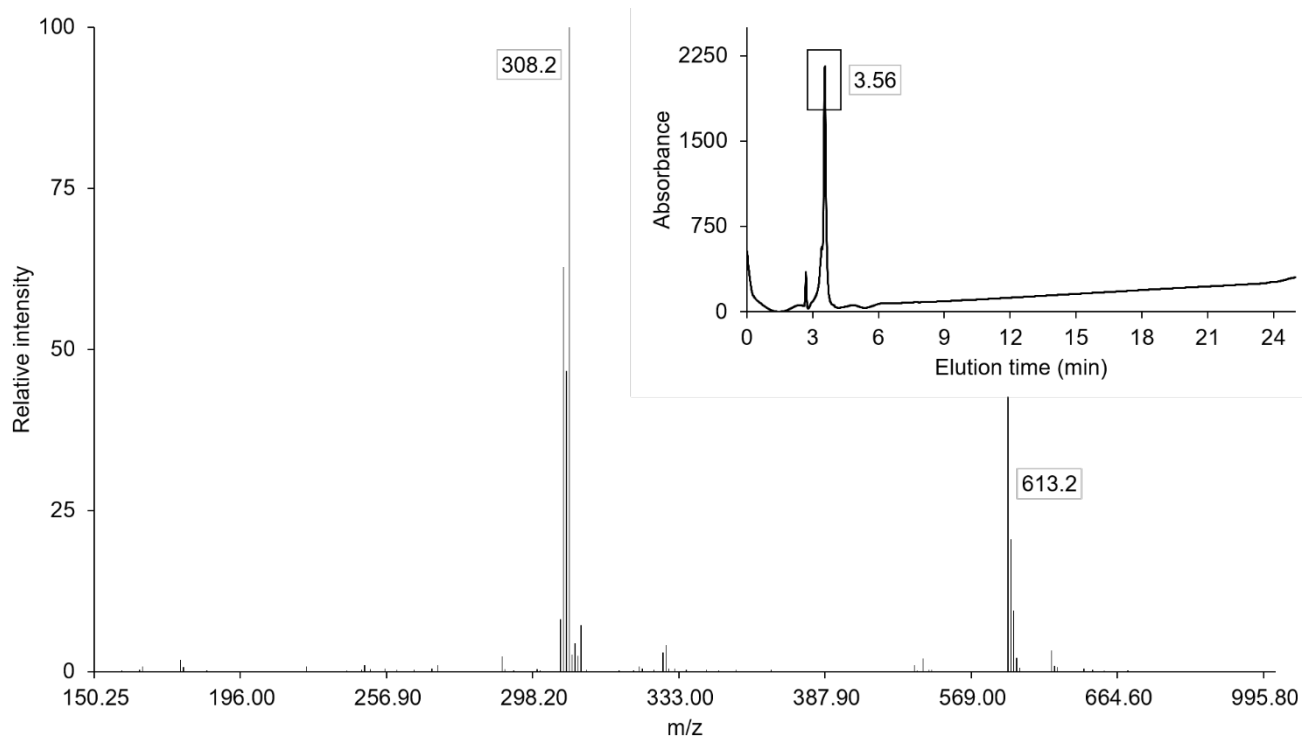


Fig. S2 | LC-MS analysis of glutathione solution before irradiation. One peak was detected in the chromatogram (inset, elution time: 3.56 min, detector: 215 nm) which corresponds to glutathione, as shown by the mass spectrum.

**Fig. S3.**

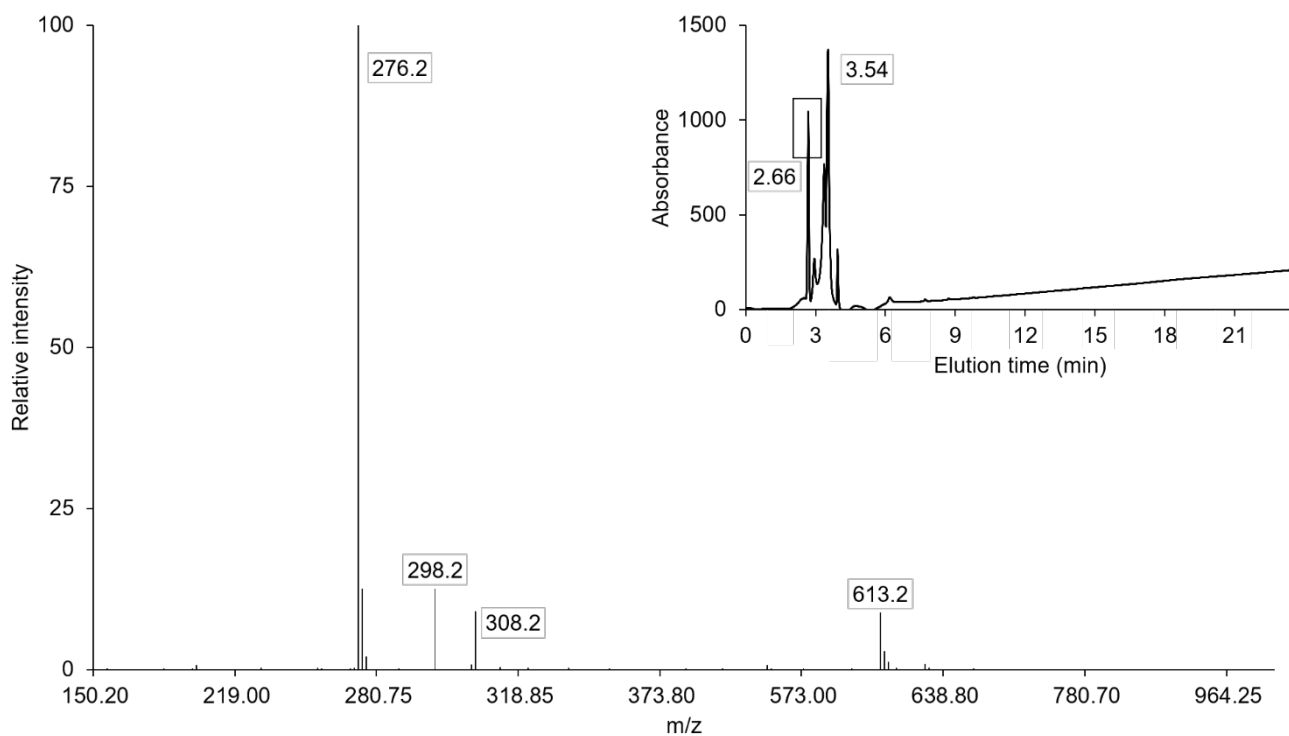


Fig. S3 | LC-MS analysis of glutathione solution after 15 min irradiation. Two peaks were detected in the chromatogram (inset, elution time: 2.66 and 3.54 min, detector: 215 nm), which correspond to the alanyl analogue of glutathione, as shown by the mass spectrum, and glutathione.

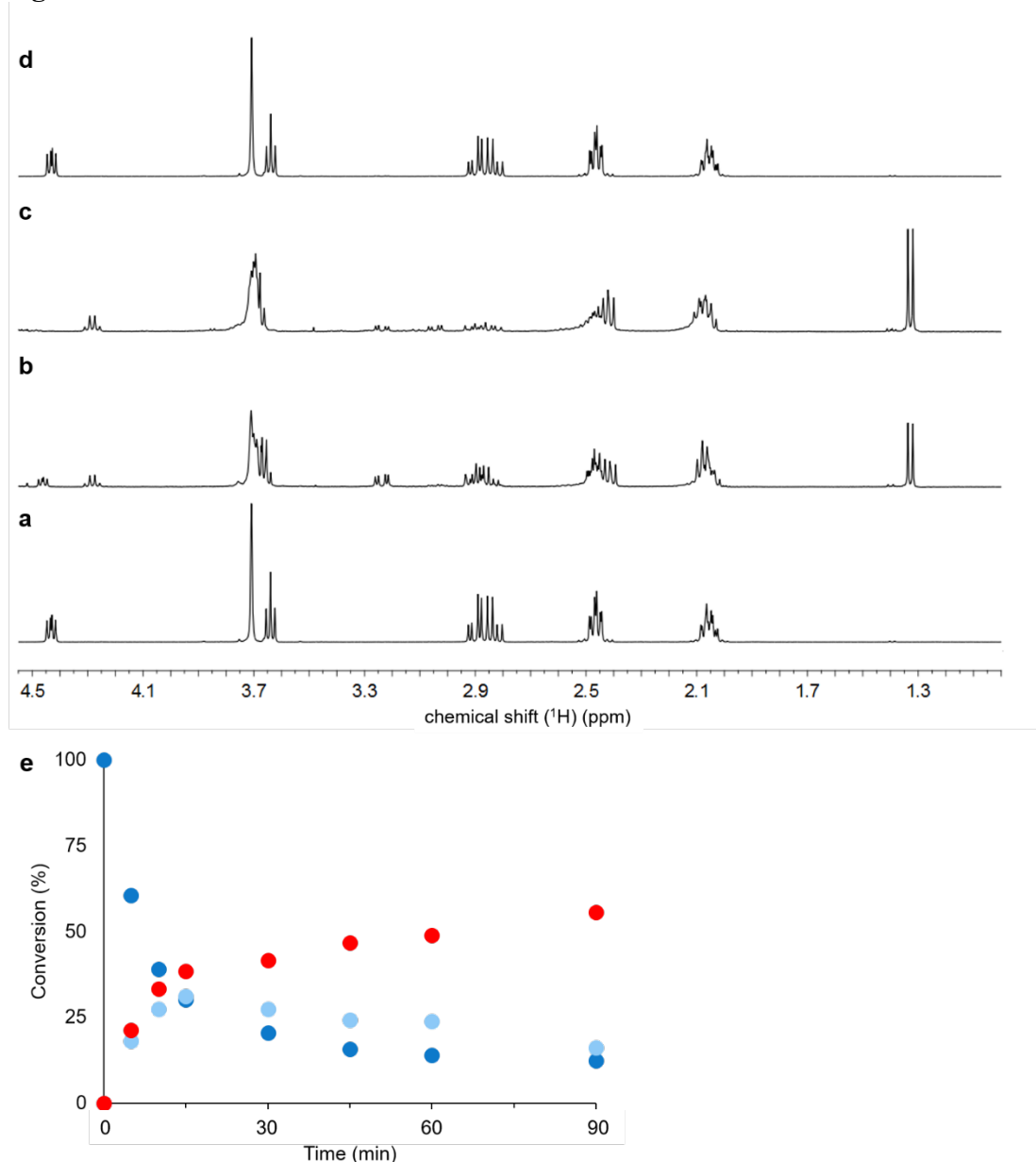
**Fig. S4.**

Fig. S4 | **a**, <sup>1</sup>H-NMR spectrum of a glutathione solution before exposure to UV light in the absence of hypophosphite. **b**, <sup>1</sup>H-NMR spectrum of a glutathione solution after 15 min exposure to UV light in the absence of hypophosphite. The alanyl species is already detectable at 1.33 ppm together with the disulfide species of glutathione at 2.94 and 3.23 ppm. **c**, The conversion to the alanyl-analogue is almost complete after 90 min of exposure to UV light. **d**, <sup>1</sup>H-NMR spectrum of a glutathione solution without exposure to UV light after 90 min. **e**, Time course of conversion as obtained by integration of NMR peaks for the irradiated solution of glutathione in the absence of hypophosphite. Blue, reduced glutathione; light blue, oxidized glutathione; red, alanyl-analogue.

**Fig. S5.**

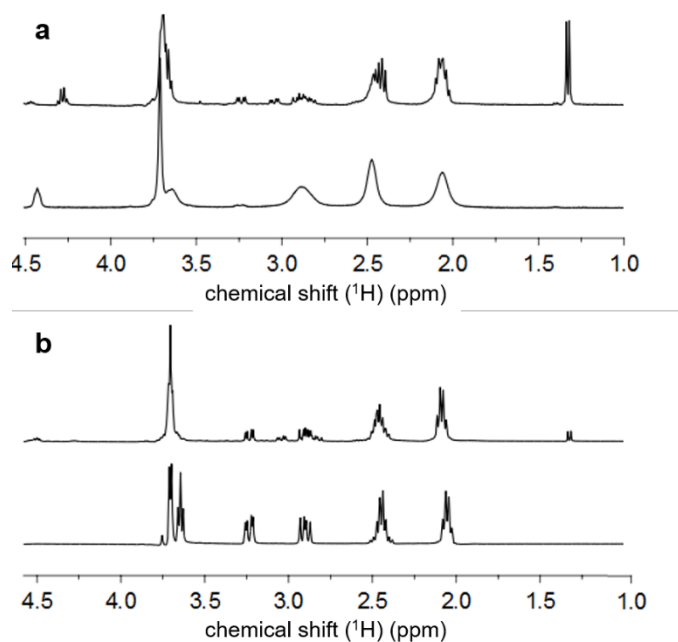


Fig. S5 | **a**, <sup>1</sup>H-NMR spectra of an irradiated solution of glutathione in the presence of ferric ions. The bottom spectrum is of the starting solution. The top spectrum is after 15 min of irradiation, which shows a new peak at 1.33 ppm indicating that photolysis occurs also in the presence of iron ions. Significant line broadening due to the paramagnetism of the iron ions and ligand exchange were observed<sup>5</sup>. **b**, <sup>1</sup>H-NMR spectra of an irradiated solution of oxidized glutathione. Upon prolonged irradiation up to 90 min of the starting material (bottom spectrum) it is possible to detect the appearance of a peak at 1.33 ppm due to the alanyl-analogue (top spectrum).

**Fig. S6.**

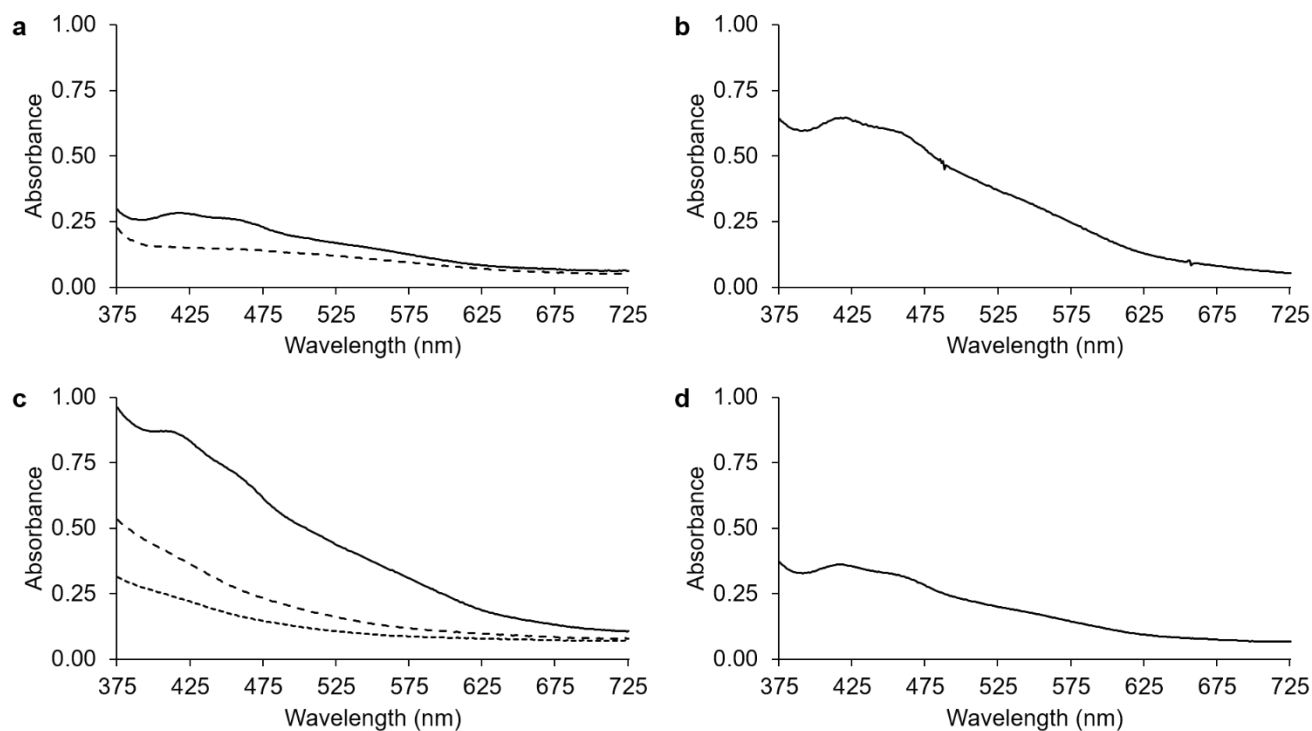


Fig. S6 | **a**, Starting from a solution of  $\text{Fe}^{2+}$ ,  $\text{S}^{2-}$ , and glutathione (dashed line), a  $[\text{2Fe-2S}]$  cluster could not be synthesized unless subsequently exposed to air to oxidize the iron ions (solid line). **b**, When  $\text{S}^{2-}$  is premixed with glutathione, the addition of  $\text{Fe}^{3+}$  leads to the formation of a  $[\text{2Fe-2S}]$  cluster. **c**, If  $\text{Fe}^{3+}$  is incubated with glutathione prior to the addition of  $\text{S}^{2-}$ , then the  $[\text{2Fe-2S}]$  cluster does not form. Here we report the sulfide addition after 60 s from premixing of glutathione and iron ions (solid line), after 60 min (dashed line) and after 6 h (dotted line). **d**, The  $[\text{2Fe-2S}]$  cluster can form by irradiation of a solution of glutathione and  $\text{Fe}^{2+}$  ions.

**Fig. S7.**

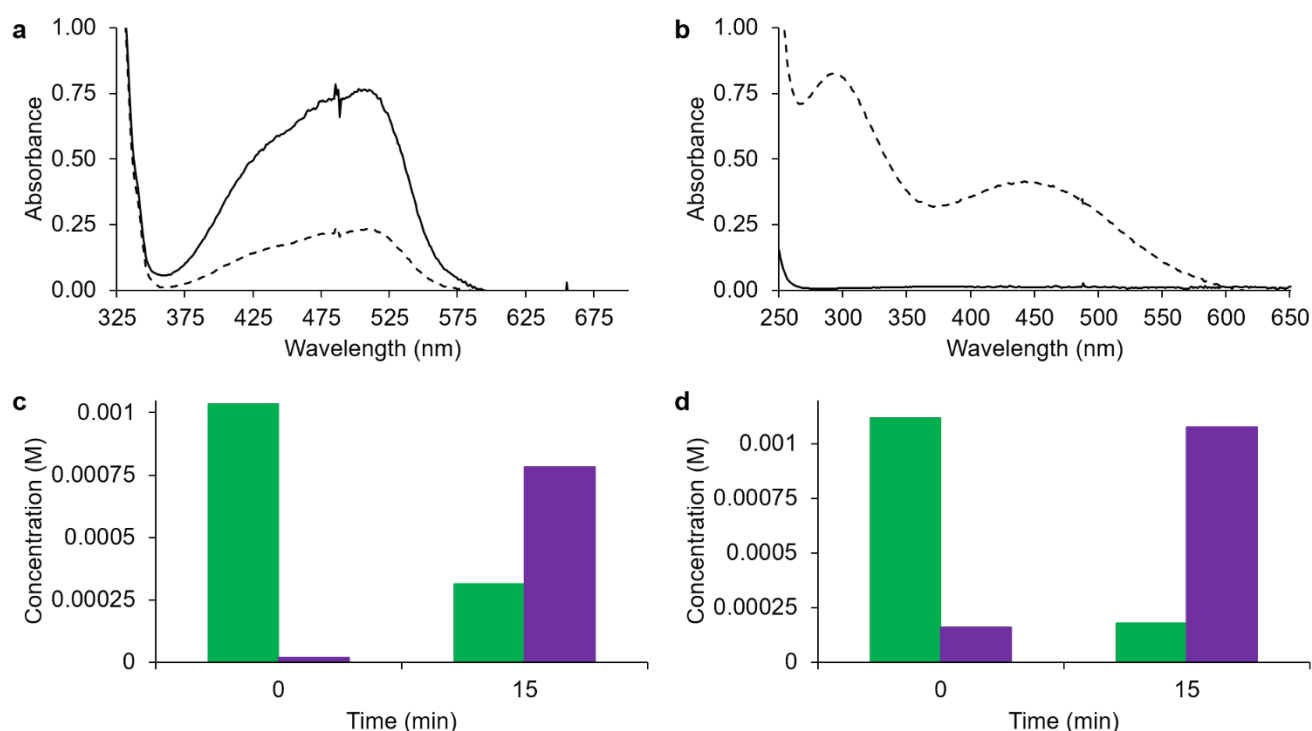


Fig. S7 | **a**, UV-vis absorption spectra of a solution of  $\text{Fe}^{2+}$  ions in water before (solid line) and after (dotted line) exposure to UV light (254 nm) for up to 15 min in the presence of 1,10-phenanthroline, an indicator of  $\text{Fe}^{2+}$  ions. **b**, UV-vis spectra of a solution of  $\text{Fe}^{2+}$  ions in water before (solid line) and after (dotted line) exposure to UV light (254 nm) in the presence of thiocyanate, an indicator of  $\text{Fe}^{3+}$  ions, for 15 min. **c**, Change in concentration of  $\text{Fe}^{2+}$  (green bars) and  $\text{Fe}^{3+}$  (violet bars) ions upon exposure to UV light in aqueous solution. **d**, Change in concentration of  $\text{Fe}^{2+}$  (green bars) and  $\text{Fe}^{3+}$  (violet bars) ions upon exposure to UV light in the presence of glutathione.

Fig. S8.

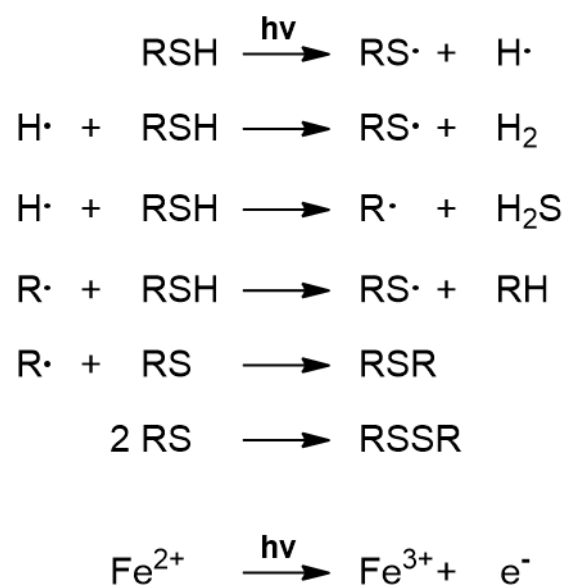


Fig. S8 | Photolysis<sup>6</sup> and photooxidation reactions during the synthesis of iron-sulfur clusters in the presence of ferrous ions and organic thiols.

**Fig. S9.**

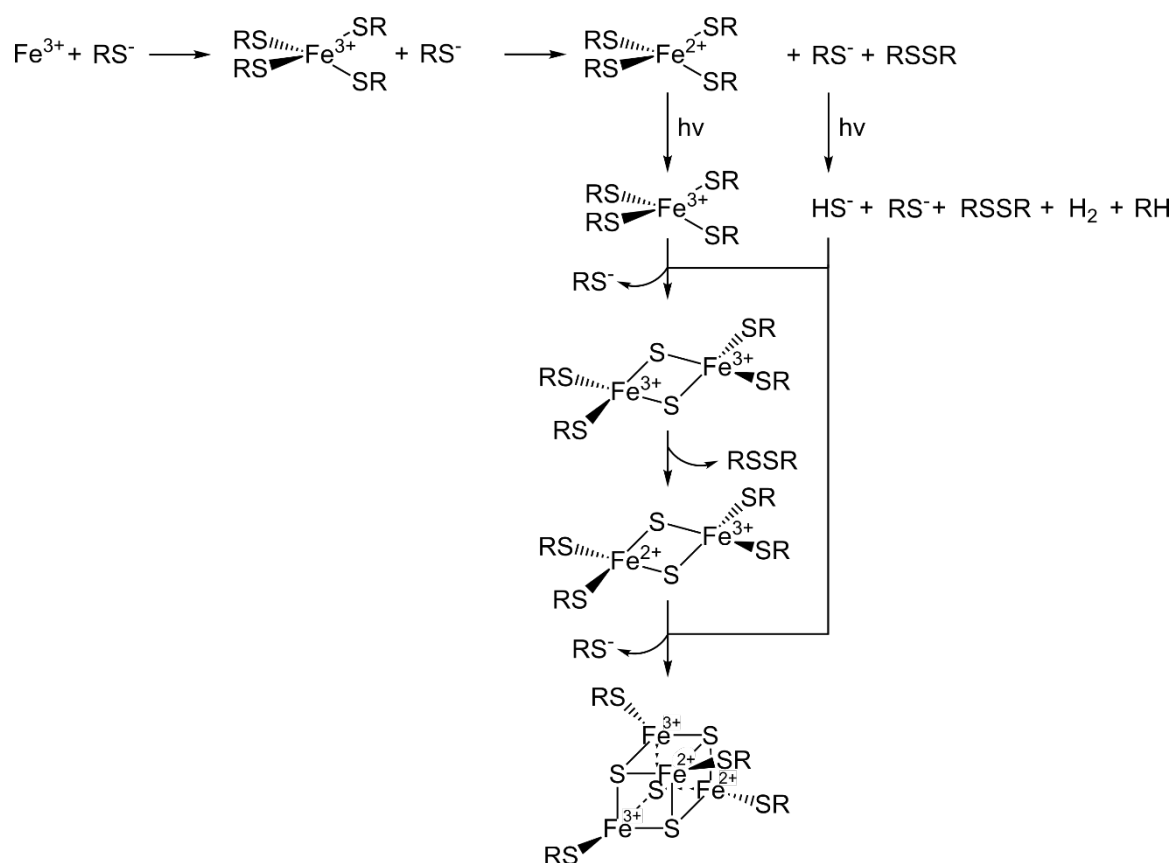


Fig. S9 | Proposed light-driven conversion routes to iron-sulfur clusters from mononuclear  $\text{Fe}^{3+}$ -thiolate complexes, showing intermediate structures.

Fig. S10.

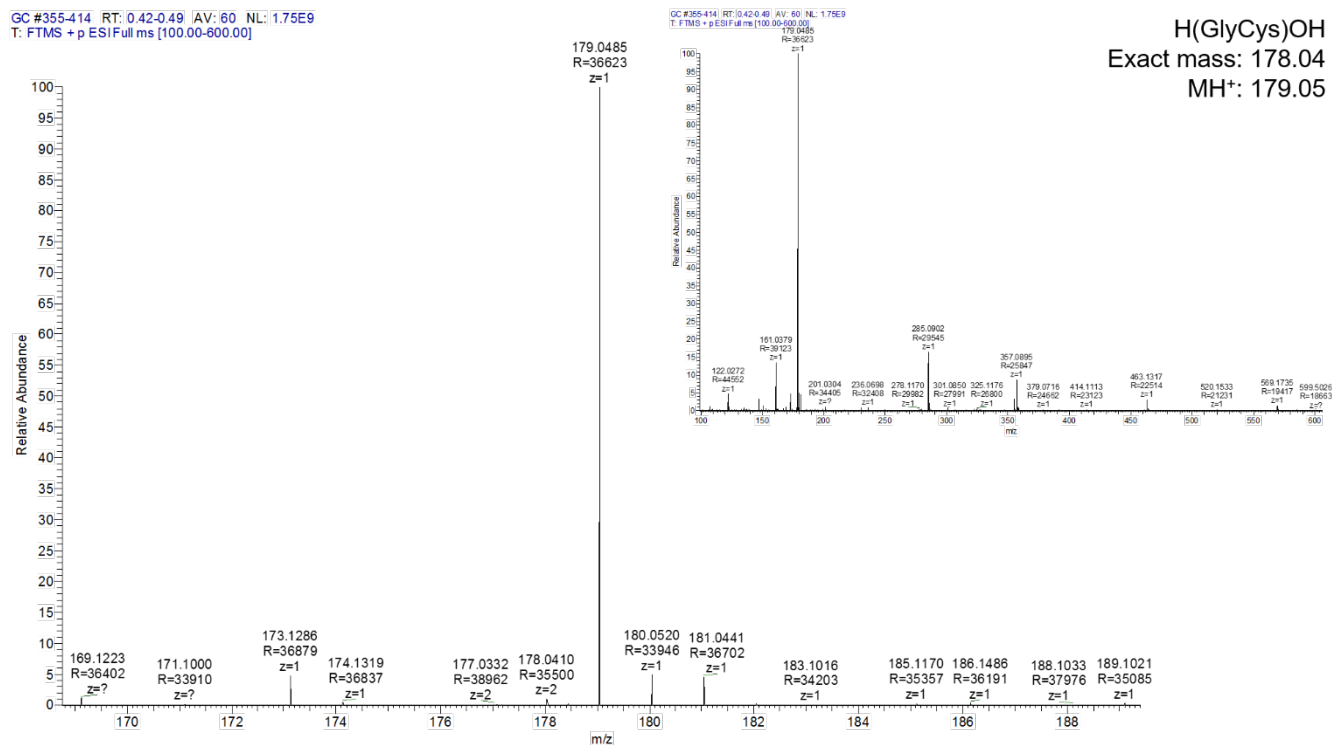


Fig. S10 | MS analysis of the peptide GC. The overall mass spectrum is shown as an inset.

Fig. S11.

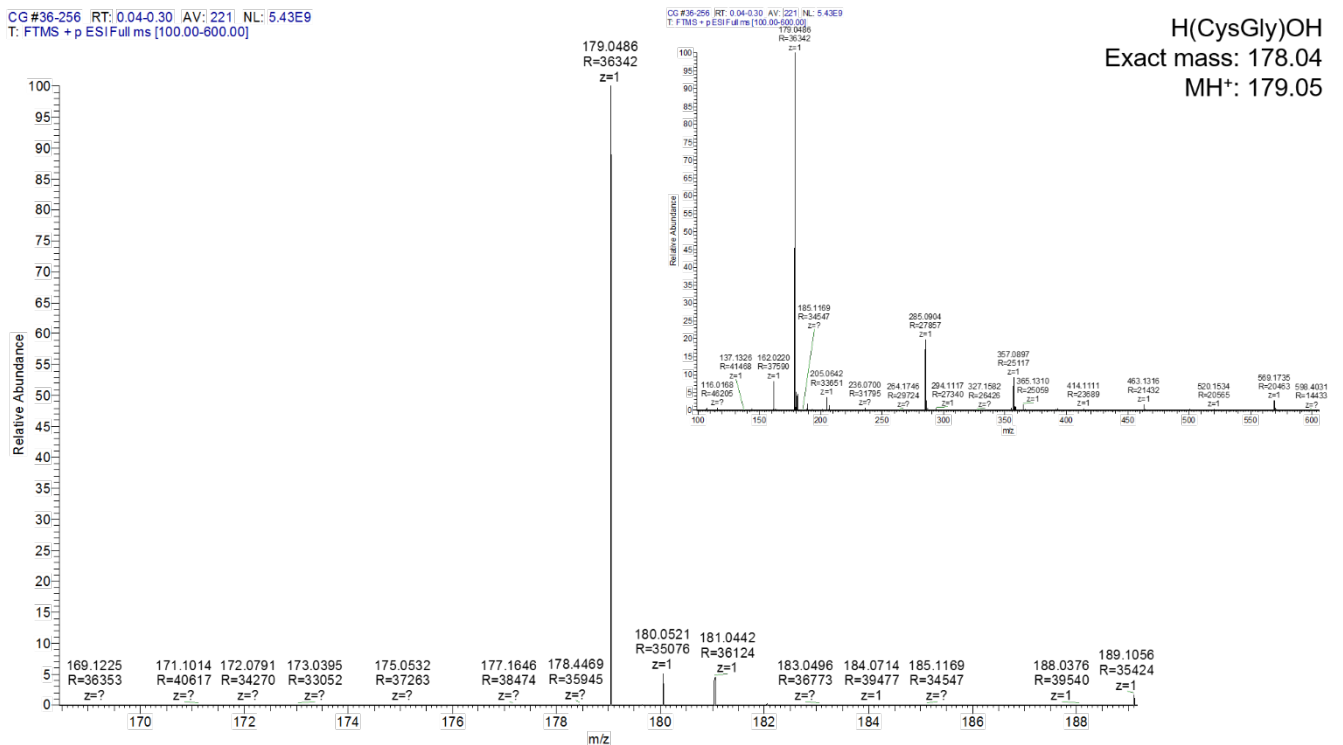


Fig. S11 | MS analysis of the peptide CG. The overall mass spectrum is shown as an inset.

Fig. S12.

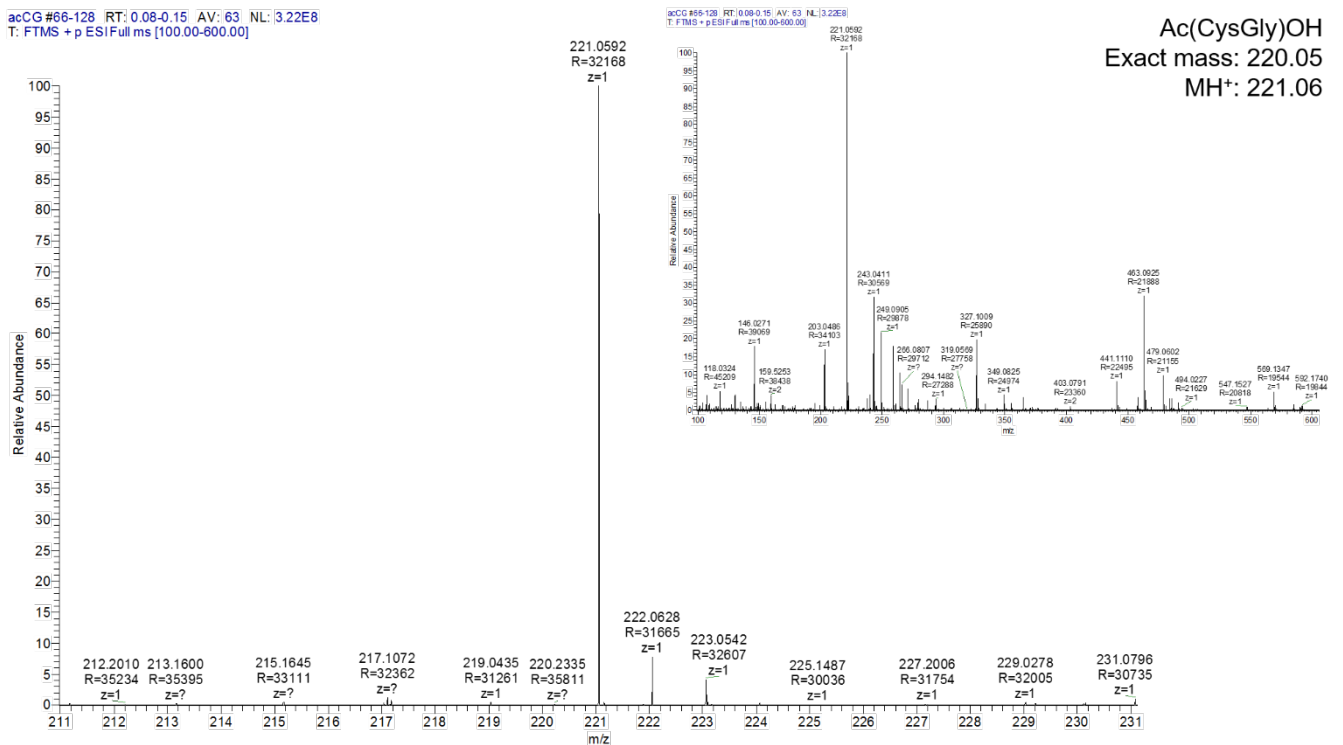


Fig. S12 | MS analysis of the peptide AcCG. The overall mass spectrum is shown as an inset.

Fig. S13.

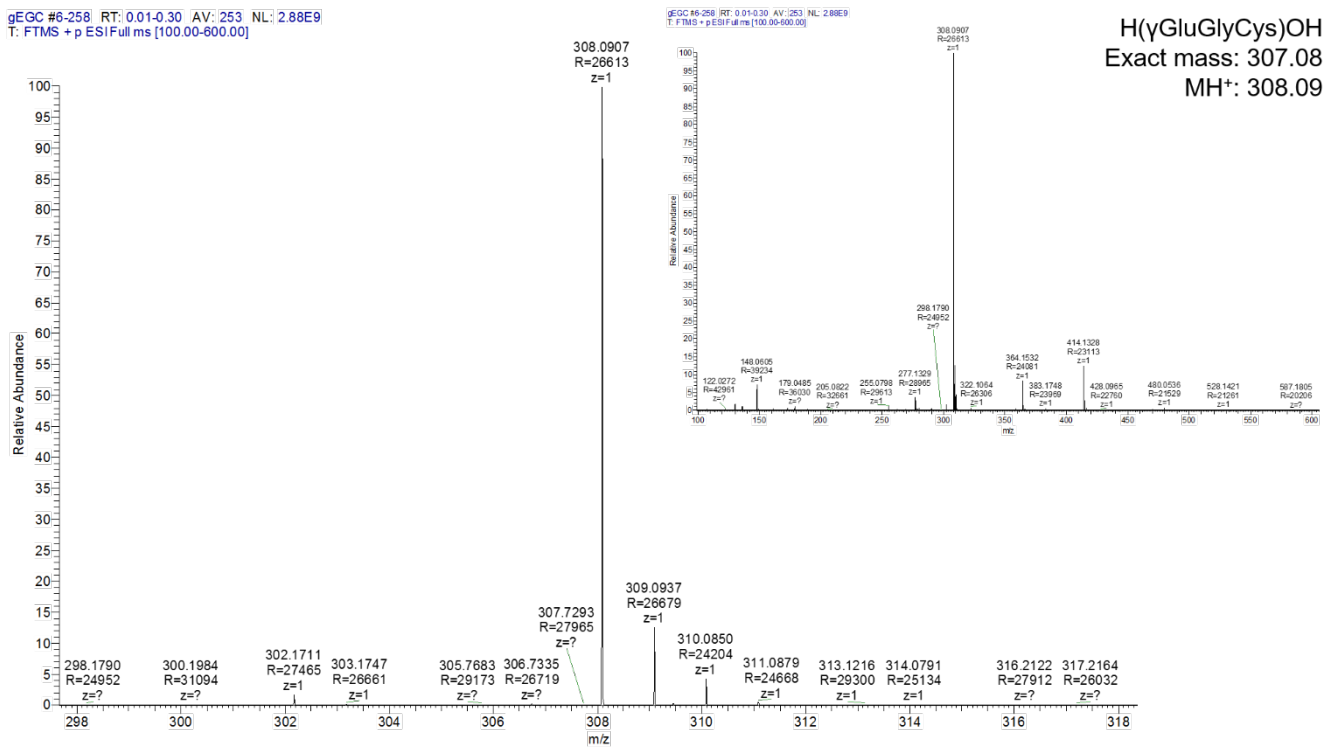


Fig. S13 | MS analysis of the peptide  $\gamma$ EGC. The overall mass spectrum is shown as an inset.

Fig. S14.

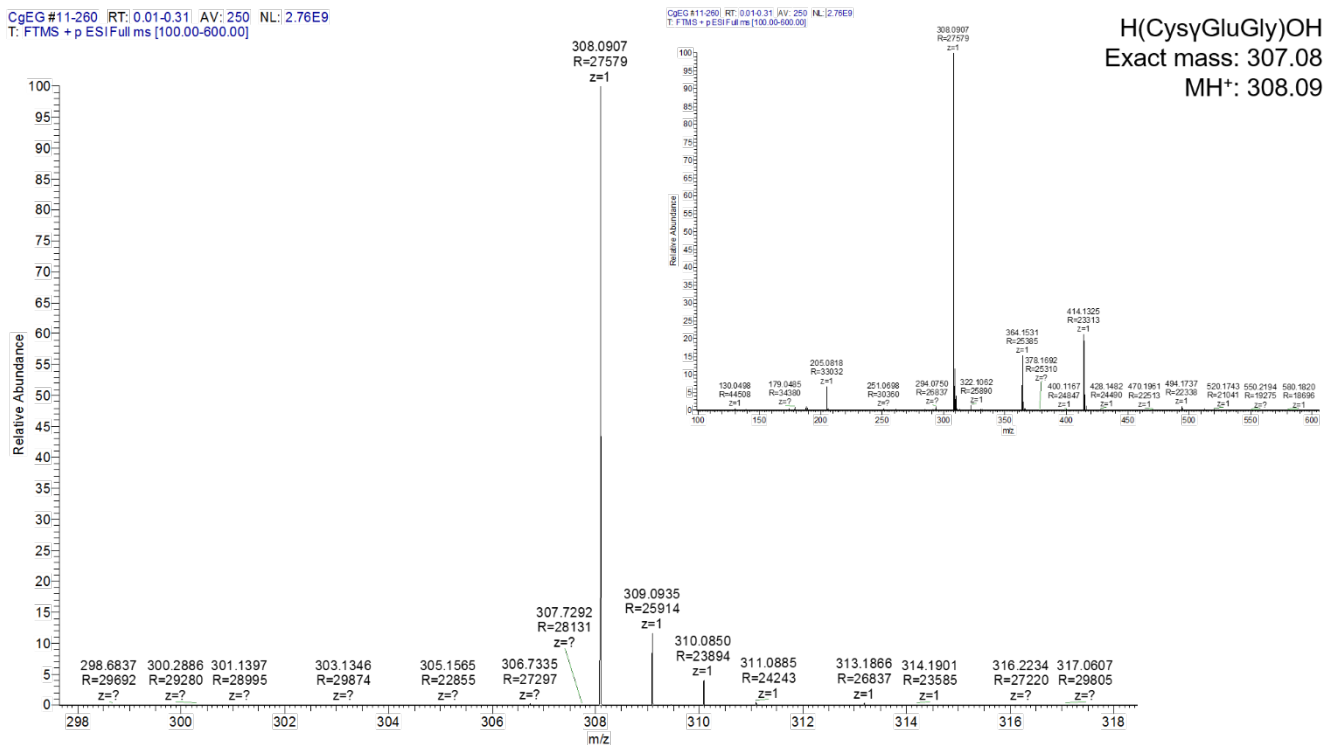


Fig. S14 | MS analysis of the peptide C $\gamma$ EG. The overall mass spectrum is shown as an inset.

Fig. S15.

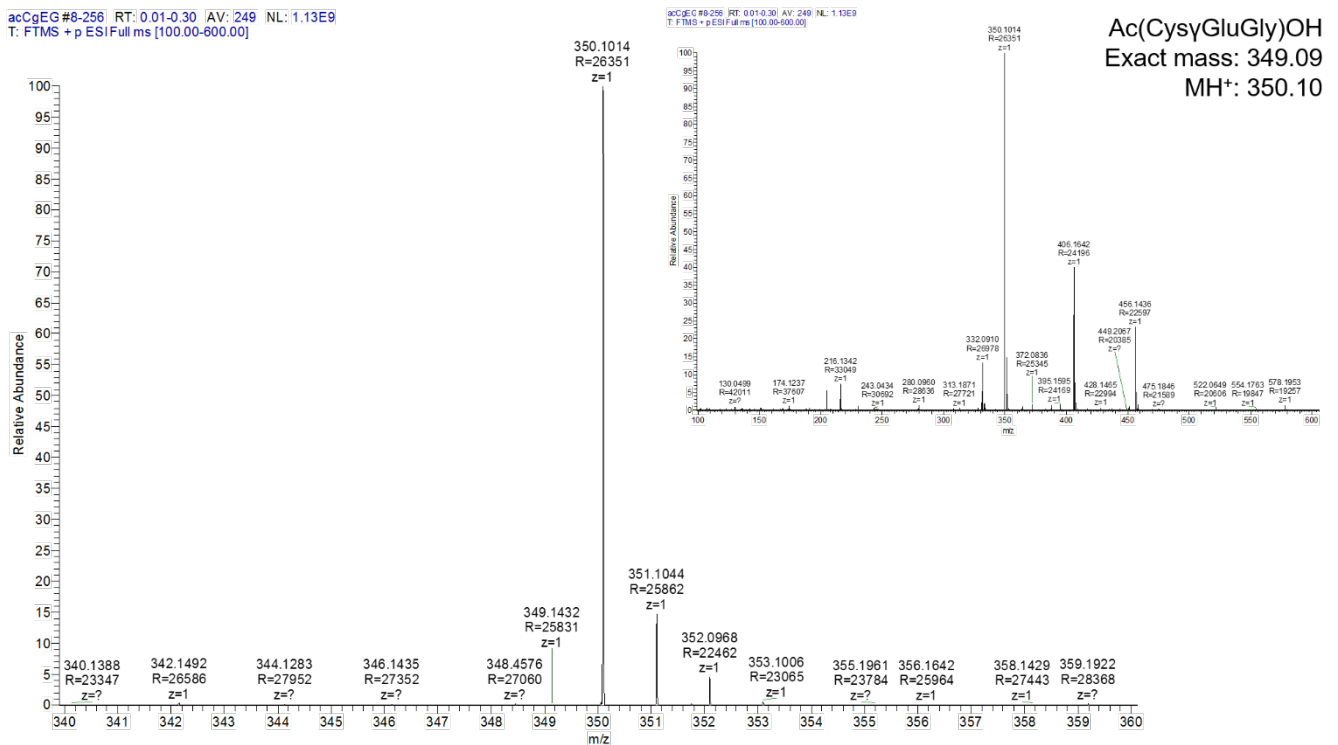


Fig. S15 | MS analysis of the peptide AcCγEG. The overall mass spectrum is shown as an inset.

Fig. S16.

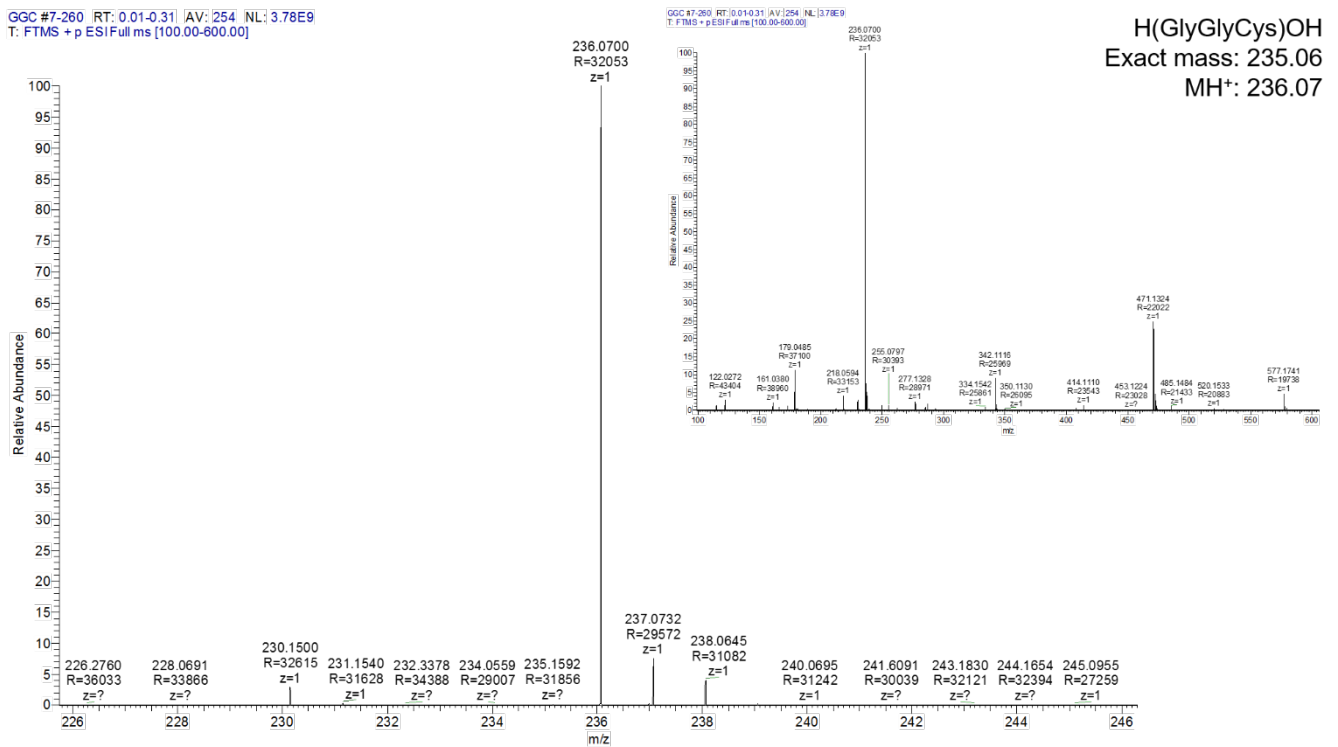


Fig. S16 | MS analysis of the peptide GGC. The overall mass spectrum is shown as an inset.

Fig. S17.

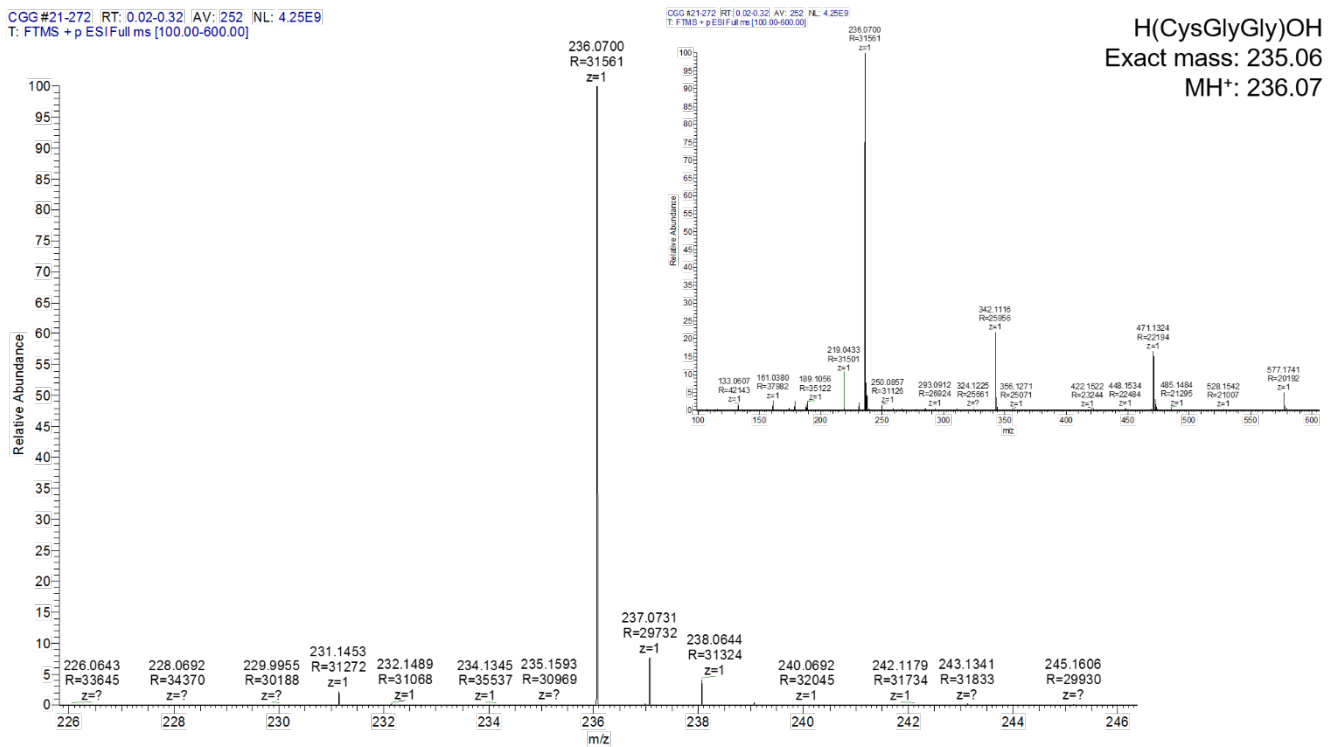


Fig. S17 | MS analysis of the peptide CGG. The overall mass spectrum is shown as an inset.

Fig. S18.

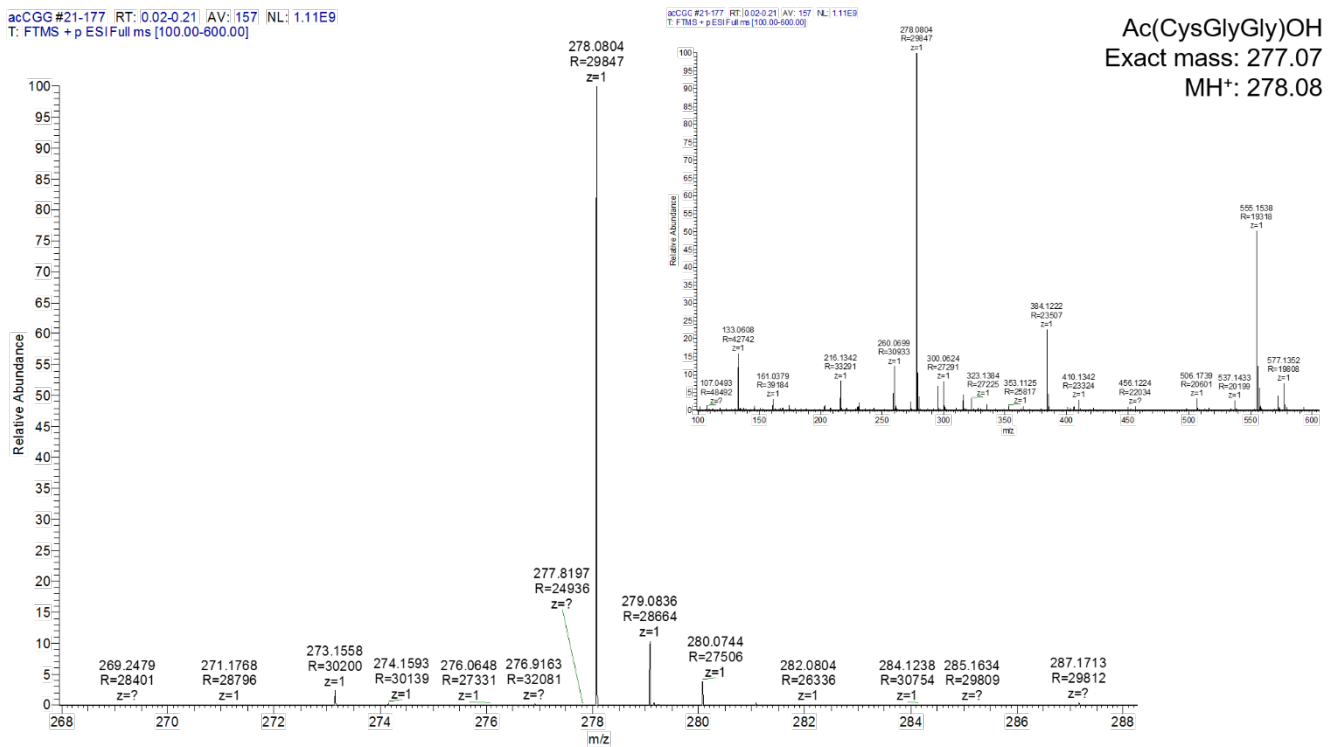


Fig. S18 | MS analysis of the peptide AcCGG. The overall mass spectrum is shown as an inset.

**Fig. S19.**

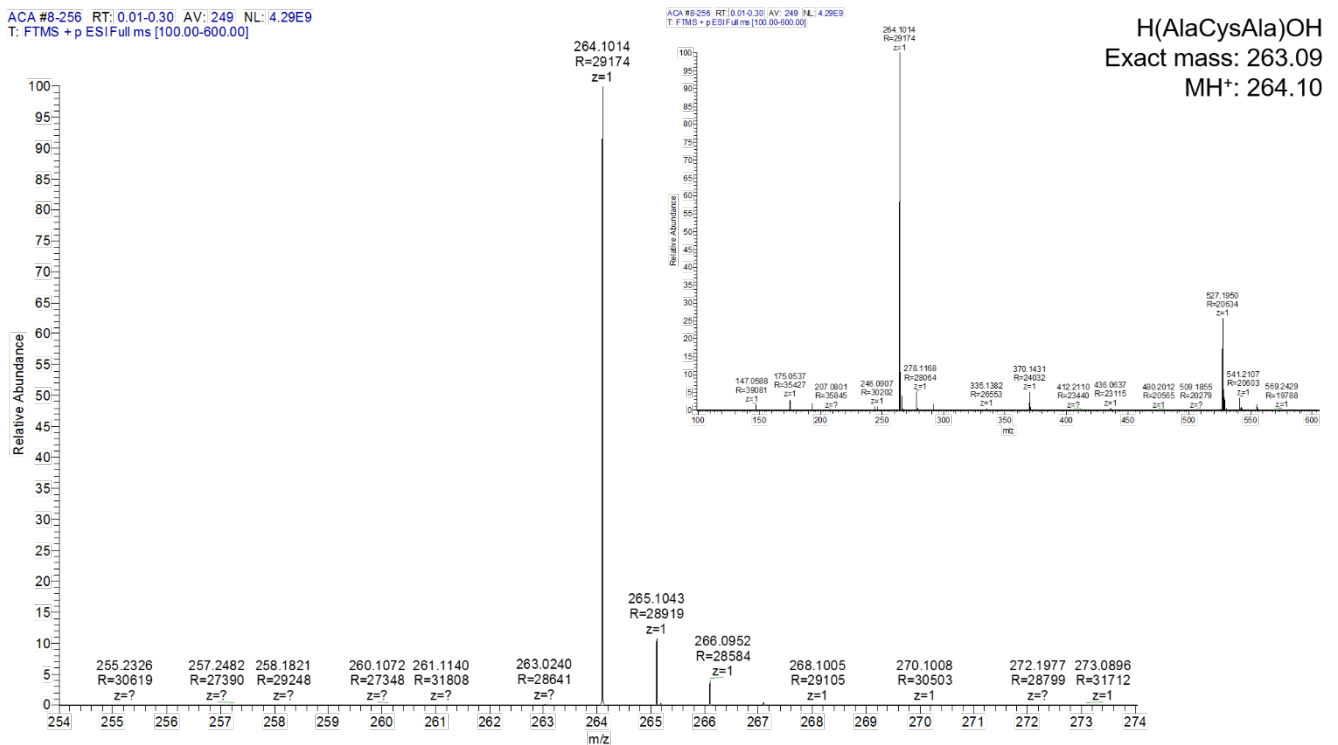


Fig. S19 | MS analysis of the peptide ACA. The overall mass spectrum is shown as an inset.

Fig. S20.

ACT#13-253 RT: 0.01-0.30 AV: 241 NL: 249E9  
T: FTMS + p ESI Full ms [100.00-800.00]

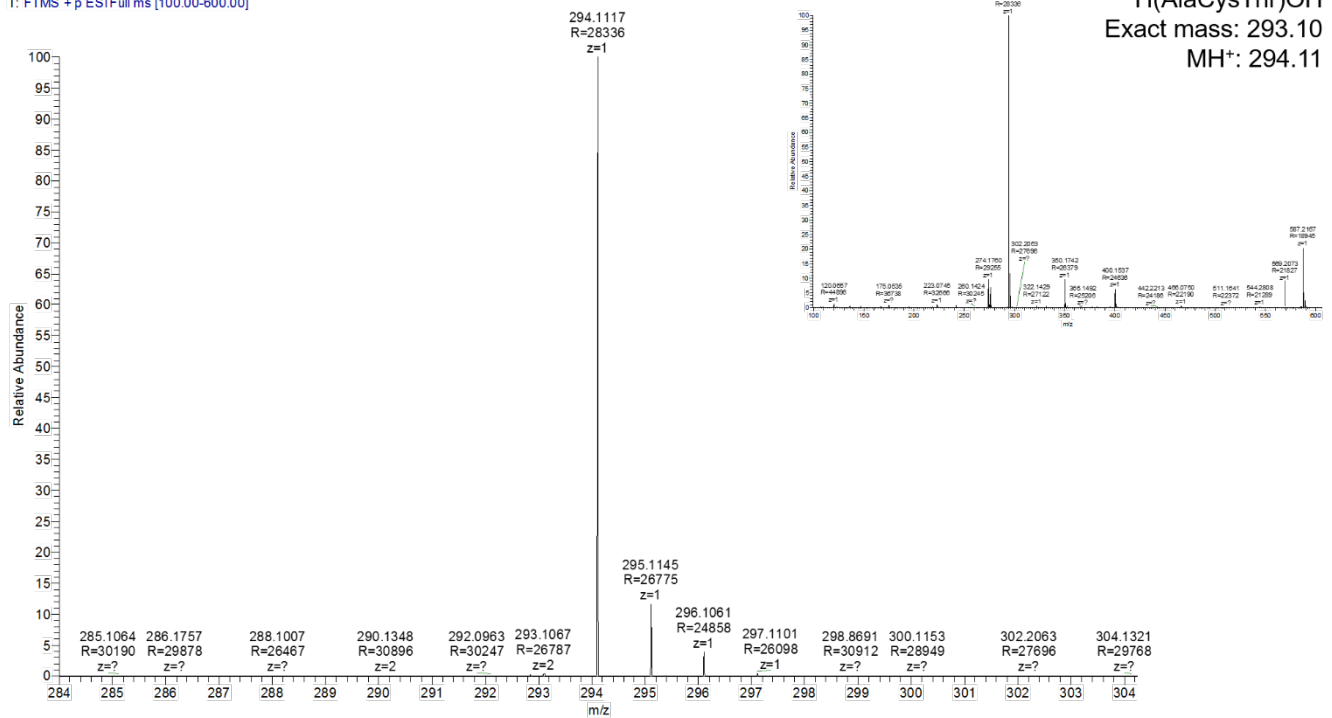


Fig. S20 | MS analysis of the peptide ACT. The overall mass spectrum is shown as an inset.

Fig. S21.

DCG #7-258 RT: 0.01-0.30 AV: 252 NL: 2.18E9  
T: FTMS + p ESI Full ms [100.00-800.00]

DCG #7-258 RT: 0.01-0.30 AV: 252 NL: 2.18E9  
T: FTMS + p ESI Full ms [100.00-800.00]

H(AspCysGly)OH  
Exact mass: 293.08  
MH<sup>+</sup>: 294.08

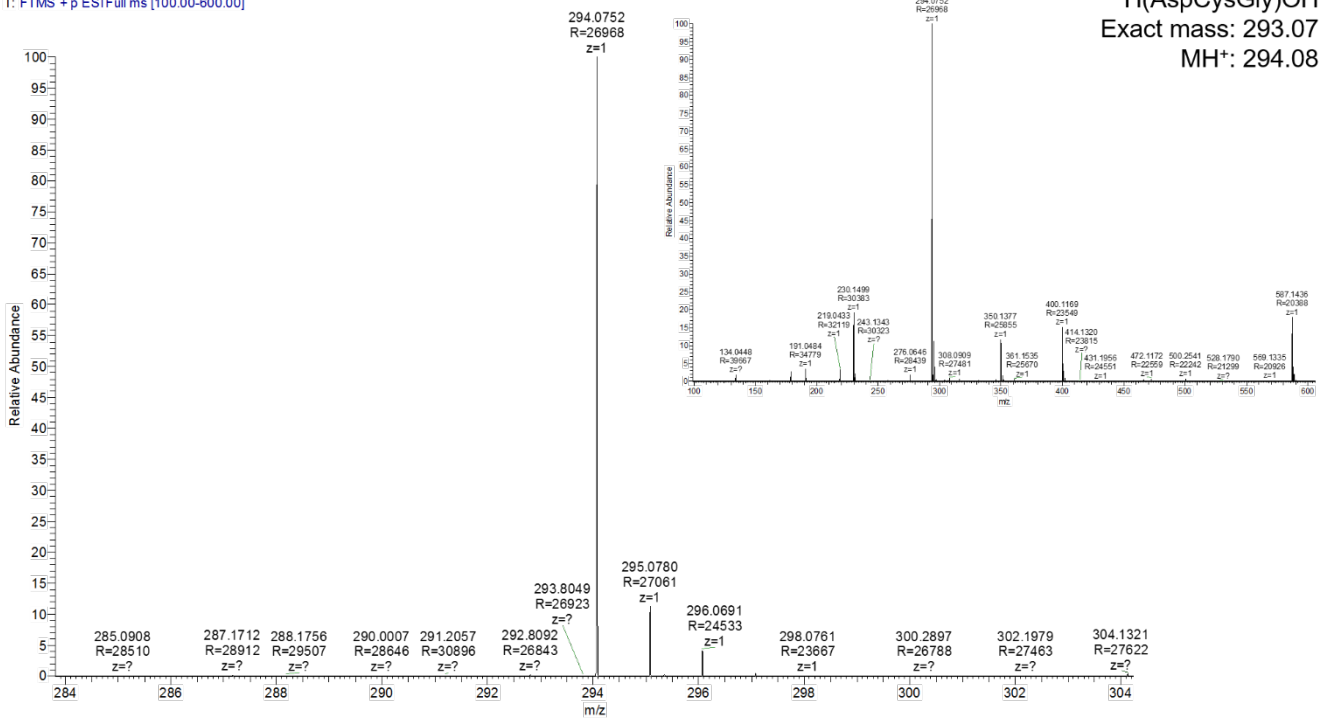


Fig. S21 | MS analysis of the peptide DCG. The overall mass spectrum is shown as an inset.

Fig. S22.

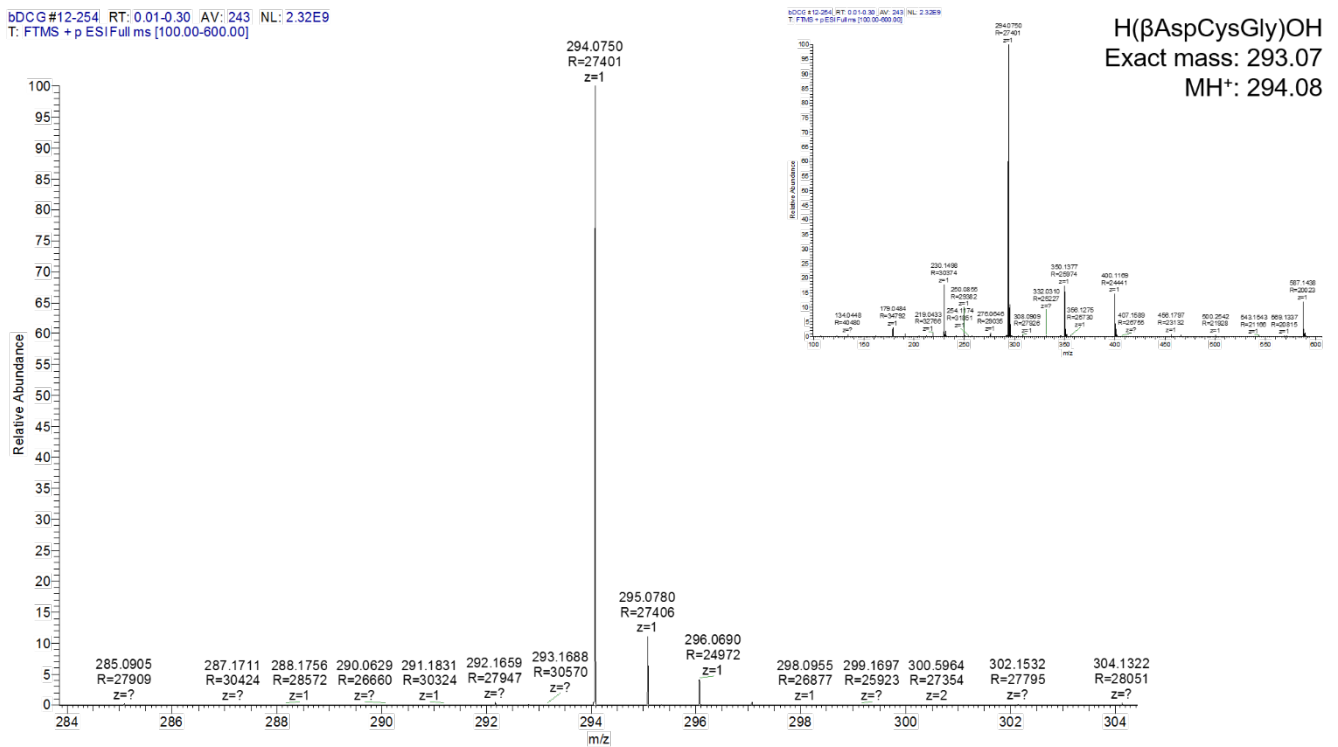


Fig. S22 | MS analysis of the peptide  $\beta$ DCG. The overall mass spectrum is shown as an inset.

Fig. S23.

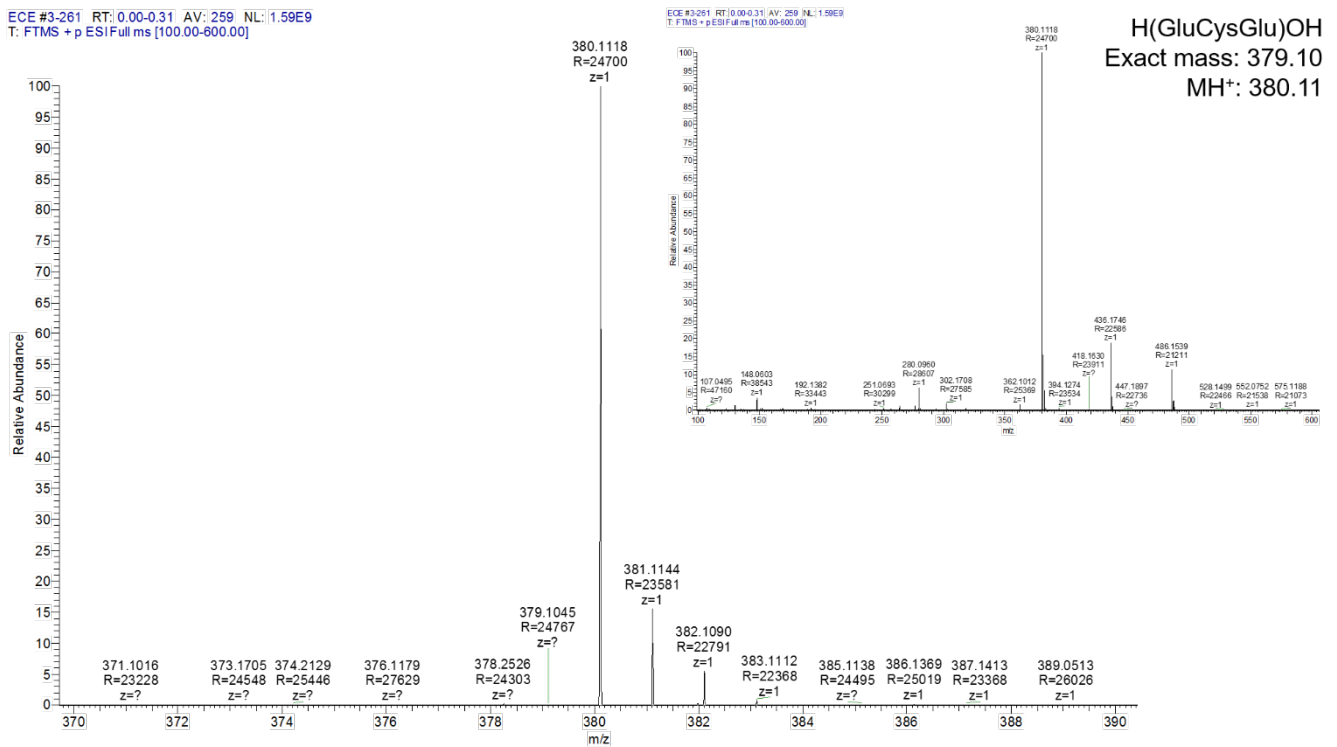


Fig. S23 | MS analysis of the peptide ECE. The overall mass spectrum is shown as an inset.

Fig. S24.

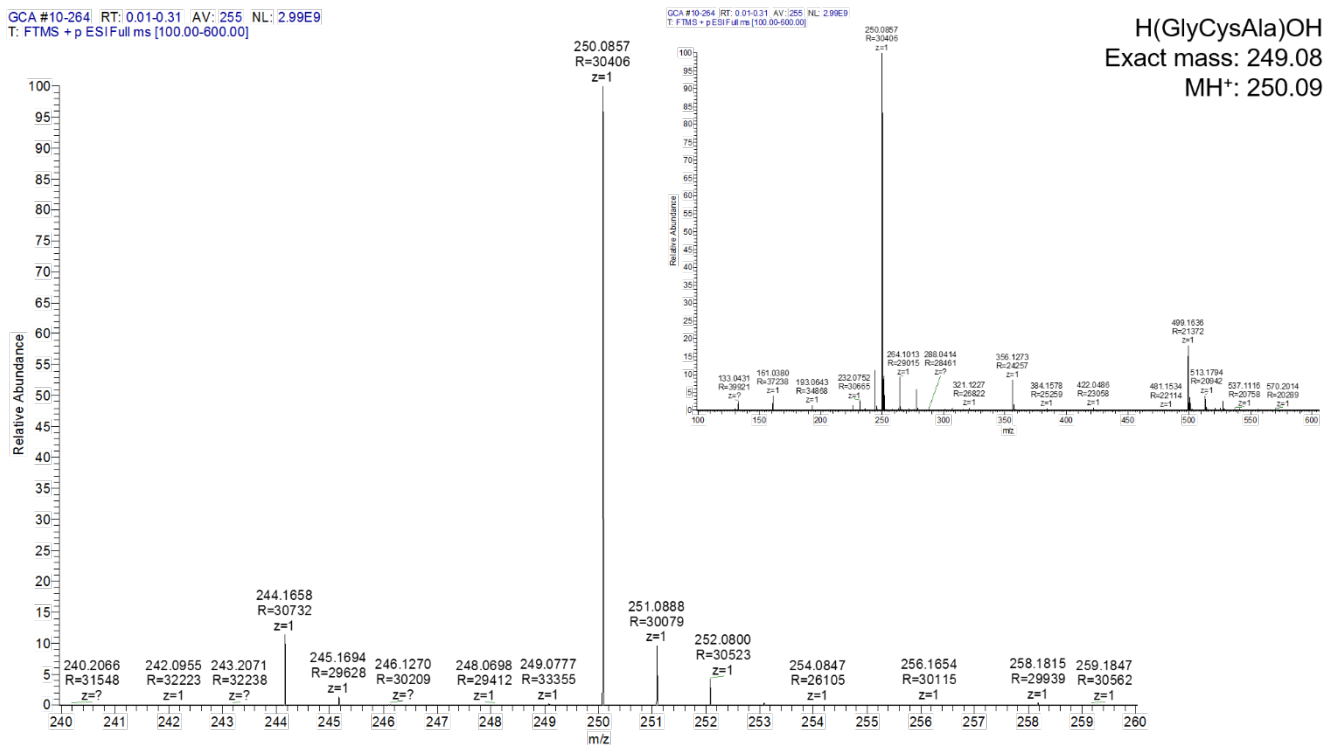


Fig. S24 | MS analysis of the peptide GCA. The overall mass spectrum is shown as an inset.

Fig. S25.

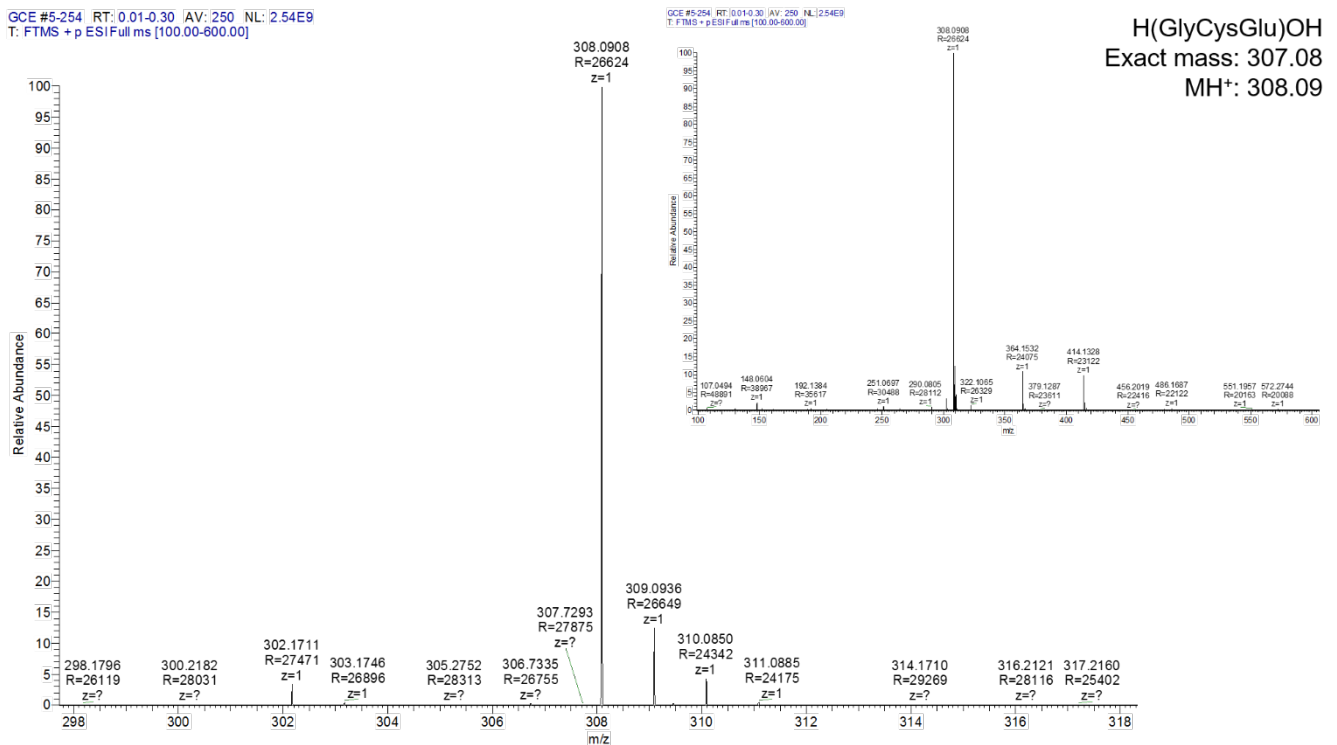


Fig. S25 | MS analysis of the peptide GCE. The overall mass spectrum is shown as an inset.

Fig. S26.

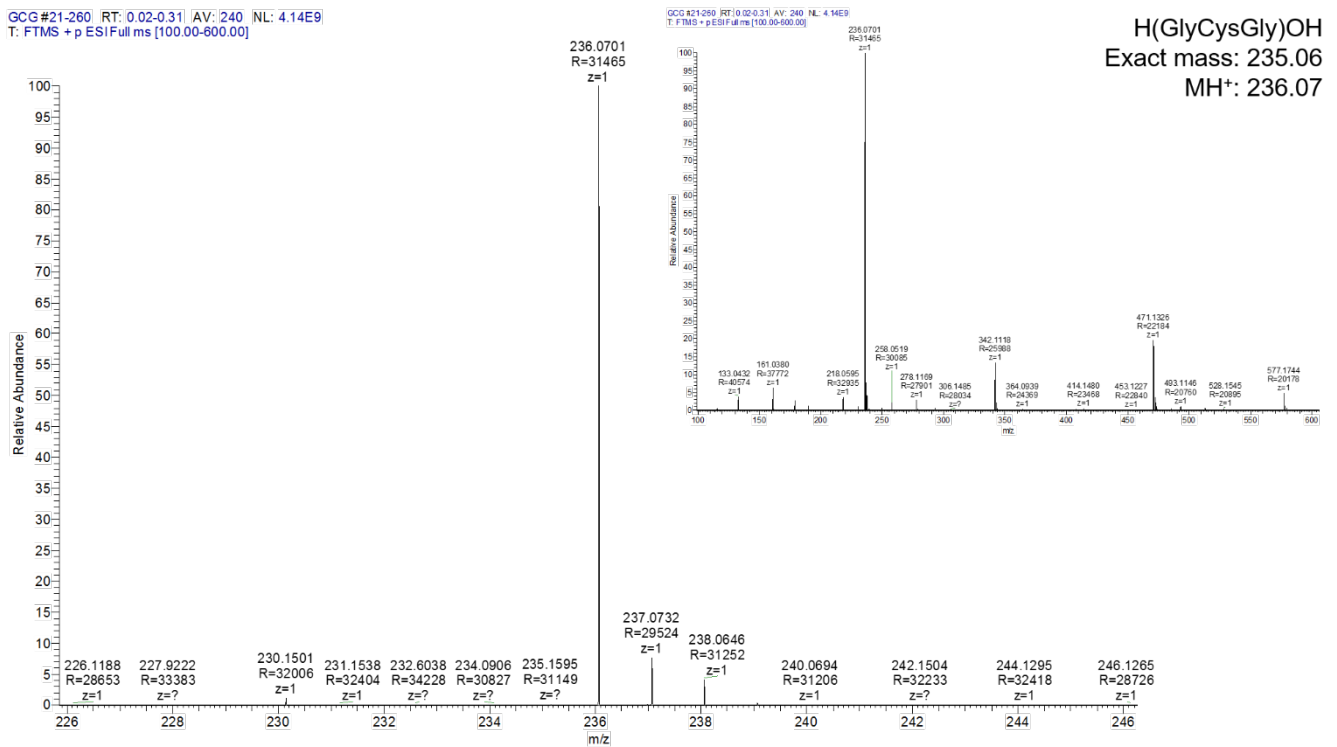


Fig. S26 | MS analysis of the peptide GCG. The overall mass spectrum is shown as an inset.

Fig. S27.

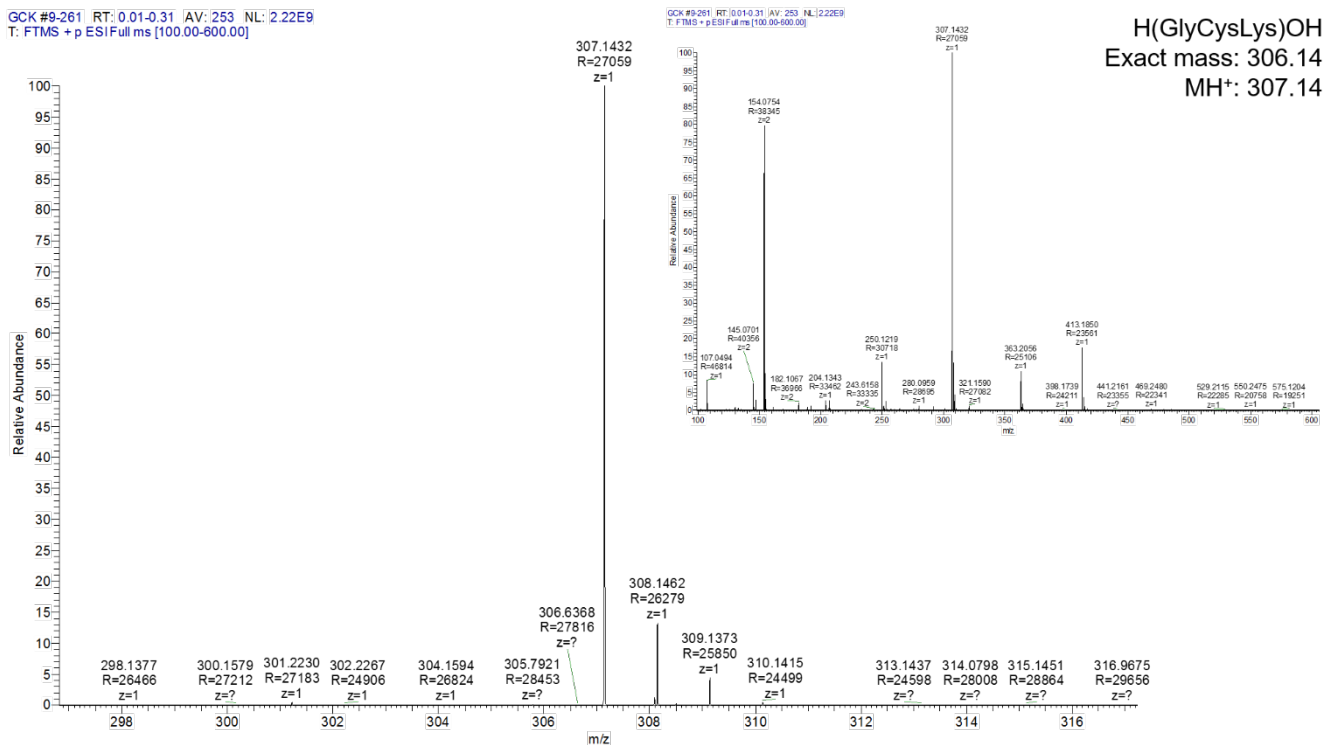


Fig. S27 | MS analysis of the peptide GCK. The overall mass spectrum is shown as an inset.

Fig. S28.

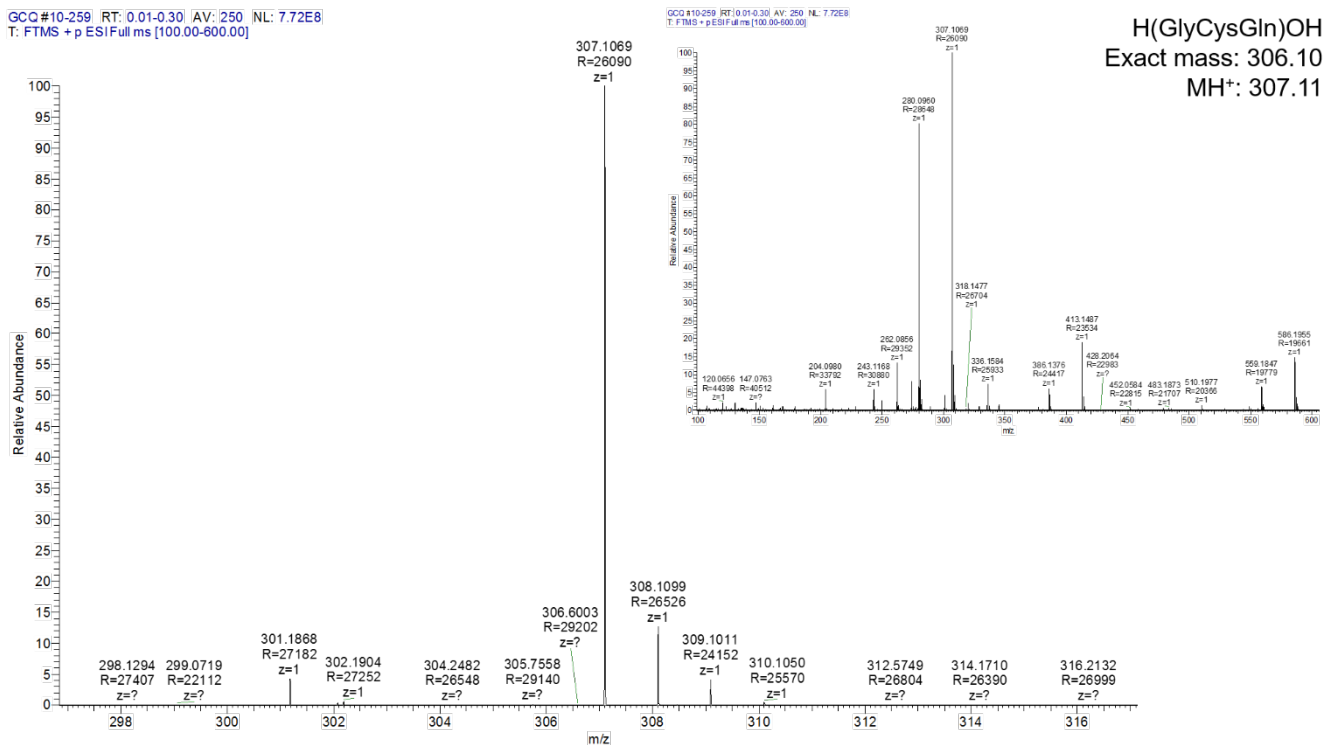


Fig. S28 | MS analysis of the peptide GCC. The overall mass spectrum is shown as an inset.

Fig. S29.

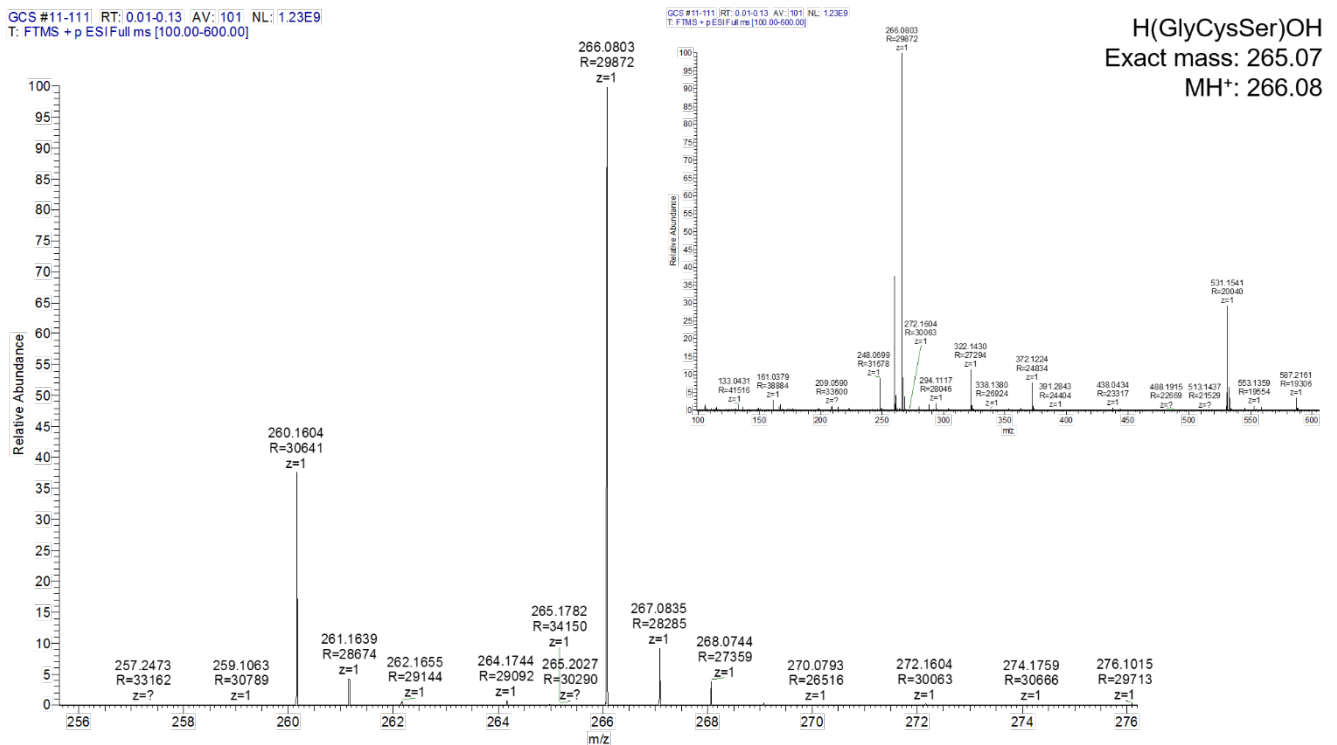


Fig. S29 | MS analysis of the peptide GCS. The overall mass spectrum is shown as an inset.

Fig. S30.

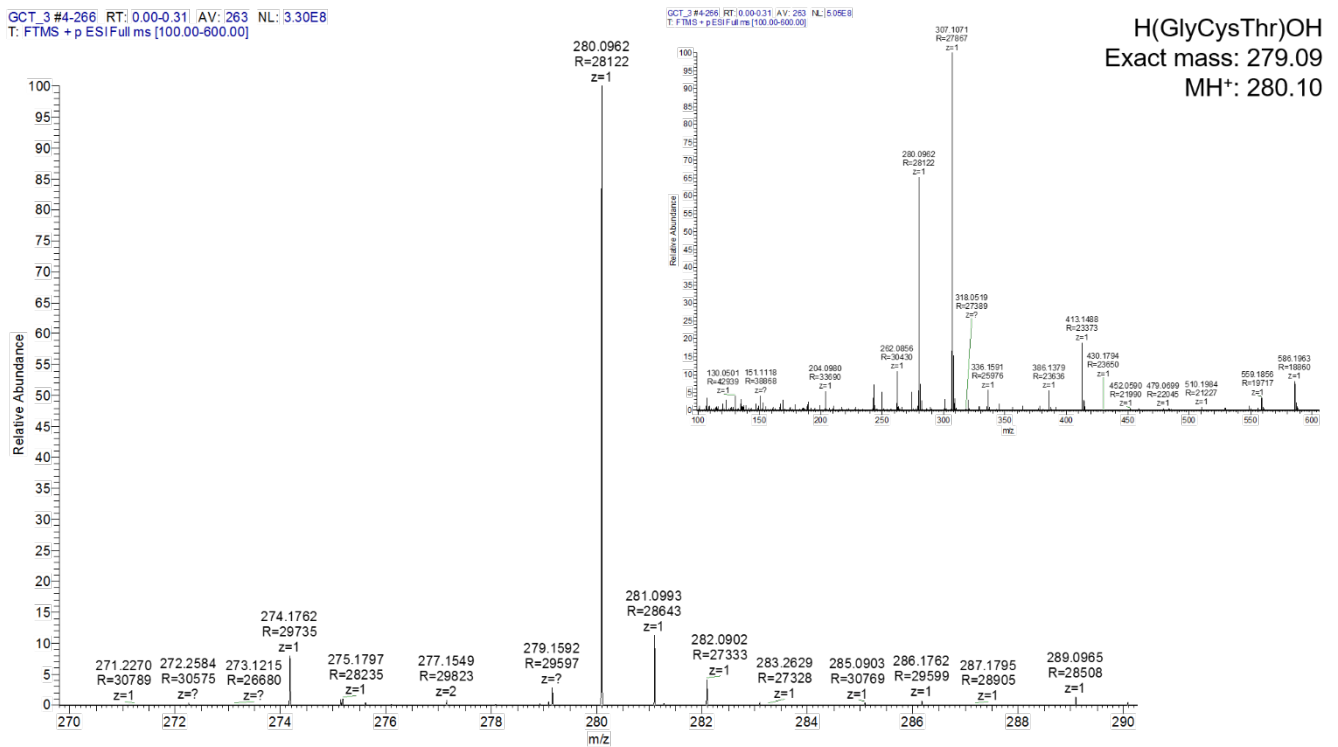


Fig. S30 | MS analysis of the peptide GCT. The overall mass spectrum is shown as an inset.



Fig. S32.

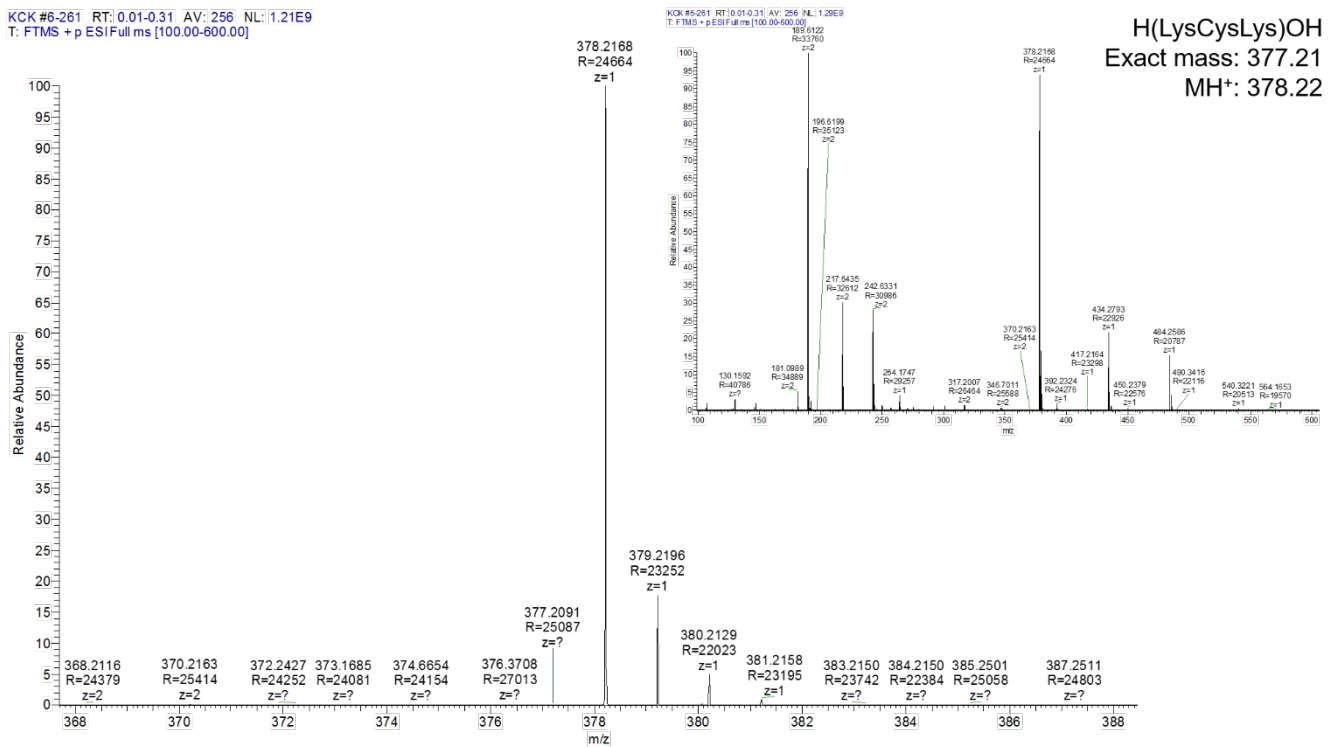


Fig. S32 | MS analysis of the peptide KCK. The overall mass spectrum is shown as an inset.

Fig. S33.

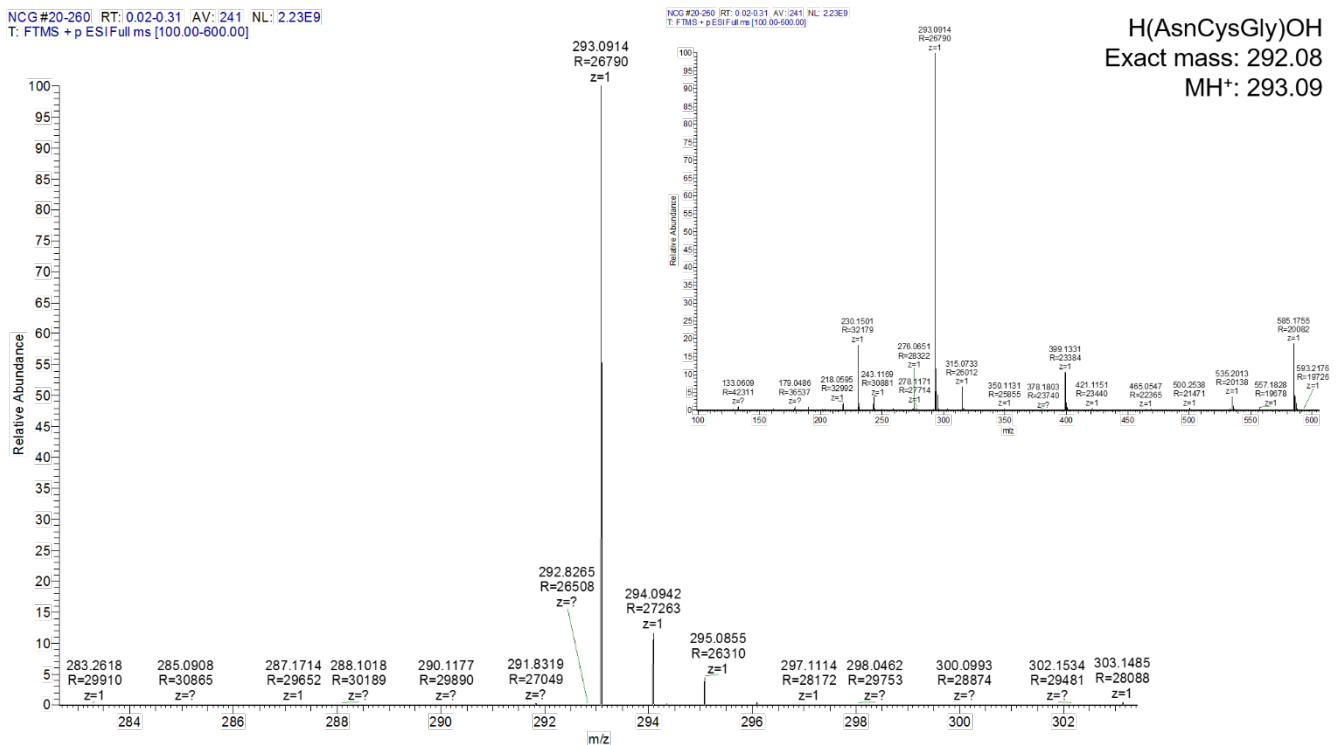


Fig. S33 | MS analysis of the peptide NCG. The overall mass spectrum is shown as an inset.

Fig. S34.

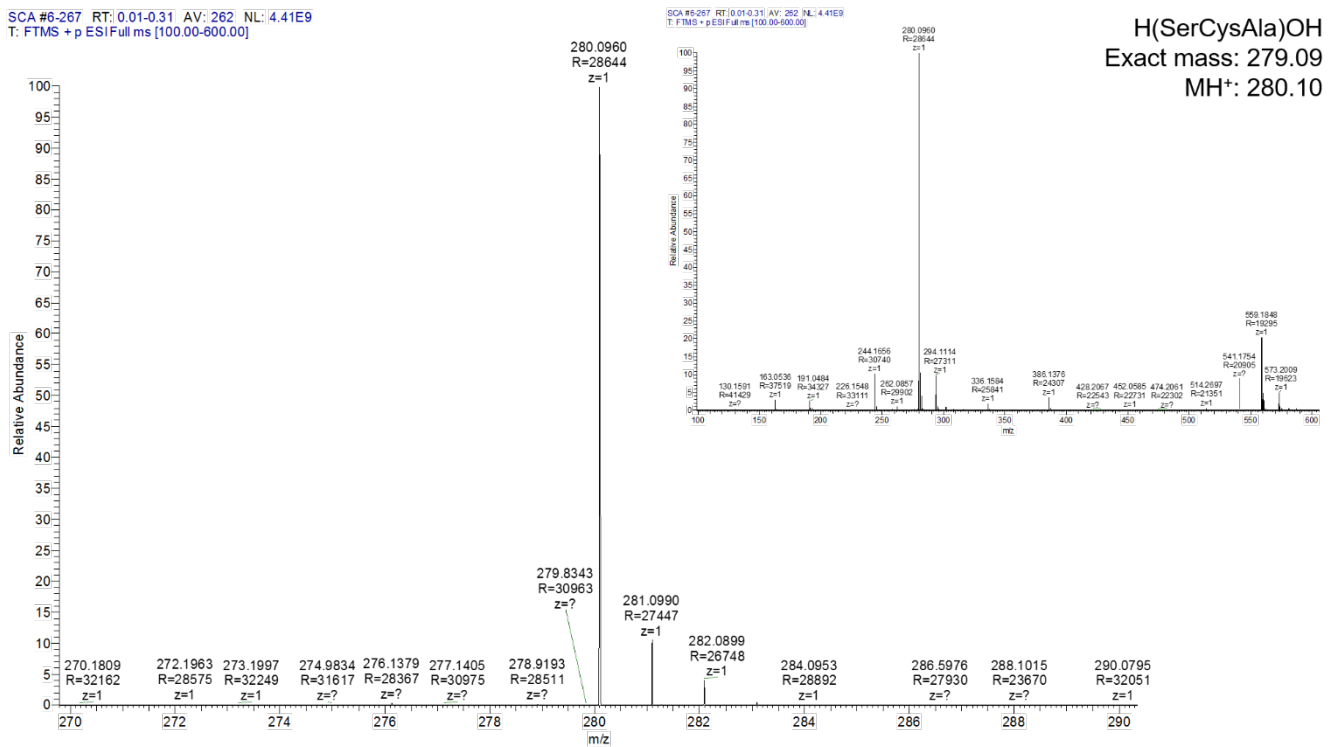


Fig. S34 | MS analysis of the peptide SCA. The overall mass spectrum is shown as an inset.

Fig. S35.

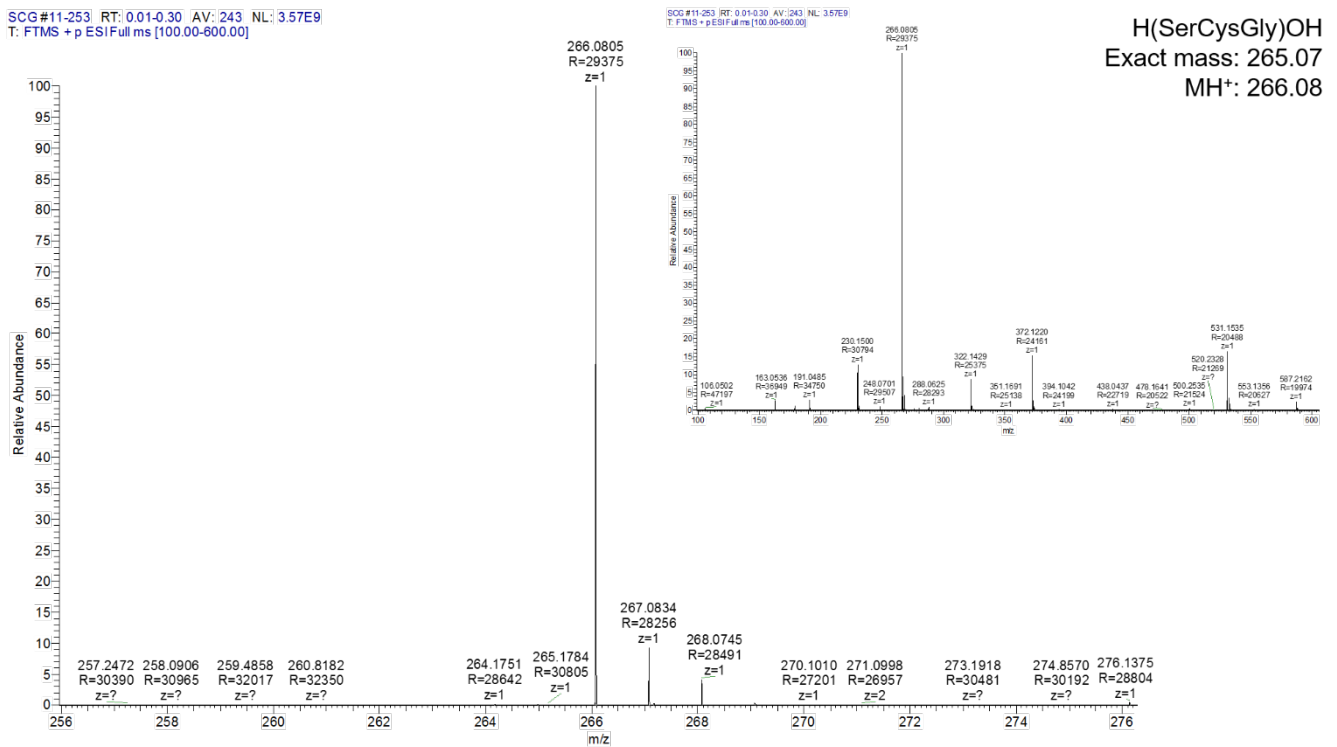


Fig. S35 | MS analysis of the peptide SCG. The overall mass spectrum is shown as an inset.

Fig. S36.

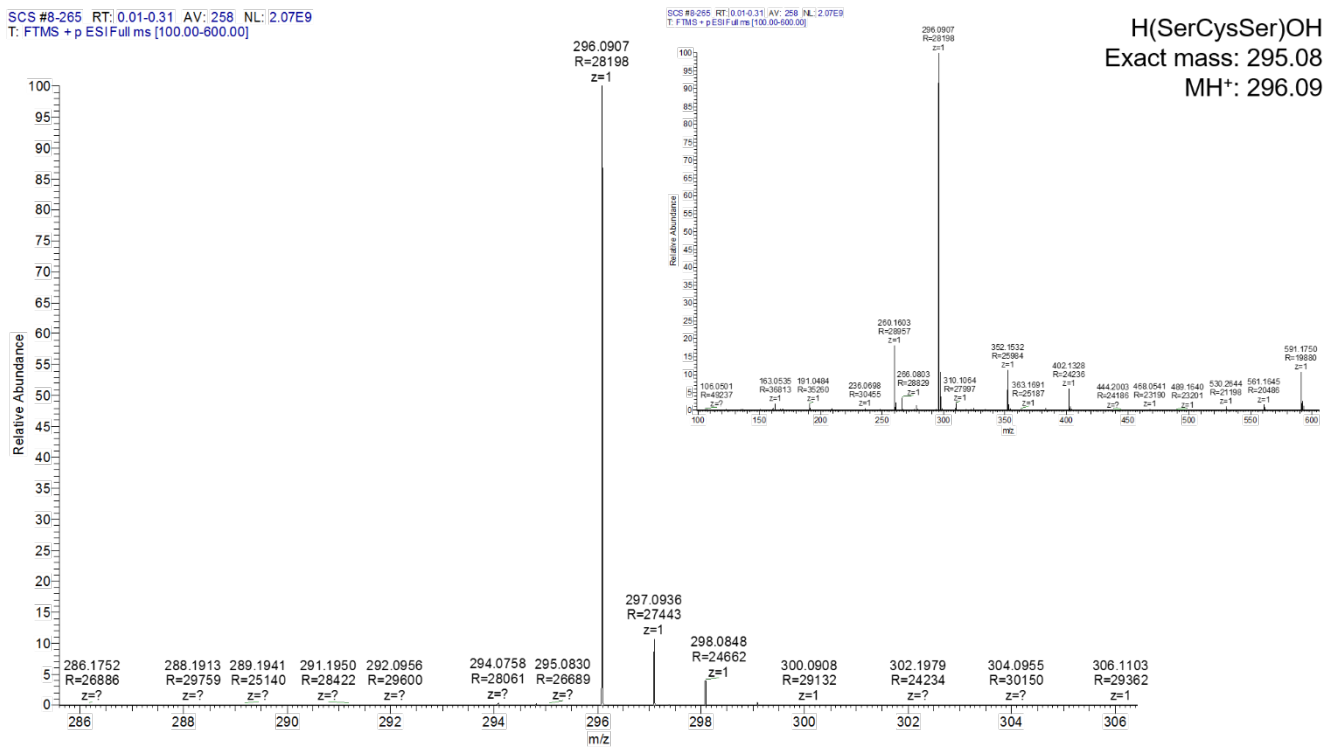


Fig. S36 | MS analysis of the peptide SCS. The overall mass spectrum is shown as an inset.

Fig. S37.

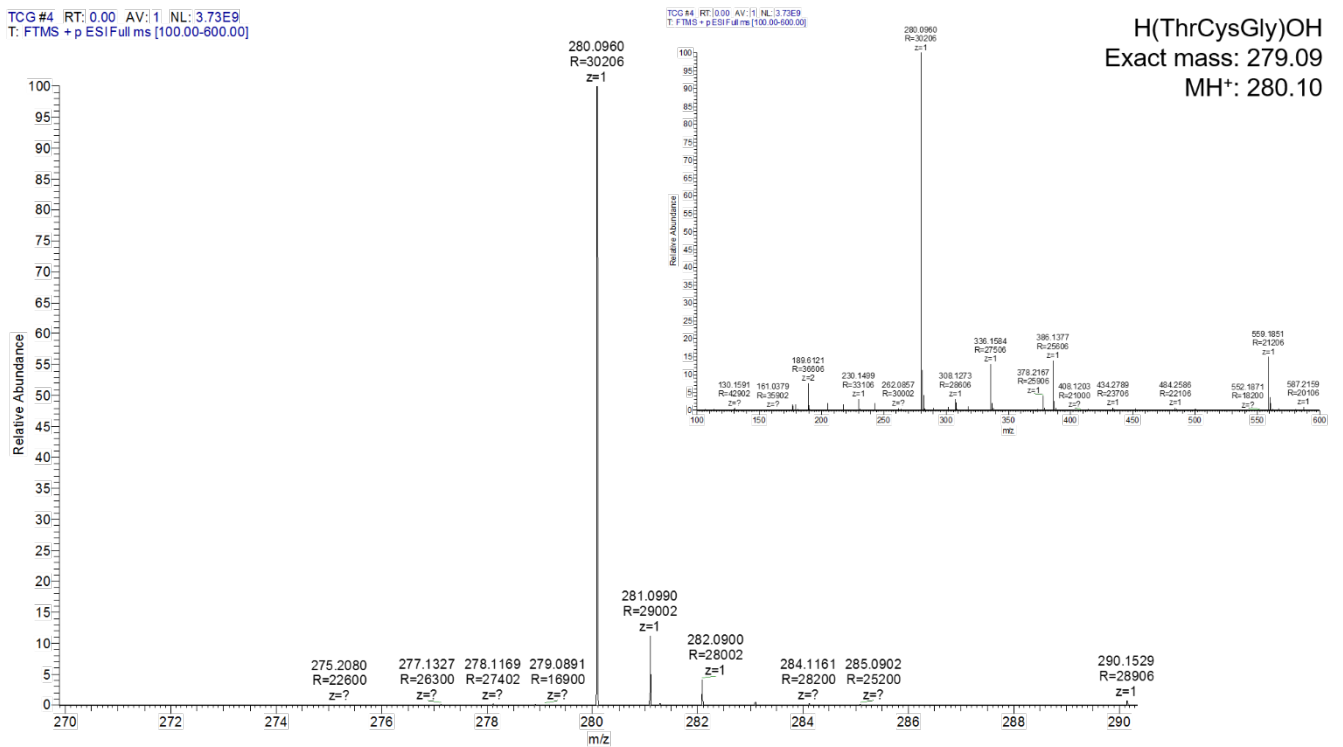


Fig. S37 | MS analysis of the peptide TCG. The overall mass spectrum is shown as an inset.

Fig. S38.

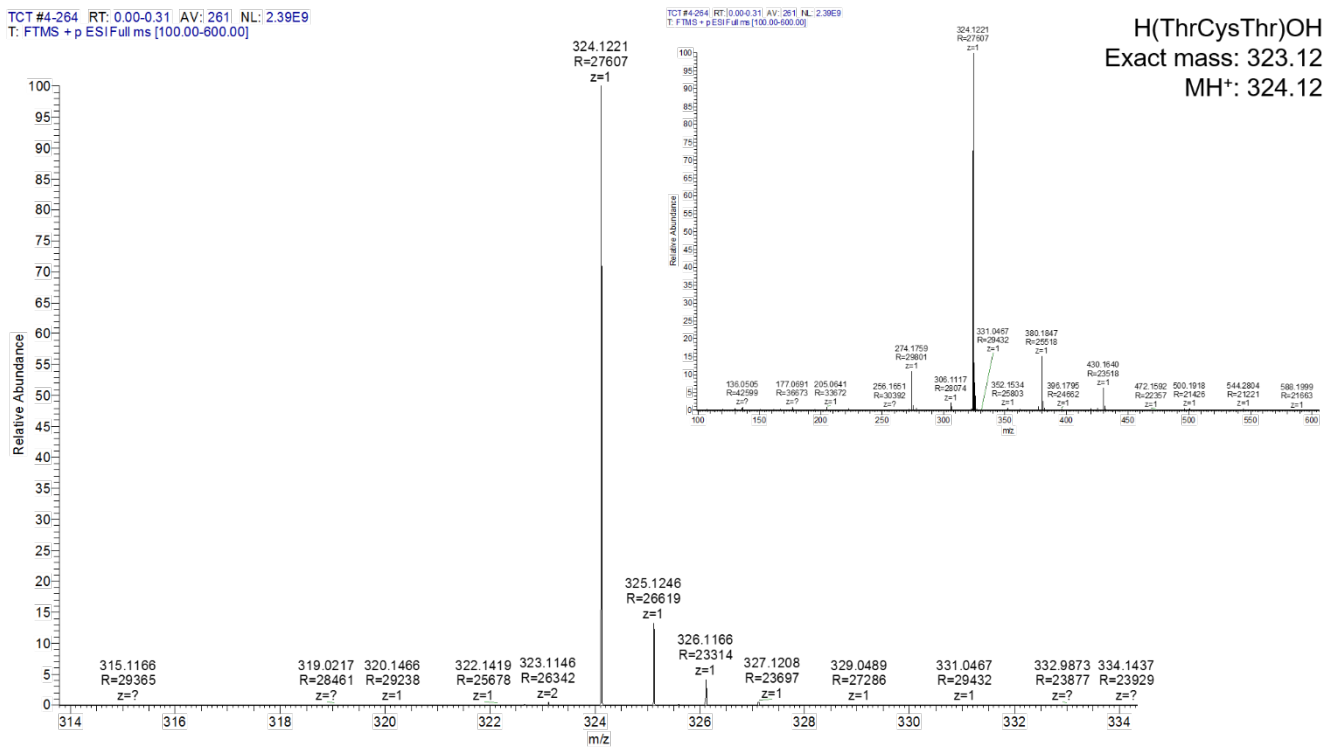


Fig. S38 | MS analysis of the peptide TCT. The overall mass spectrum is shown as an inset.

Fig. S39.

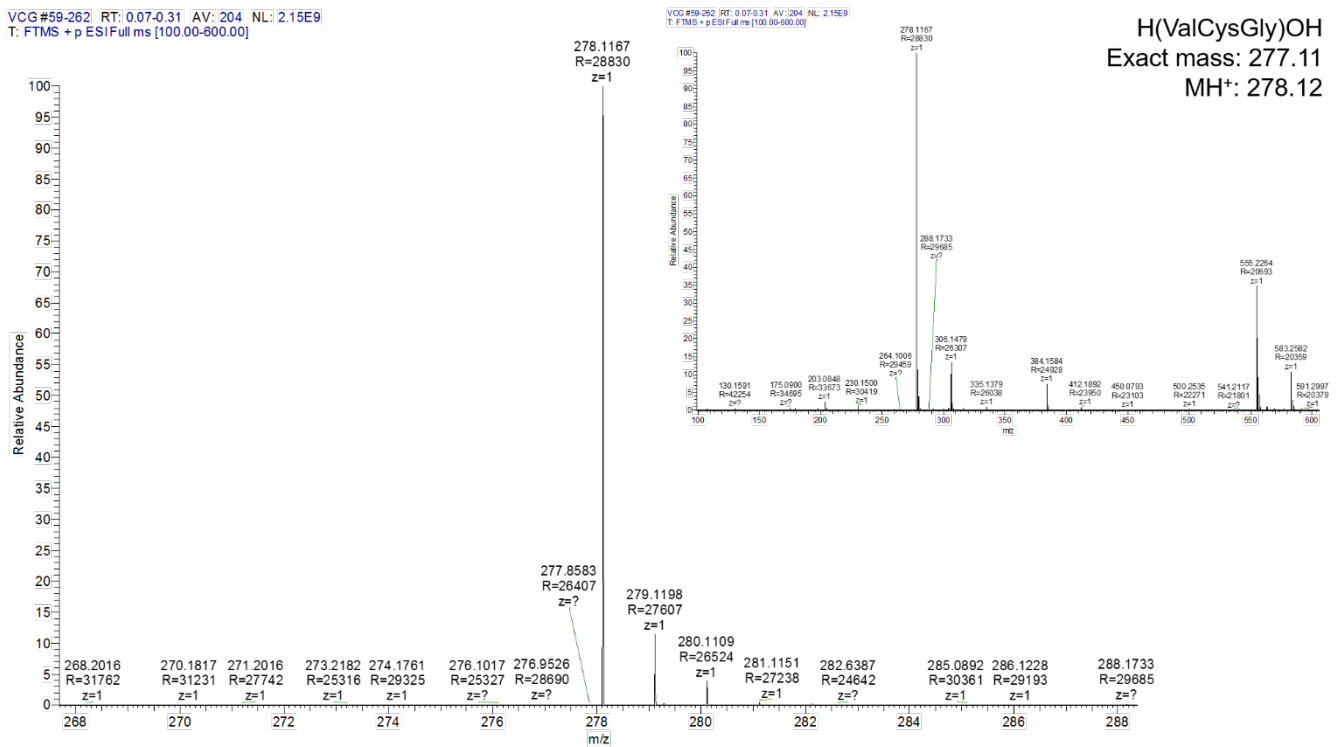


Fig. S39 | MS analysis of the peptide VCG. The overall mass spectrum is shown as an inset.

Fig. S40.

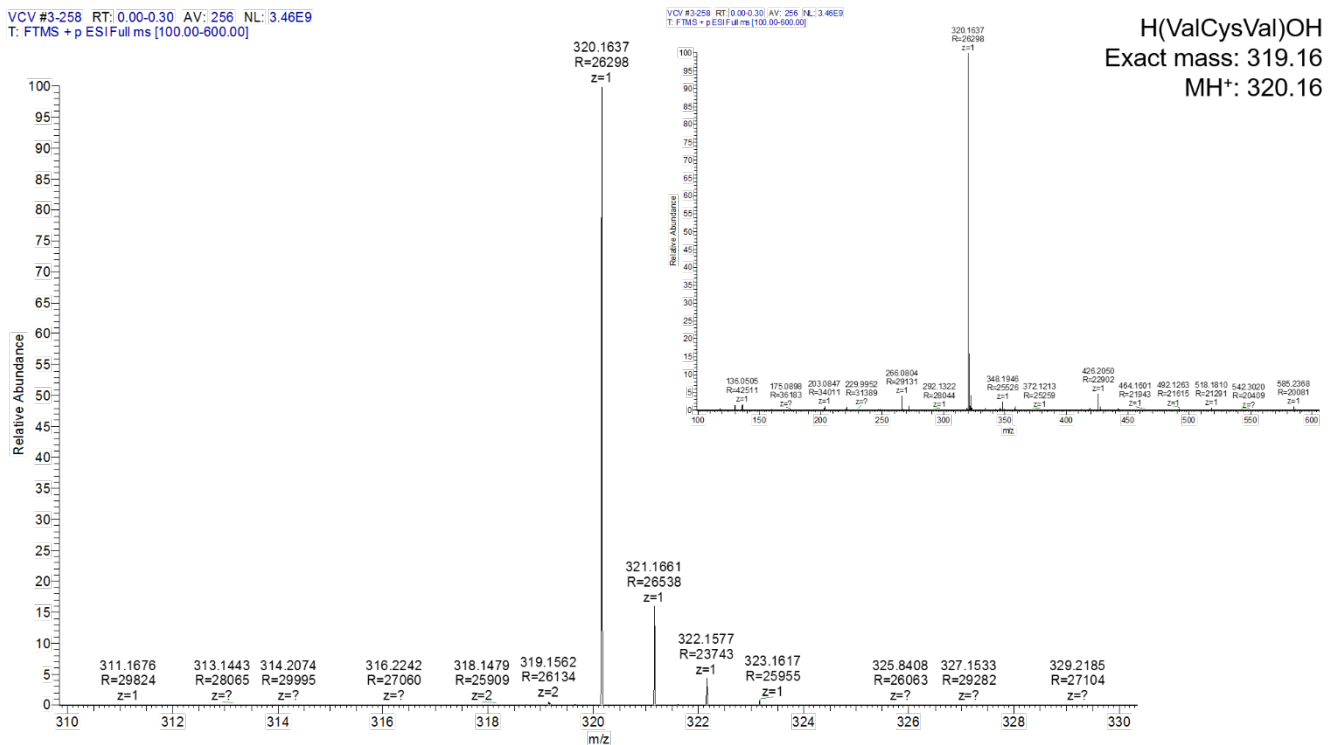


Fig. S40 | MS analysis of the peptide VCV. The overall mass spectrum is shown as an inset.

**Fig. S41.**

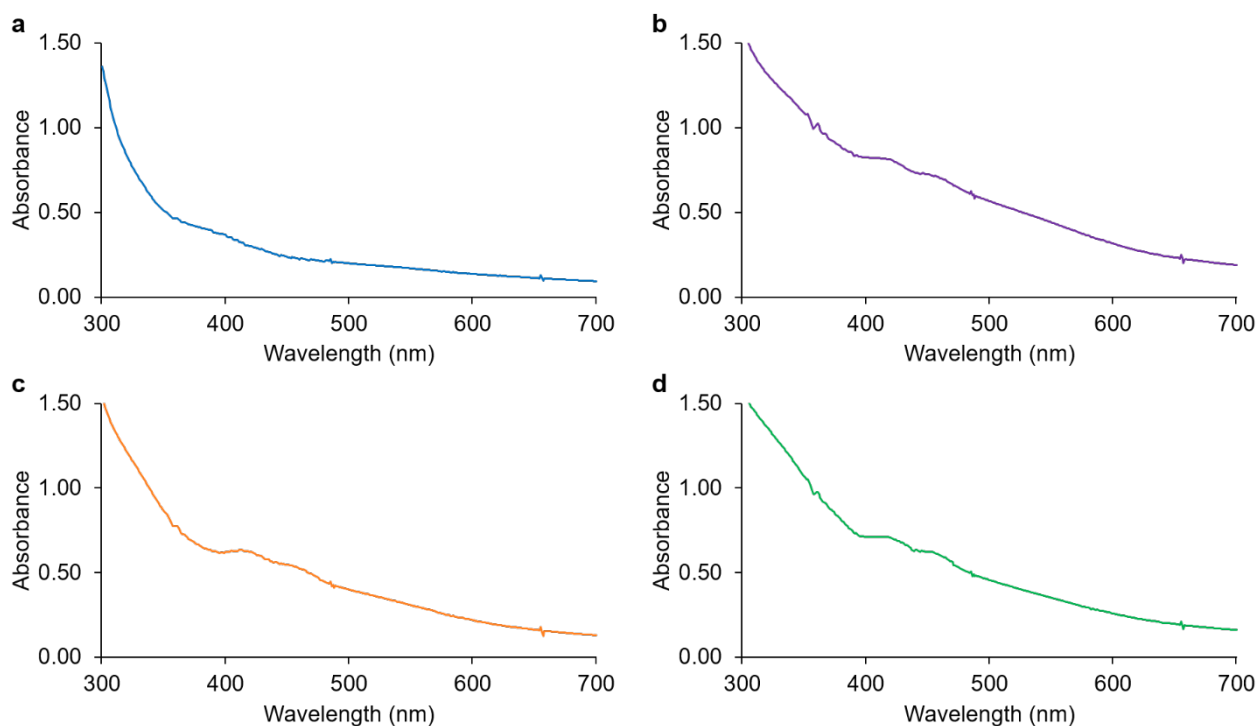


Fig. S41 | **a**, UV-vis spectrum of the C $\gamma$ EG peptide in the presence of Fe<sup>3+</sup> and S<sup>2-</sup> ions. The [2Fe-2S] cluster is not detectable. **b**, UV-vis spectrum of [2Fe-2S] cluster coordinated by  $\gamma$ ECG. **c**, UV-vis spectrum of [2Fe-2S] cluster coordinated to  $\gamma$ EGC. **d**, UV-vis spectrum of [2Fe-2S] cluster coordinated to AcC $\gamma$ EG.

**Fig. S42.**

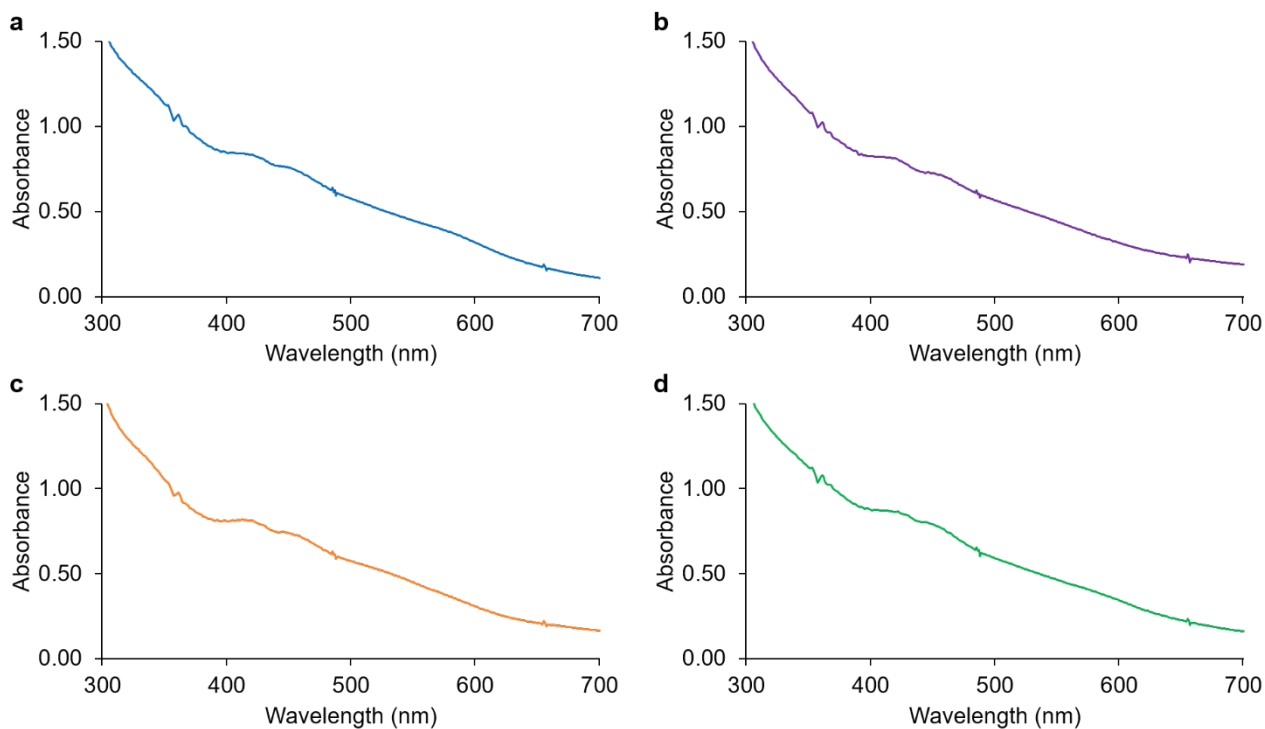


Fig. S42 | **a**, UV-vis spectrum of [2Fe-2S] cluster coordinated to DCG. **b**, UV-vis spectrum of [2Fe-2S] cluster coordinated to  $\gamma$ ECG. **c**, UV-vis spectrum of [2Fe-2S] cluster coordinated to  $\beta$ DCG. **d**, UV-vis spectrum of [2Fe-2S] cluster coordinated to ECG.

**Fig. S43.**

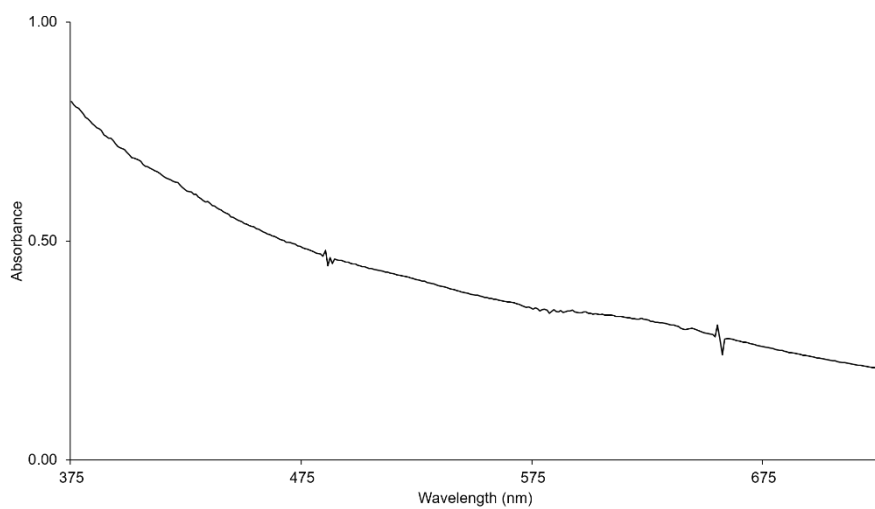


Fig. S43 | UV-vis spectrum of a solution containing 40 mM GMG, 0.5 mM iron ions, 0.2 mM sulfide at pH 8. The [2Fe-2S] cluster is not detectable.

**Fig. S44.**

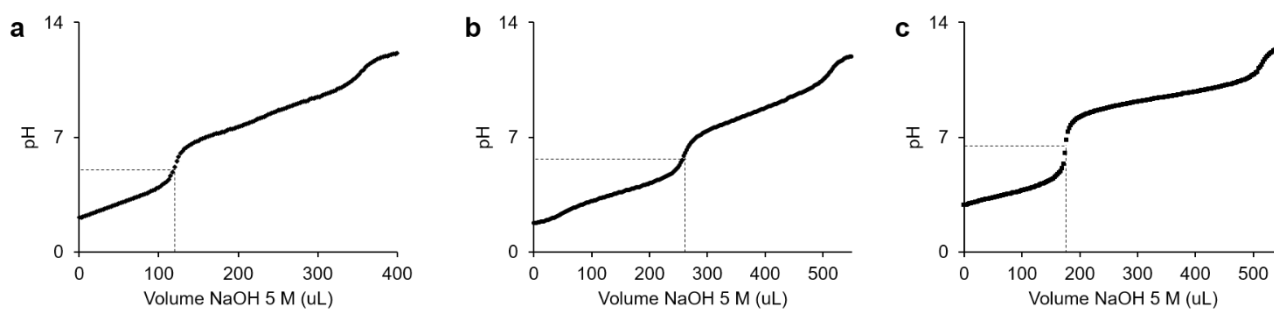


Fig. S44 | **a**, pH titration of SCG. **b**, pH titration of ECG. **c**, pH titration of  $\gamma$ ECG. The first inflection point is highlighted for each titration. Acetylation of the amino-terminus increased the  $pK_a$  of the thiol to 8.1. For amino-terminal cysteine peptides, the  $pK_a$  was lower (ca. 6.9) due to the proximity of the  $\alpha$ -amino group to the side-chain thiol. For these cases, the pH was adjusted to 6.9 or 7.3, in order to shift the equilibrium of  $H_2S$  dissociation. However, N-terminal Cys peptides failed to coordinate a  $[2Fe-2S]$  cluster in both the cases.

**Fig. S45.**

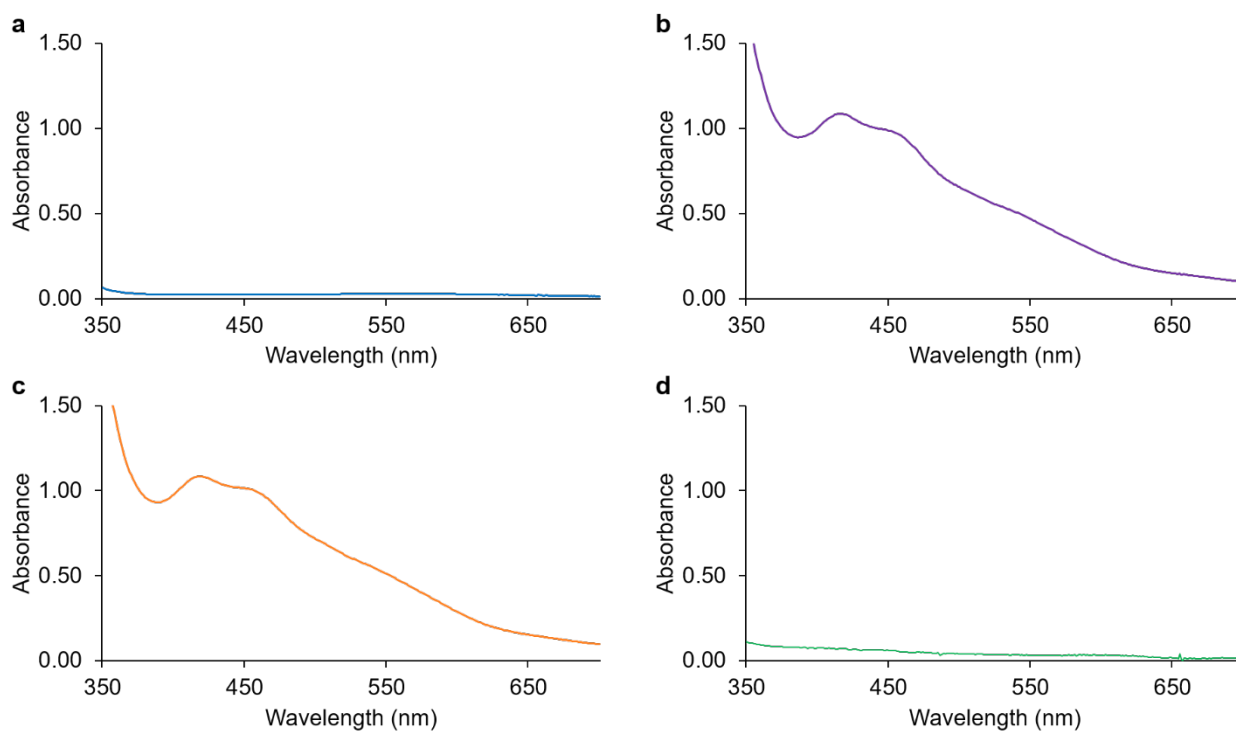


Fig. S45 | **a**, UV-vis spectrum of L-cysteine methyl ester in the presence of  $\text{Fe}^{3+}$  and  $\text{S}^{2-}$  ions. The  $[\text{2Fe-2S}]$  cluster is not detectable. **b**, UV-vis spectrum of  $[\text{2Fe-2S}]$  cluster coordinated by *N*-acetyl L-cysteine methyl ester. **c**, UV-vis spectrum of  $[\text{2Fe-2S}]$  cluster coordinated by *N*-acetyl L-cysteine. **d**, UV-vis spectrum of L-cysteine in the presence of  $\text{Fe}^{3+}$  and  $\text{S}^{2-}$  ions. The  $[\text{2Fe-2S}]$  cluster is not detectable.

Fig. S46.

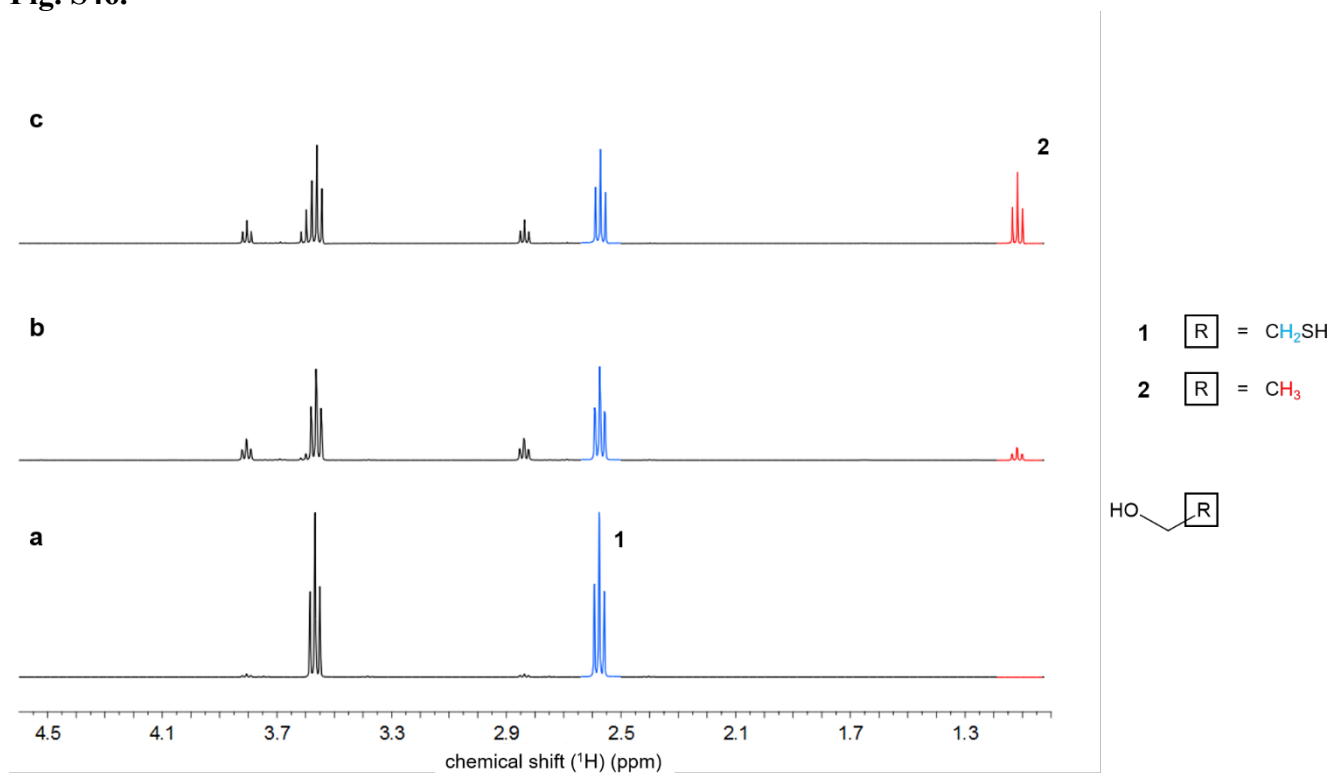


Fig. S46 | **a**,  $^1\text{H-NMR}$  of 2-mercaptoethanol solution before UV light (254 nm) irradiation. **b**,  $^1\text{H-NMR}$  of 2-mercaptoethanol solution after 15 min UV light irradiation. **c**,  $^1\text{H-NMR}$  of irradiated 2-mercaptoethanol solution after spiking with ethanol.

Fig. S47.

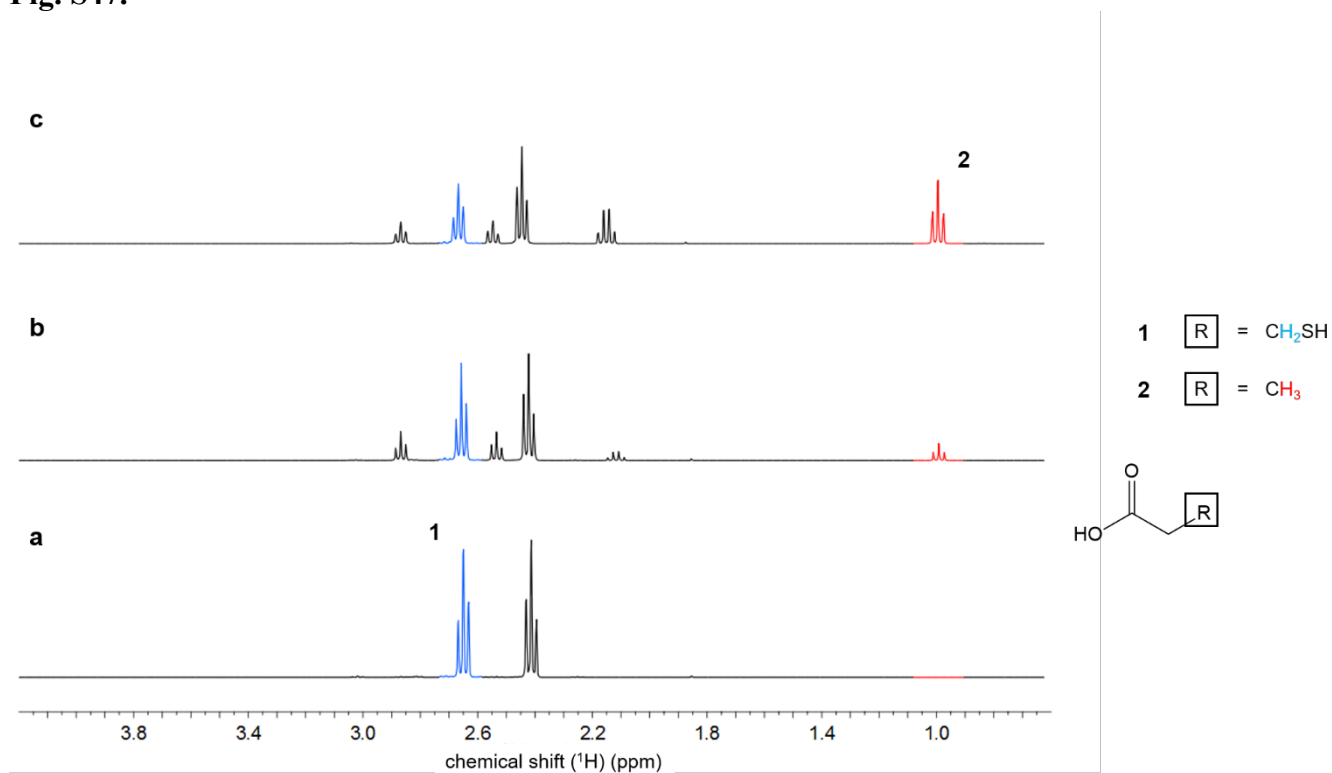


Fig. S47 | **a**, <sup>1</sup>H-NMR of 3-mercaptopropionic acid solution before UV light (254 nm) irradiation. **b**, <sup>1</sup>H-NMR of a 3-mercaptopropionic acid solution after 15 min UV light irradiation. **c**, <sup>1</sup>H-NMR of an irradiated 3-mercaptopropionic acid solution after spiking with propionic acid.

Fig. S48.

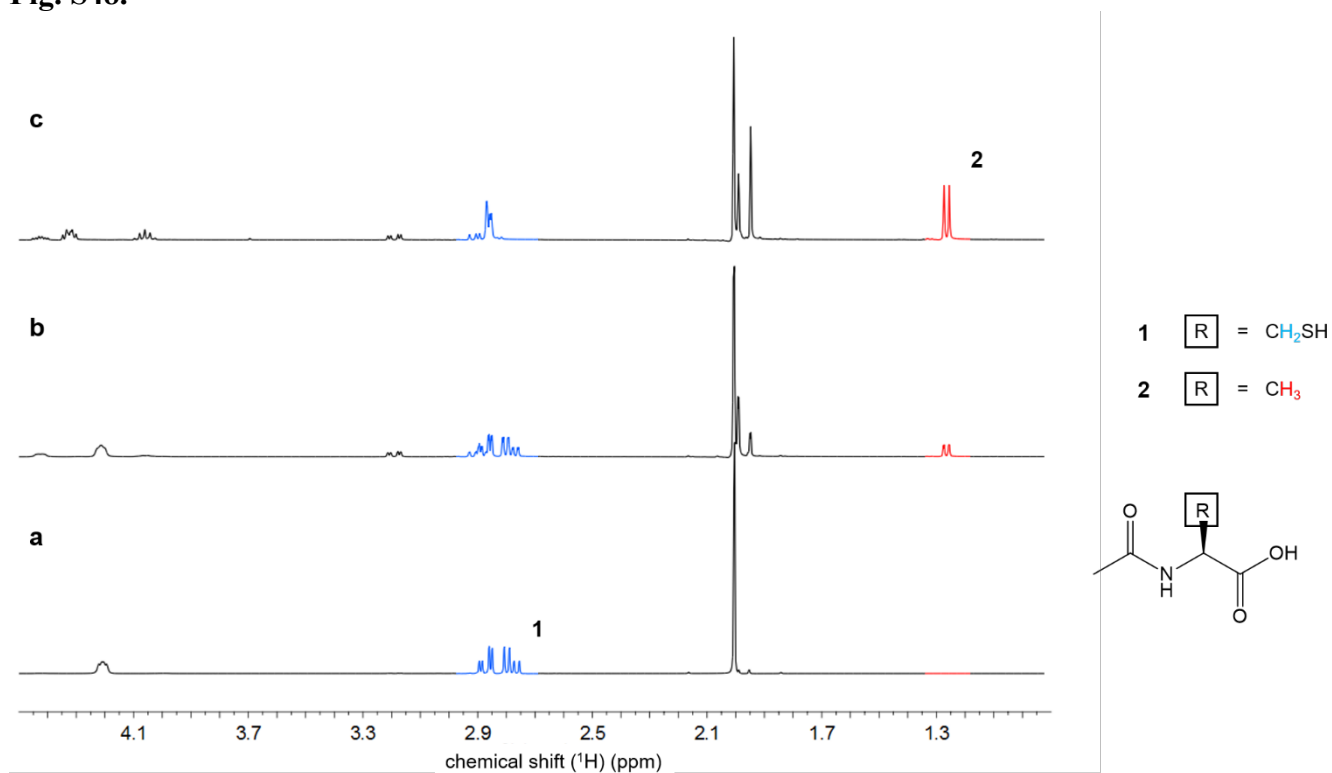


Fig. S48 | **a**,  $^1\text{H-NMR}$  of a  $N$ -acetyl L-cysteine solution before UV light (254 nm) irradiation. **b**,  $^1\text{H-NMR}$  of  $N$ -acetyl L-cysteine solution after 15 min UV light irradiation. **c**,  $^1\text{H-NMR}$  of an irradiated  $N$ -acetyl L-cysteine solution after spiking with  $N$ -acetyl alanine.

Fig. S49.

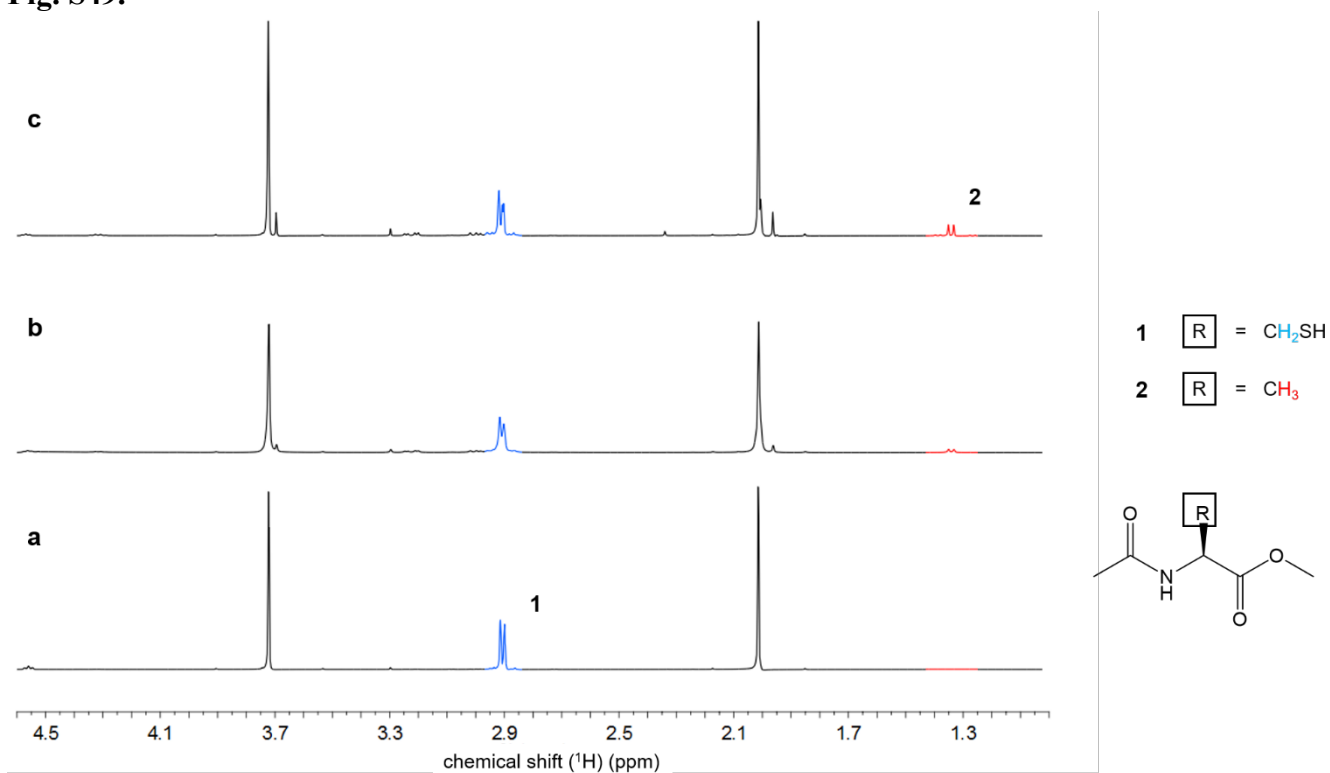


Fig. S49 | **a**,  $^1\text{H}$ -NMR of *N*-acetyl L-cysteine methyl ester solution before UV light (254 nm) irradiation. **b**,  $^1\text{H}$ -NMR of *N*-acetyl L-cysteine methyl ester solution after 15 min UV light irradiation. **c**,  $^1\text{H}$ -NMR of irradiated *N*-acetyl L-cysteine methyl ester solution after spiking with *N*-acetyl alanine methyl ester.

**Fig. S50.**

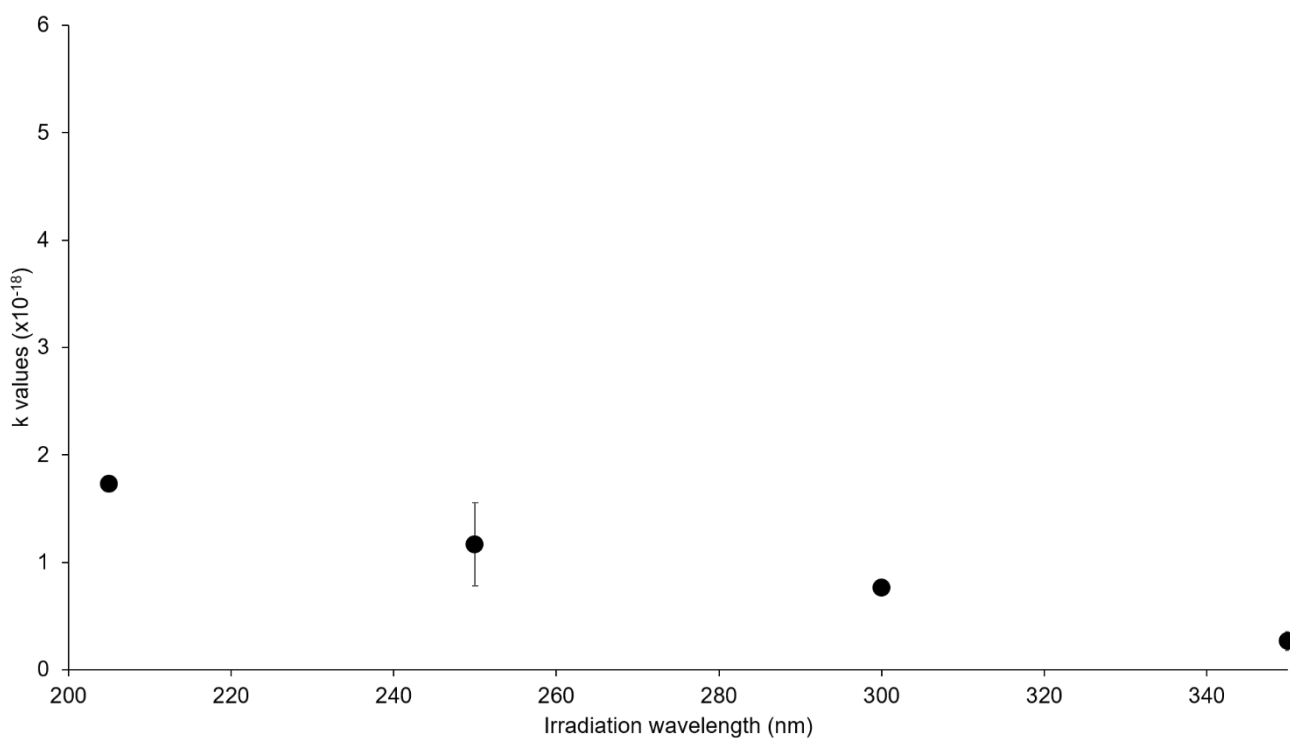


Fig. S50 | Dependence of the conversion rate constant on the irradiation wavelength for 2-mercaptoethanol. The rate constant (expressed as  $s^{-1}$ ) was normalized by the photon flux (expressed as  $s$ ) and each wavelength measurement had a bandwidth of 10 nm. Data represent  $n \geq 3$  replicates for kinetic analysis (mean and SEM).

**Fig. S51.**

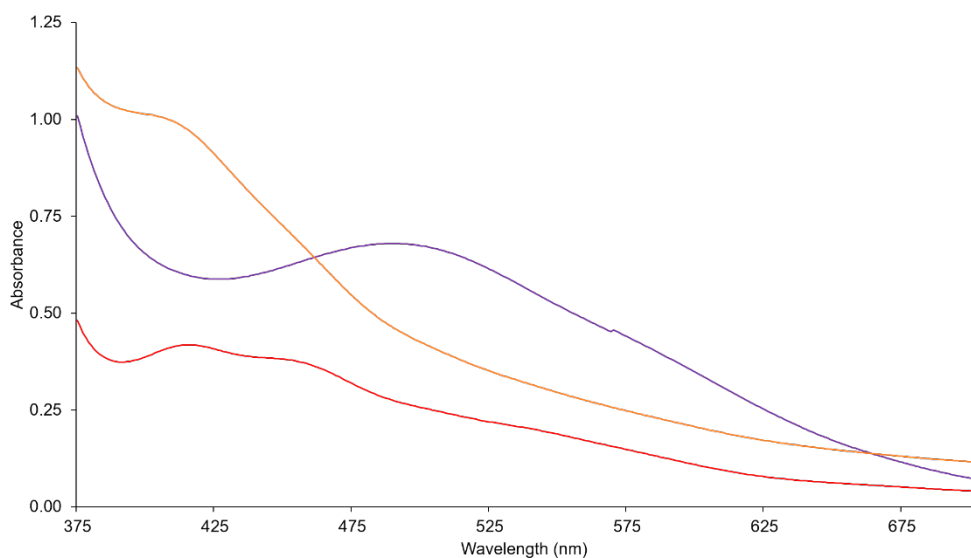


Fig. S51 | UV-vis spectra of a solution of 2-mercaptoethanol and Fe<sup>3+</sup> exposed to UV light (254 nm). The Fe<sup>3+</sup>-mononuclear complex (violet line) is converted within 30 s to the corresponding [2Fe-2S] cluster (red line). Upon further irradiation (180 s) the formation of the [4Fe-4S] cluster can be detected (orange line).

**Fig. S52.**

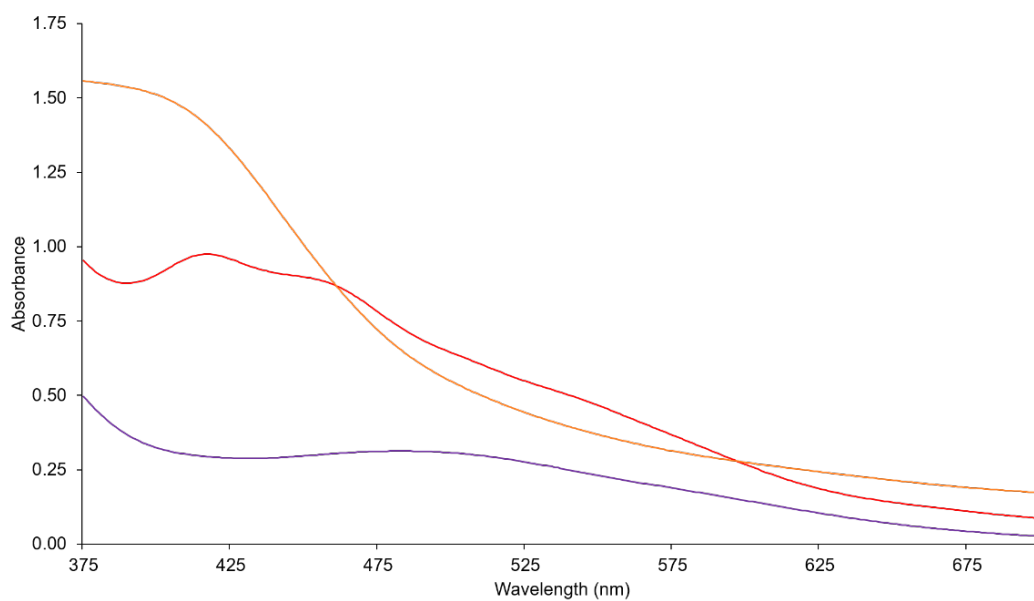


Fig. S52 | UV-vis spectra of a solution of 3-mercaptopropionic acid and Fe<sup>3+</sup> exposed to UV light (254 nm). The Fe<sup>3+</sup>-mononuclear complex (violet line) is converted within 30 s of exposure to UV light to the corresponding [2Fe-2S] cluster (red line). Upon further irradiation (180 s) the formation of the [4Fe-4S] cluster can be detected (orange line).

**Fig. S53.**

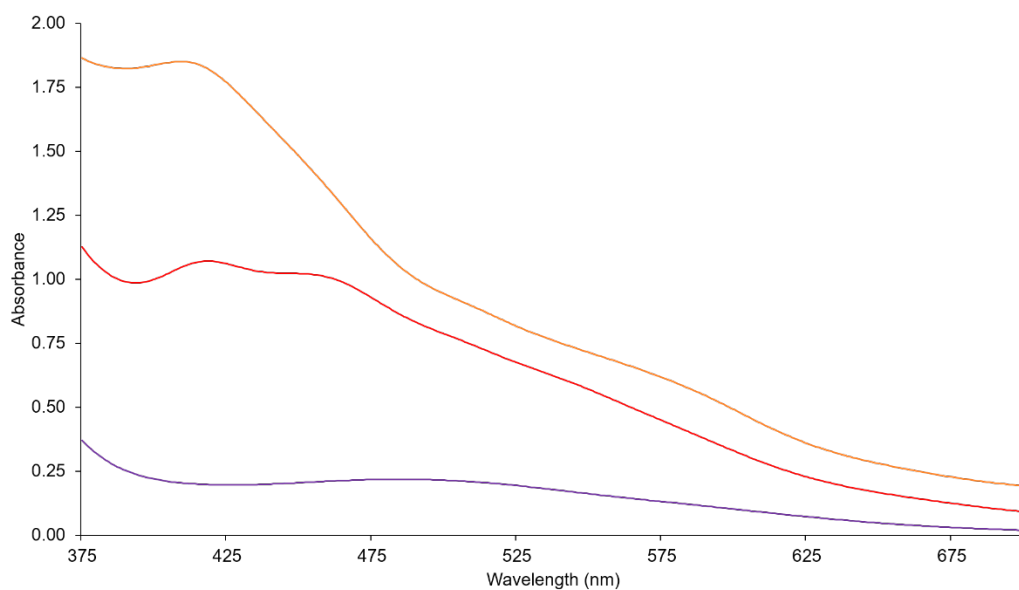


Fig. S53 | UV-vis spectra of a solution of *N*-acetyl L-cysteine and Fe<sup>3+</sup> exposed to UV light (254 nm). The Fe<sup>3+</sup>-mononuclear complex (violet line) is converted within 30 s of exposure to UV light to the corresponding [2Fe-2S] cluster (red line). Upon further irradiation (180 s) the formation of the [4Fe-4S] cluster can be detected (orange line).

**Fig. S54.**

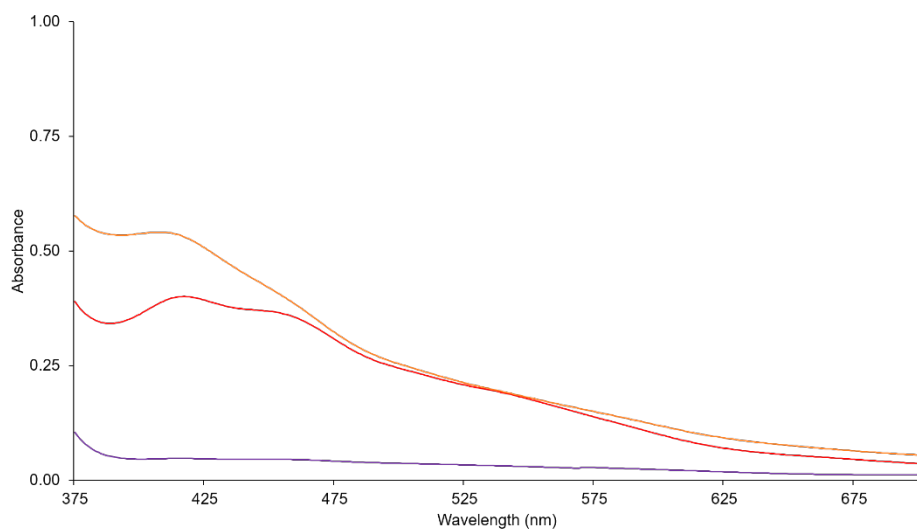


Fig. S54 | UV-vis spectra of a solution of *N*-acetyl L-cysteine methyl ester and  $\text{Fe}^{3+}$  exposed to UV light (254 nm). The  $\text{Fe}^{2+}$ -mononuclear complex (violet line) is converted within 30 s of exposure to UV light to the corresponding [2Fe-2S] cluster (red line). Upon further irradiation (180 s) the formation of the [4Fe-4S] cluster can be detected (orange line).

**Fig. S55.**

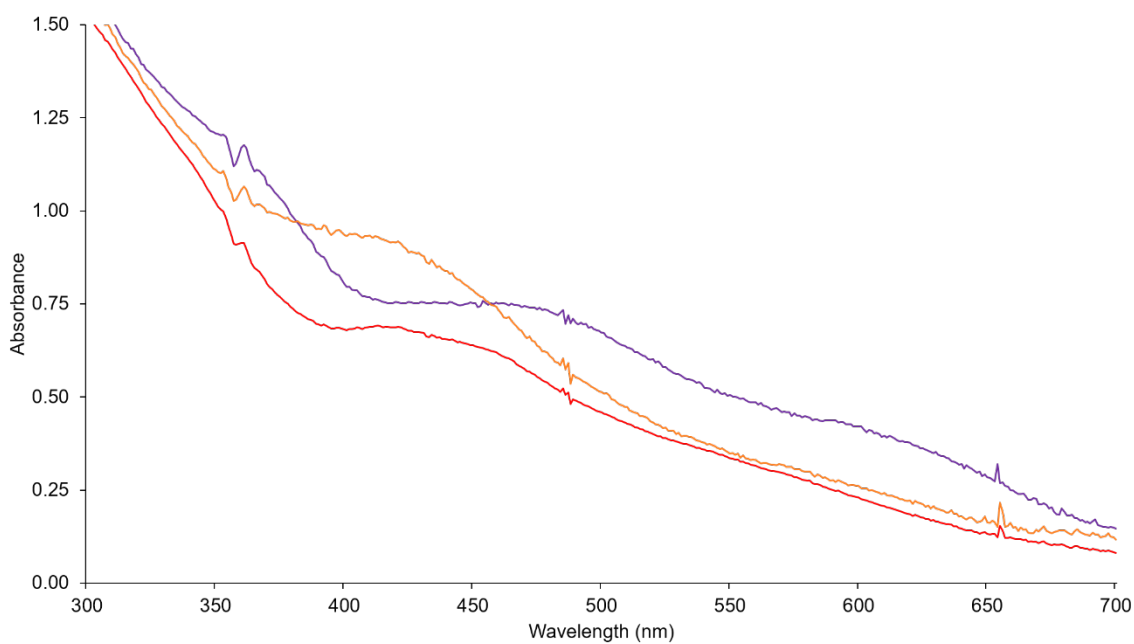


Fig. S55 | UV-vis spectra of a solution of ACG and Fe<sup>3+</sup> exposed to UV light (254 nm). The Fe<sup>2+</sup>-mononuclear complex (violet line) is converted within 30 s of exposure to UV light to the corresponding [2Fe-2S] cluster (red line). Upon further irradiation (180 s) the formation of the [4Fe-4S] cluster can be detected (orange line).

**Fig. S56.**

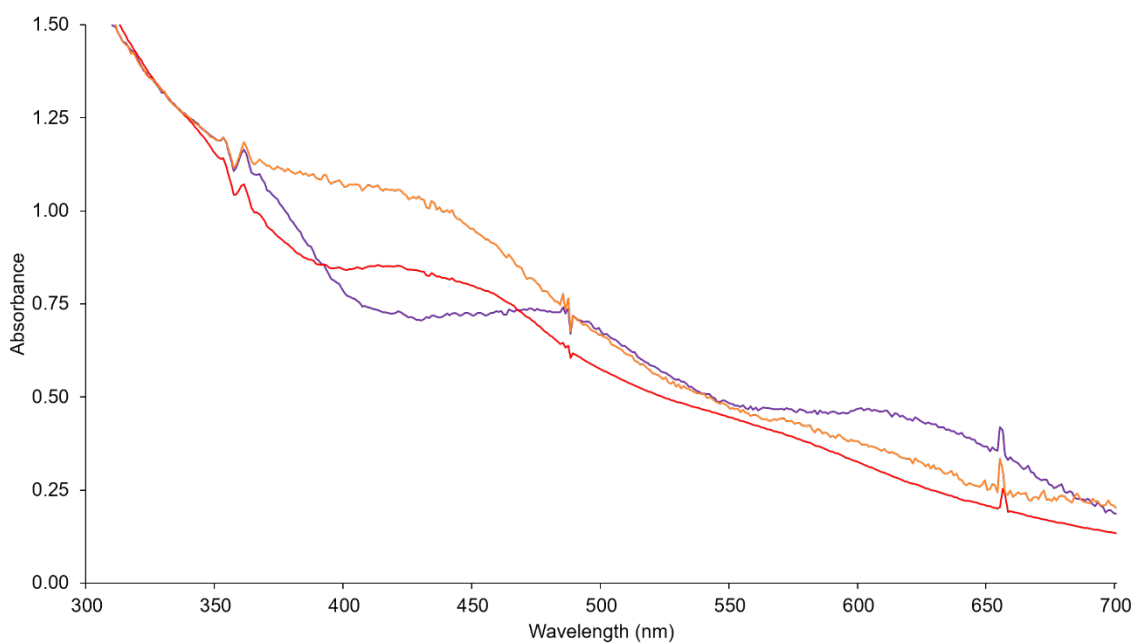


Fig. S56 | UV-vis spectra of a solution of KCG and Fe<sup>3+</sup> exposed to UV light (254 nm). The Fe<sup>2+</sup>-mononuclear complex (violet line) is converted within 30 s of exposure to UV light to the corresponding [2Fe-2S] cluster (red line). Upon further irradiation (180 s) the formation of the [4Fe-4S] cluster can be detected (orange line).

**Fig. S57.**

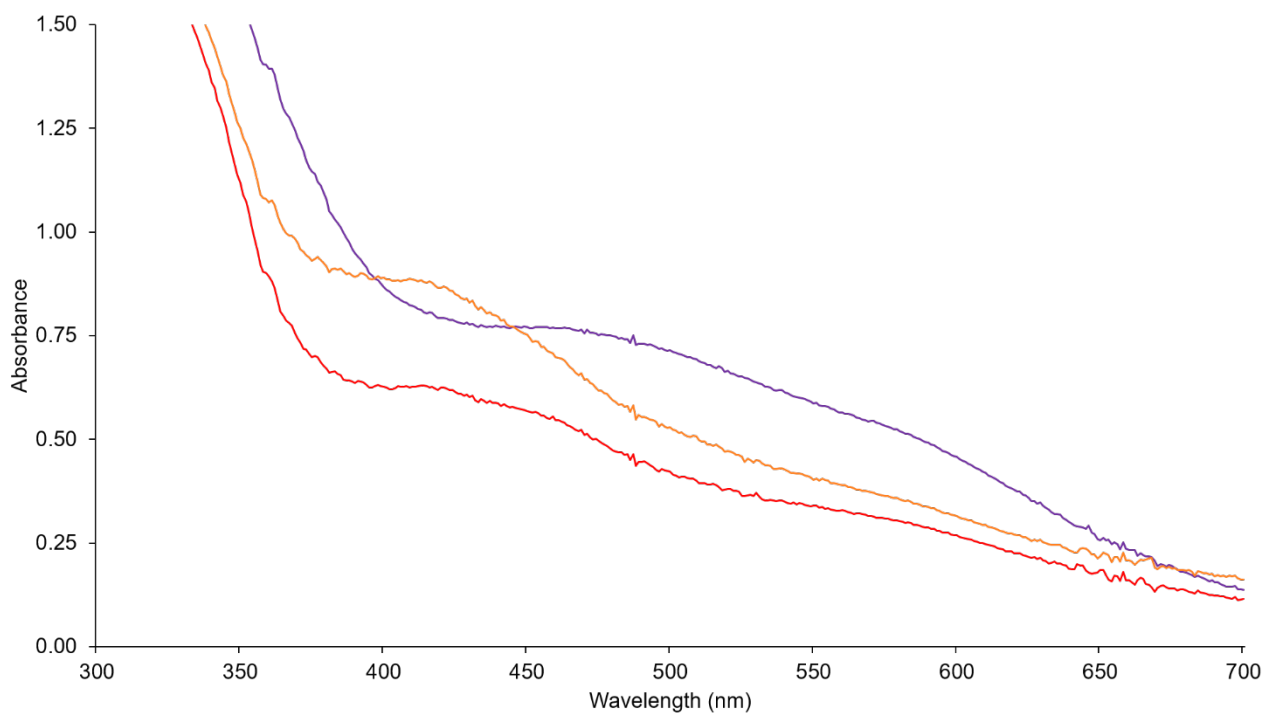


Fig. S57 | UV-vis spectra of a solution of GCK and Fe<sup>3+</sup> exposed to UV light (254 nm). The Fe<sup>2+</sup>-mononuclear complex (violet line) is converted within 30 s of exposure to UV light to the corresponding [2Fe-2S] cluster (red line). Upon further irradiation (180 s) the formation of the [4Fe-4S] cluster can be detected (orange line).

**Fig. S58.**

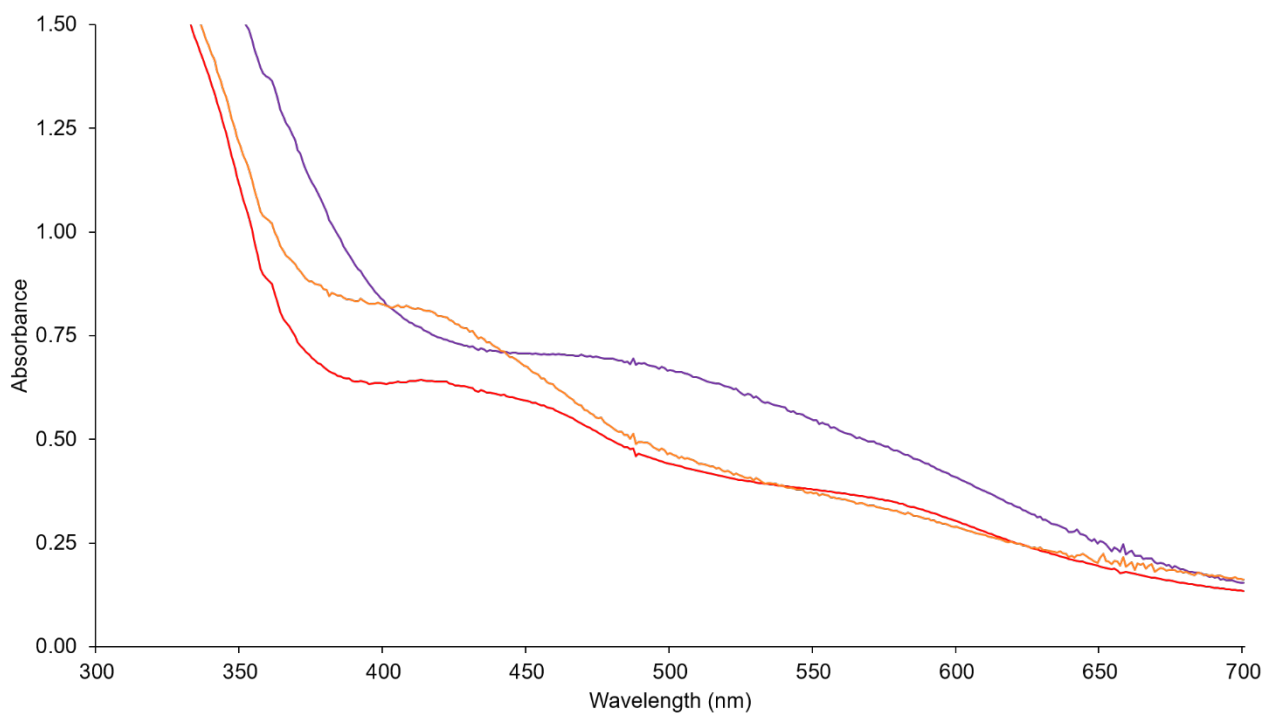


Fig. S58 | UV-vis spectra of a solution of TCT and Fe<sup>3+</sup> exposed to UV light (254 nm). The Fe<sup>2+</sup>-mononuclear complex (violet line) is converted within 30 s of exposure to UV light to the corresponding [2Fe-2S] cluster (red line). Upon further irradiation (180 s) the formation of the [4Fe-4S] cluster can be detected (orange line).

**Fig. S59.**

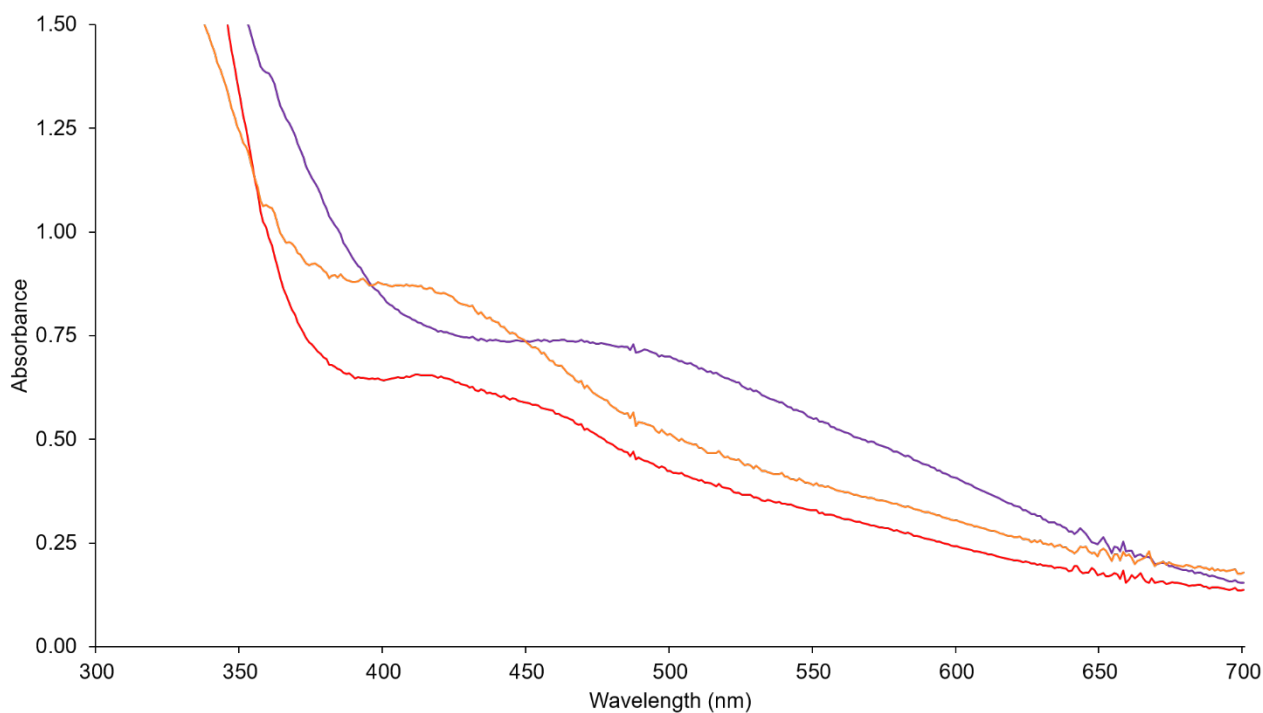


Fig. S59 | UV-vis spectra of a solution of ACT and Fe<sup>3+</sup> exposed to UV light (254 nm). The Fe<sup>2+</sup>-mononuclear complex (violet line) is converted within 30 s of exposure to UV light to the corresponding [2Fe-2S] cluster (red line). Upon further irradiation (180 s) the formation of the [4Fe-4S] cluster can be detected (orange line).

**Fig. S60.**

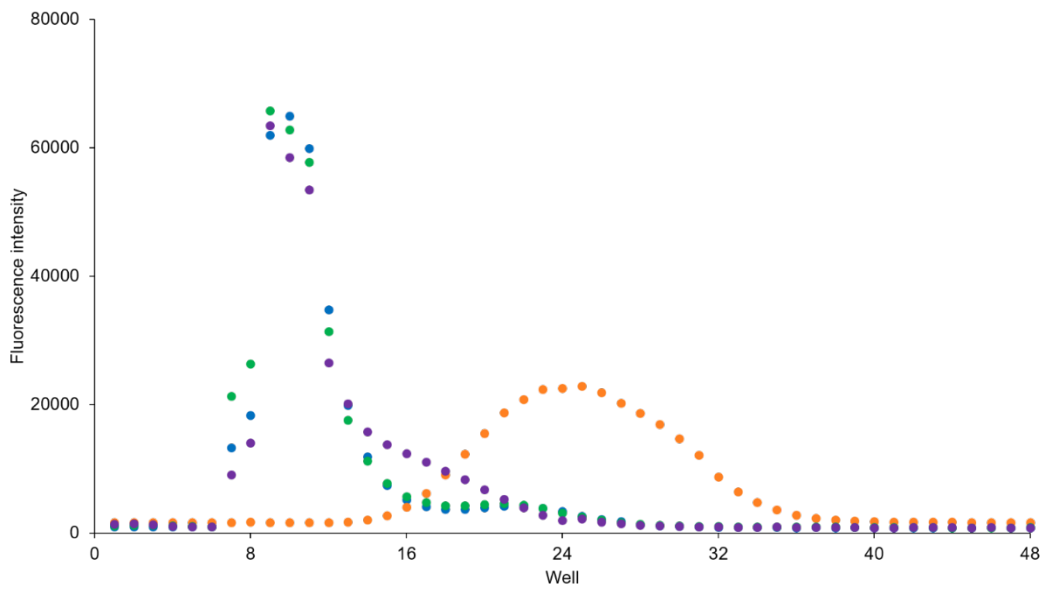


Fig. S60 | Oleate vesicle stability in the presence of Fe<sup>2+</sup> and Fe<sup>2+</sup>- glutathione. Oleate vesicles containing encapsulated FITC-dextran were incubated with either 200 mM Tris-HCl, pH 8.5 (blue dots), 200 mM glutathione (green dots), 5 mM Fe<sup>2+</sup> (orange dots), or 5 mM Fe<sup>2+</sup> plus 200 mM glutathione (violet dots) for 60 min. The integrity of the vesicles was then assessed by quantifying unencapsulated, leaked FITC-dextran by size exclusion chromatography with Sepharose 4b followed by fluorescence spectroscopy.

**Fig. S61.**

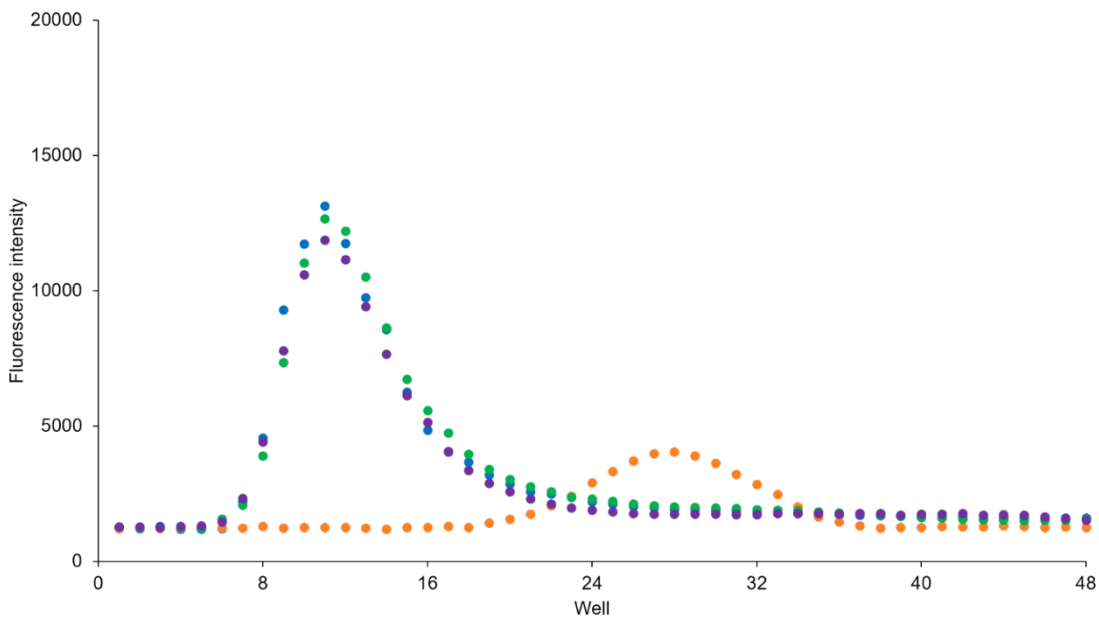


Fig. S61 | 4:1:1 decanoic acid:decanol:monocaprin vesicle stability to Fe<sup>2+</sup> and Fe<sup>2+</sup>-glutathione. 4:1:1 decanoic acid:decanol:monocaprin vesicles containing encapsulated FITC-dextran were incubated with either 200 mM Tris-HCl, pH 8.5 (blue dots), 200 mM glutathione (green dots), 5 mM Fe<sup>2+</sup> (orange dots), or 5 mM Fe<sup>2+</sup> plus 5 mM glutathione (violet dots) for 60 min. The integrity of the vesicles was then assessed by quantifying unencapsulated, leaked FITC-dextran by size exclusion chromatography with Sepharose 4B followed by fluorescence spectroscopy.

**Fig. S62.**

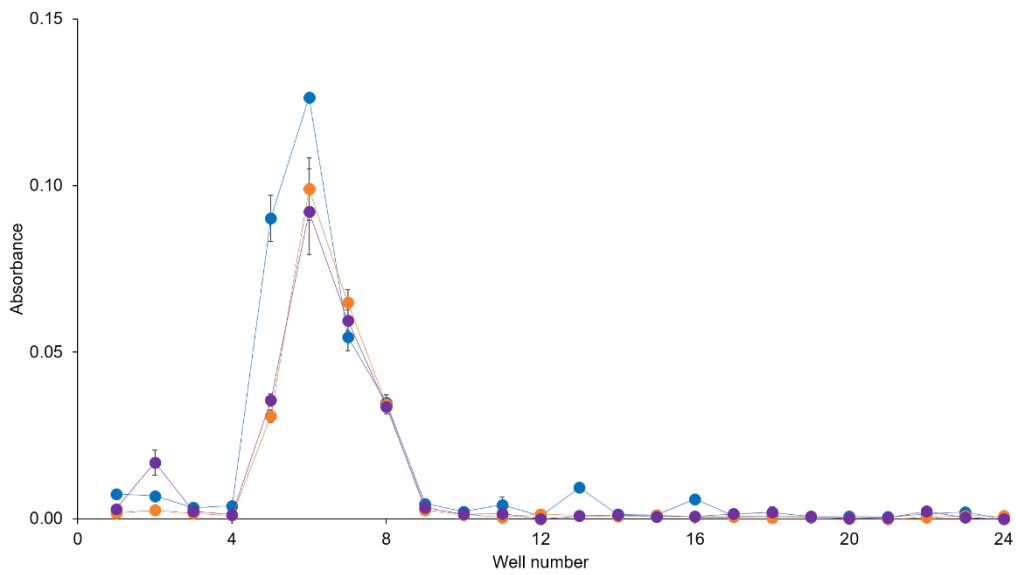


Fig. S62 | Oleate vesicle stability assay to UV light. Oleate vesicles containing encapsulated  $\text{Fe}^{2+}$ -glutathione was irradiated at 254 nm for 60 min (orange dots). Control reactions included an aliquot of the same sample prior to exposure to UV light (blue dots) and vesicles kept at room temperature for 60 min (violet dots) without exposure to UV. Absorbance of the tiron-iron complex was exploited to detect leaked iron ions, thus indicating structurally compromised vesicles. No leaked iron ions were detected.

**Fig. S63.**

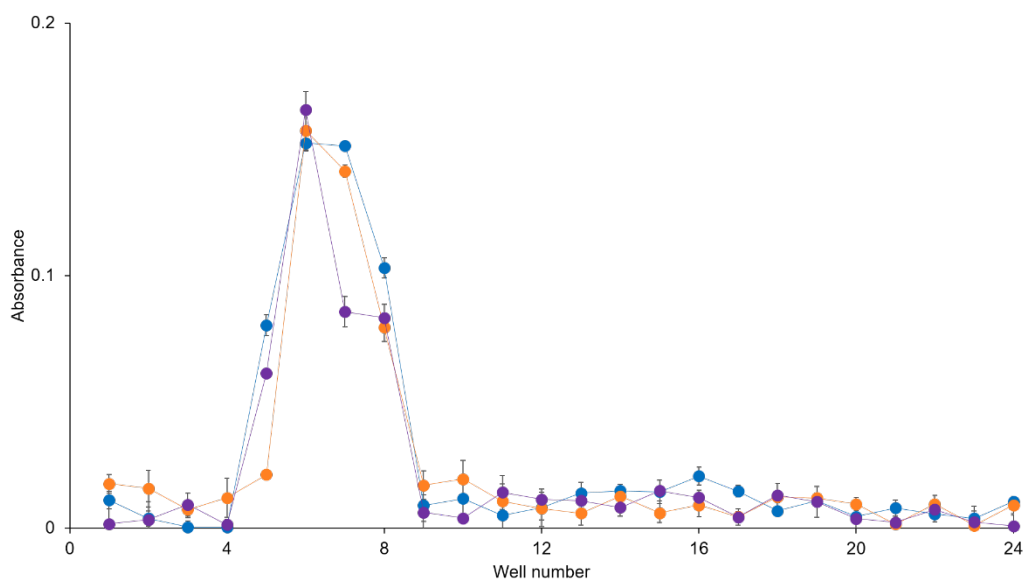


Fig. S63 | 4:1:1 decanoic acid:decanol:monocaprin vesicle stability to UV light. 4:1:1 decanoic acid:decanol:monocaprin vesicles containing encapsulated  $\text{Fe}^{2+}$ -glutathione was irradiated at 254 nm for 60 min (orange dots). Control reactions included an aliquot of the same sample prior to exposure to UV light (blue dots) and vesicles kept at room temperature for 60 min (violet dots) without exposure to UV. Absorbance of the tiron-iron complex was exploited to detect leaked iron ions, thus indicating structurally compromised vesicles. No leaked iron ions were detected.

**Fig. S64.**

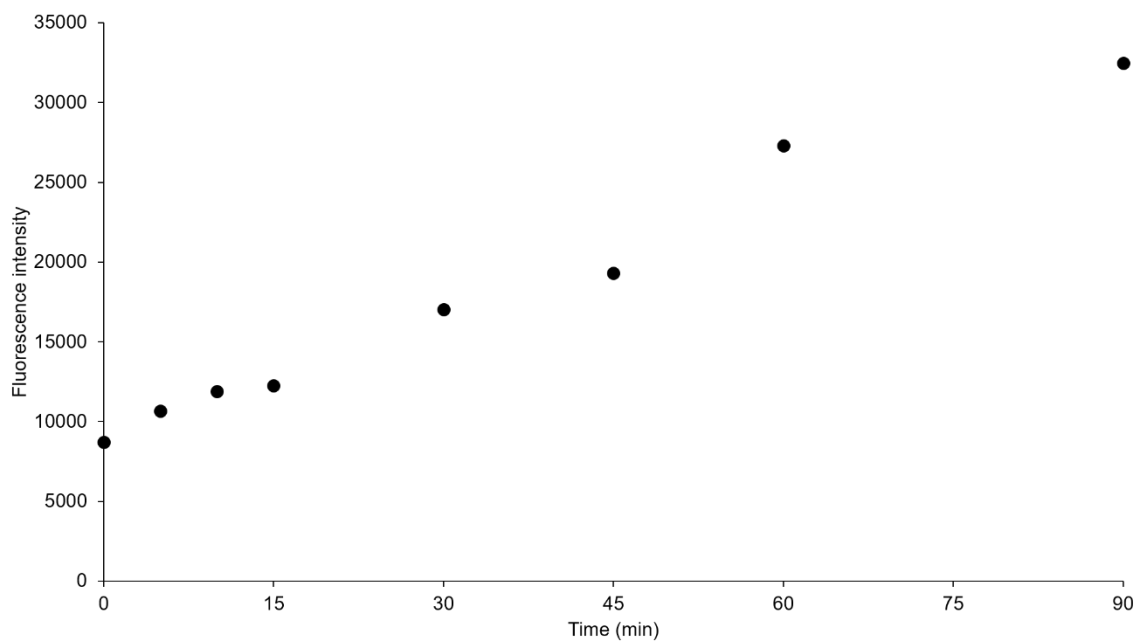


Fig. S64 | 7-amino-4-methyl coumarin assay for sulfide production within oleate vesicles induced by UV-light. Aliquots of oleate vesicles were irradiated for 5, 10, 15, 30, 45, 60 and 90 min. 7-azido-4-methyl coumarin was added to each aliquot and left to react for 1 h. The formation of 7-amino-4-methyl coumarin upon reaction with sulfide ions was detected by fluorescence (excitation wavelength: 345 nm, emission wavelength: 440 nm).

**Fig. S65.**

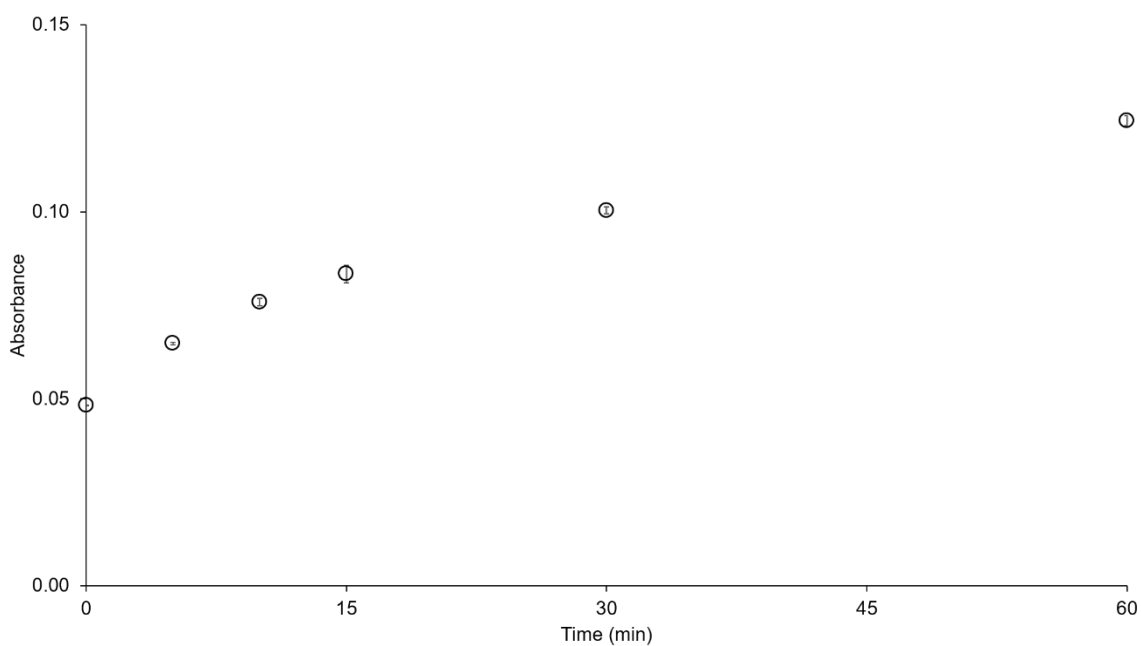


Fig. S65 | Methylene blue assay for sulfide production within 4:1:1 decanoic acid:decanol:monocaprin vesicles induced by UV-light. Aliquots of 4:1:1 decanoic acid:decanol:monocaprin vesicles were irradiated for 5, 10, 15, 30, 45 and 60 min. DMPD solution (2.5 mM) was added to each aliquot upon the addition of  $\text{Fe}^{3+}$  ions (1.25 mM) and left to react for 1 h. The absorbance at 668 nm was then recorded. Colorimetric data represent mean and SEM in  $n \geq 3$  replicates.

**Table S1.**

Table S1. Absorbance maxima for Fe<sup>3+</sup> mononuclear complex, [2Fe-2S] and [4Fe-4S] clusters with thiol containing molecules synthesized by photolysis and photooxidation.

<b>Ligand</b>	<b>iron-sulfur system</b>	<b>Absorbance maximum (nm)</b>	<b>Absorbance maximum (nm)</b>
<b>2-mercaptoethanol</b>	Fe <sup>3+</sup> mononuclear complex	492	-
	[2Fe-2S] cluster	420	455
	[4Fe-4S] cluster	404	-
<b>3-mercaptopropionic acid</b>	Fe <sup>3+</sup> mononuclear complex	496	-
	[2Fe-2S] cluster	419	451
	[4Fe-4S] cluster	405	-
<b>N-acetyl L-cysteine</b>	Fe <sup>3+</sup> mononuclear complex	498	-
	[2Fe-2S] cluster	420	454
	[4Fe-4S] cluster	412	-
<b>N-acetyl L-cysteine methyl ester</b>	Fe <sup>3+</sup> mononuclear complex	505	-
	[2Fe-2S] cluster	422	451
	[4Fe-4S] cluster	413	-

**Table S2.**

Table S2. Mössbauer data obtained on Fe<sup>3+</sup> mononuclear complex, [2Fe-2S] and [4Fe-4S] clusters with glutathione (mms<sup>-1</sup>, errors  $\leq \pm 0.01$  mms<sup>-1</sup> unless shown otherwise in parenthesis, at 80 K).

<b>Irradiation time</b>	<b>IS*</b>	<b>QS*</b>	<b>h.w.h.m.*</b>	<b>Molar contribution (%)</b>	<b>Identity</b>	<b>Geometry</b>
0 s	0.68	3.26	0.22	100	Fe <sup>2+</sup>	4-coord., T <sub>d</sub>
30 s	0.68	3.26	0.23	79	Fe <sup>2+</sup>	4-coord., T <sub>d</sub>
	0.27	0.52	0.21	21	Fe <sup>3+</sup>	[2Fe-2S], T <sub>d</sub>
180 s	0.68	3.32	0.23	26	Fe <sup>2+</sup>	4-coord., T <sub>d</sub>
	0.31	0.57	0.22	64	Fe <sup>3+</sup>	[2Fe-2S], T <sub>d</sub>
	0.48	1.06(2)	0.26(2)	10	Fe <sup>2+/3+</sup>	[4Fe-4S], T <sub>d</sub>

\*IS, isomeric shift; QS, quadrupole splitting; h.w.h.m., half of the line width at half maximum.

**Table S3.**

Table S3. Chemical shift (ppm) data collected from <sup>1</sup>H-NMR spectra of thiol containing solutions exposed to UV irradiation at 254 nm.

	Reduced thiol (ppm)		Oxidized thiol (ppm)		Desulfurized analogue (ppm)	
	R-CH <sub>2</sub> -CH <sub>2</sub> -SH	R-CH <sub>2</sub> -CH <sub>2</sub> -SH	(R-CH <sub>2</sub> -CH <sub>2</sub> -S) <sub>2</sub>	(R-CH <sub>2</sub> -CH <sub>2</sub> -S) <sub>2</sub>	R-CH <sub>2</sub> -CH <sub>3</sub>	R-CH <sub>2</sub> -CH <sub>3</sub>
<b>2-Mercaptoethanol</b>	δ 2.57 (t, 2H)	δ 3.55 (t, 2H)	δ 2.83 (t, 2H)	δ 3.81 (t, 2H)	δ 1.11 (t, 2H)	δ 3.59 (q, 3H)
<b>3-Mercaptopropionic acid</b>	δ 2.62 (t, 2H)	δ 2.37 (t, 2H)	δ 2.83 (t, 2H)	δ 3.81 (t, 2H)	δ 1.11 (t, 2H)	δ 3.59 (q, 3H)
<b>Cysteamine</b>	δ 2.69 (t, 2H)	δ 3.04 (t, 2H)	δ 2.91 (t, 2H)	δ 3.25 (t, 2H)	δ 1.20 (t, 2H)	δ 2.98 (q, 3H)

**Table S4.**

Table S4. Chemical shift (ppm) data collected from  $^1\text{H-NMR}$  spectra of protected and unprotected L-cysteine and L-glutathione solutions exposed to UV irradiation at 254 nm.

	Reduced thiol (ppm)		Oxidized thiol (ppm)		Desulfurized analogue (ppm)	
	<b>R-CH-CH<sub>2</sub>-SH</b>	<b>R-CH-CH<sub>2</sub>-SH</b>	<b>(R-CH-CH<sub>2</sub>-S)<sub>2</sub></b>	<b>(R-CH-CH<sub>2</sub>-S)<sub>2</sub></b>	<b>R-CH-CH<sub>3</sub></b>	<b>R-CH-CH<sub>3</sub></b>
<b>L-cysteine</b>	$\delta$ 2.89 - 2.75 (m, 2H)	$\delta$ 4.21 (m, 1H)	$\delta$ 3.20 - 2.88 (m, 2H)	-	$\delta$ 1.26 (d, 3H)	$\delta$ 4.06 (m, 1H)
<b>L-cysteine methyl ester</b>	$\delta$ 2.89 - 2.75 (m, 2H)	$\delta$ 4.21 (m, 1H)	$\delta$ 3.20 - 2.88 (m, 2H)	-	$\delta$ 1.26 (d, 3H)	$\delta$ 4.06 (m, 1H)
<b>N-acetyl L-cysteine</b>	$\delta$ 2.89 - 2.75 (m, 2H)	$\delta$ 4.21 (m, 1H)	$\delta$ 3.20 - 2.88 (m, 2H)	-	$\delta$ 1.26 (d, 3H)	$\delta$ 4.06 (m, 1H)
<b>N-acetyl L-cysteine methyl ester</b>	$\delta$ 2.89 - 2.75 (m, 2H)	$\delta$ 4.21 (m, 1H)	$\delta$ 3.20 - 2.88 (m, 2H)	-	$\delta$ 1.26 (d, 3H)	$\delta$ 4.06 (m, 1H)
<b>L-Glutathione</b>	$\delta$ 2.93 - 2.80 (m, 2H)	$\delta$ 4.43 (m, 1H)	$\delta$ 3.26 - 2.90 (m, 2H)	-	$\delta$ 1.33 (d, 3H)	$\delta$ 4.29 (q, 1H)

**Table S5.**

Table S5. Absorbance maxima for Fe<sup>3+</sup> mononuclear complex, [2Fe-2S] and [4Fe-4S] clusters with different tripeptides synthesized by photolysis-photooxidation and by the addition of Na<sub>2</sub>S.\*

Ligand		iron-sulfur system	Absorbance maximum (nm)	Absorbance maximum (nm)	
<b>G CX</b>	GCA	Fe <sup>3+</sup> mononuclear complex	490	-	
		[2Fe-2S] cluster	413	459	
		[4Fe-4S] cluster	415	-	
	GCE	Fe <sup>3+</sup> mononuclear complex	474	-	
		[2Fe-2S] cluster	415	456	
		[4Fe-4S] cluster	409	-	
	GCK	Fe <sup>3+</sup> mononuclear complex	480	-	
		[2Fe-2S] cluster	422	447	
		[4Fe-4S] cluster	420	-	
	GCQ	Fe <sup>3+</sup> mononuclear complex	495	-	
		[2Fe-2S] cluster	430	455	
		[4Fe-4S] cluster	421	-	
	GCS	Fe <sup>3+</sup> mononuclear complex	501	-	
		[2Fe-2S] cluster	420	454	
		[4Fe-4S] cluster	417	-	
	GCT	Fe <sup>3+</sup> mononuclear complex	497	-	
		[2Fe-2S] cluster	419	453	
		[4Fe-4S] cluster	419	-	
	GCV	Fe <sup>3+</sup> mononuclear complex	499	-	
		[2Fe-2S] cluster	418	457	
		[4Fe-4S] cluster	420	-	
	<b>X CG</b>	ACG	Fe <sup>3+</sup> mononuclear complex	496	-
			[2Fe-2S] cluster	421	457
			[4Fe-4S] cluster	414	-

	DCG	Fe <sup>3+</sup> mononuclear complex	491	-
		[2Fe-2S] cluster	415	451
		[4Fe-4S] cluster	415	-
	βDCG	Fe <sup>3+</sup> mononuclear complex	503	-
		[2Fe-2S] cluster	417	459
		[4Fe-4S] cluster	415	-
	ECG	Fe <sup>3+</sup> mononuclear complex	482	-
		[2Fe-2S] cluster	425	455
		[4Fe-4S] cluster	409	-
	γECG	Fe <sup>3+</sup> mononuclear complex	495	-
		[2Fe-2S] cluster	423	457
		[4Fe-4S] cluster	411	-
	FCG	Fe <sup>3+</sup> mononuclear complex	499	-
		[2Fe-2S] cluster	422	456
		[4Fe-4S] cluster	415	-
	KCG	Fe <sup>3+</sup> mononuclear complex	498	-
		[2Fe-2S] cluster	424	451
		[4Fe-4S] cluster	407	-
	NCG	Fe <sup>3+</sup> mononuclear complex	470	-
		[2Fe-2S] cluster	423	451
		[4Fe-4S] cluster	415	-
	QCG	Fe <sup>3+</sup> mononuclear complex	470	-
		[2Fe-2S] cluster	418	454
		[4Fe-4S] cluster	418	-
SCG	Fe <sup>3+</sup> mononuclear complex	475	-	
	[2Fe-2S] cluster	420	447	
	[4Fe-4S] cluster	411	-	
TCG	Fe <sup>3+</sup> mononuclear complex	470	-	

		[2Fe-2S] cluster	419	447	
		[4Fe-4S] cluster	418	-	
	VCG	Fe <sup>3+</sup> mononuclear complex	487	-	
		[2Fe-2S] cluster	422	456	
		[4Fe-4S] cluster	406	-	
	WCG	-	-	-	
<b>XCX</b>	ACA	Fe <sup>3+</sup> mononuclear complex	486	-	
		[2Fe-2S] cluster	417	449	
		[4Fe-4S] cluster	417	-	
	ECE	Fe <sup>3+</sup> mononuclear complex	476	-	
		[2Fe-2S] cluster	423	459	
		[4Fe-4S] cluster	414	-	
	GCG	Fe <sup>3+</sup> mononuclear complex	460	-	
		[2Fe-2S] cluster	421	455	
		[4Fe-4S] cluster	415	-	
	KCK	Fe <sup>3+</sup> mononuclear complex	484	-	
		[2Fe-2S] cluster	425	451	
		[4Fe-4S] cluster	416	-	
	SCS	Fe <sup>3+</sup> mononuclear complex	479	-	
		[2Fe-2S] cluster	418	447	
		[4Fe-4S] cluster	416	-	
	TCT	Fe <sup>3+</sup> mononuclear complex	473	-	
		[2Fe-2S] cluster	421	455	
		[4Fe-4S] cluster	419	-	
	VCV	Fe <sup>3+</sup> mononuclear complex	496	-	
		[2Fe-2S] cluster	418	457	
		[4Fe-4S] cluster	412	-	
	<b>XCY</b>	ACT	Fe <sup>3+</sup> mononuclear complex	472	-
			[2Fe-2S] cluster	425	453

	SCA	[4Fe-4S] cluster	411	-
		Fe <sup>3+</sup> mononuclear complex	488	-
		[2Fe-2S] cluster	422	452
		[4Fe-4S] cluster	422	-
<b>Protected and unprotected CXG</b>	CGG	-	-	-
	AcCGG	Fe <sup>3+</sup> mononuclear complex	484	-
		[2Fe-2S] cluster	413	456
		[4Fe-4S] cluster	413	-
	CγEG	-	-	-
	AcCγEG	Fe <sup>3+</sup> mononuclear complex	496	-
		[2Fe-2S] cluster	415	462
[4Fe-4S] cluster		415	-	
<b>XGC type</b>	GGC	Fe <sup>3+</sup> mononuclear complex	496	-
		[2Fe-2S] cluster	415	455
		[4Fe-4S] cluster	411	-
	γEGC	Fe <sup>3+</sup> mononuclear complex	506	-
		[2Fe-2S] cluster	416	453
		[4Fe-4S] cluster	411	-
<b>Dipeptides</b>	CG	-	-	-
	AcCG	Fe <sup>3+</sup> mononuclear complex	496	-
		[2Fe-2S] cluster	418	452
		[4Fe-4S] cluster	417	-
	GC	Fe <sup>3+</sup> mononuclear complex	500	-
		[2Fe-2S] cluster	419	453
[4Fe-4S] cluster		419	-	
<b>Negative control</b>	GMG	-	-	-

\* Iron-sulfur cluster synthesis was first carried out with the addition of Na<sub>2</sub>S and FeCl<sub>3</sub>, as described under "[2Fe-2S] cluster synthesis" above. For every single peptide that successfully coordinated a [2Fe-2S] cluster, the synthesis of the cluster was repeated by photolysis in the absence of Na<sub>2</sub>S. Both iron-sulfur cluster synthesis methods gave identical results.

**Table S6.**

Table S6. Inflection points and pK<sub>a</sub> values for model Cys-containing tripeptides.

<b>Peptide</b>	<b>pH - first inflection point</b>	<b>pH - second inflection point</b>	<b>Thiol pK<sub>a</sub></b>
GGC	5.02	10.88	8.01
GCG	6.25	11.06	8.04
CGG	5.52	10.61	6.91
AcCGG	6.12	10.47	8.06
ECG	5.83	11.03	7.74
SCG	5.20	10.99	7.28
VCG	5.32	10.70	7.68
VCV	5.74	10.44	7.61

**Table S7.**

Table S7. Absorbance maxima for [2Fe-2S] clusters coordinated to protected and unprotected L-cysteine and small molecule thiols.

<b>Ligand</b>		<b>Absorbance maximum (nm)</b>	<b>Absorbance maximum (nm)</b>
<b>Protected and unprotected Cys</b>	L-cysteine	-	-
	L-cysteine methyl ester	-	-
	<i>N</i> -acetyl L-cysteine	420	454
	<i>N</i> -acetyl L-cysteine methyl ester	420	451
<b>Small thiolates</b>	DL-dithiothreitol	419	457
	2-mercaptoethanol	420	455
	3-mercaptopropionic acid	419	451

**Table S8.**

Table S8. Mössbauer data obtained on irradiated and non-irradiated oleate vesicles containing Fe<sup>3+</sup> - L-glutathione (mms<sup>-1</sup>, errors  $\leq \pm 0.01$  mms<sup>-1</sup> unless shown otherwise in parenthesis, at 80 K).

<b>Irradiation time</b>	<b>IS*</b>	<b>QS*</b>	<b>h.w.h.m.*</b>	<b>Molar contribution (%)</b>	<b>Identity</b>	<b>Geometry</b>
0 s	0.72	3.50(3)	0.16(2)	23	Fe <sup>2+</sup>	4-coord., distorted T <sub>d</sub>
	0.70	3.11(3)	0.20	37	Fe <sup>2+</sup>	4-coord., T <sub>d</sub>
	0.38	0.70	0.29	40	Fe <sup>3+</sup>	4-coord., distorted T <sub>d</sub>
180 s	0.72	3.49(2)	0.18	32	Fe <sup>2+</sup>	4-coord., distorted T <sub>d</sub>
	0.69	3.13(2)	0.21	54	Fe <sup>2+</sup>	4-coord., T <sub>d</sub>
	0.28	0.53	0.21	14	Fe <sup>3+</sup>	[2Fe-2S], T <sub>d</sub>

\*IS, isomeric shift; QS, quadrupole splitting; h.w.h.m., half of the line width at half maximum.

## References

1. De Marco, R., Di Gioia, M. L., Leggio, A., Liguori, A. & Viscomi, M. C. Deprotection of N-Nosyl-  $\alpha$ -amino Acids by Using Solid-Supported Mercaptoacetic Acid. *European J. Org. Chem.* 3795–3800 (2009). doi:10.1002/ejoc.200900271
2. Jensen, Knud J.; Tofteng Shelton, Pernille; Pedersen, S. L. *Peptide Synthesis and Applications*. (2013). doi:10.1007/978-1-62703-544-6
3. Hanczyc, M. M., Fujikawa, S. M. & Szostak, J. W. Experimental models of primitive cellular compartments: encapsulation, growth, and division. *Science* **302**, 618–22 (2003).
4. Hassan, S. S. ., Marzouk, S. A. . & Sayour, H. E. . Methylene blue potentiometric sensor for selective determination of sulfide ions. *Anal. Chim. Acta* **466**, 47–55 (2002).
5. Scintilla, S. *et al.* Duplications of an iron–sulphur tripeptide leads to the formation of a protoferredoxin. *Chem. Commun.* **52**, 13456–13459 (2016).
6. Pryor, W. A. & Olsen, E. G. Homolytic displacement at sulfur by the hydrogen atom. Formation of hydrogen sulfide in the liquid-phase photolysis of thiols. *J. Am. Chem. Soc.* **100**, 2852–2856 (1978).